PNAS
www.pnas.org

Supplementary Information for

The process of Lewy body formation, rather than simply alpha-synuclein fibrillization, is one of the major driver of neurodegeneration in synucleinopathies.

Anne-Laure Mahul-Mellier[1], Johannes Burtscher[1], Niran Maharjan[1], Laura Weerens[1], Marie Croisier[2], Fabien Kuttler[3], Marion Leleu[4], Graham Knott[2], and Hilal A. Lashuel[1]*

Paste corresponding author name here
Email: **hilal.lashuel@epfl.ch**

This PDF file includes:

Supplementary text (Material and Method section)
Figures S1 to S15
Legends for Figures S1 to S15
SI References

Other supplementary materials for this manuscript include the following:

Datasets S1 to S4 (large dataset saved as separate files)

Supplementary Information Text

Supplemental information – Material

Antibodies and compounds

Information and RRID of the primary antibodies used in this study are listed in Figure S2. Tables include their clone name, catalog numbers, vendors, and respective epitopes.

Supplemental information – Experimental procedures

Expression and Purification of Mouse α-syn

pT7-7 plasmids were used for the expression of recombinant mouse α-syn in *E. coli*. Mouse wild type (WT) α-syn was expressed and purified using anion exchange chromatography (AEC) followed by reverse-phase High-Performance Liquid Chromatography (HPLC) and fully characterized as previously described(1, 2).

Preparation of α-syn fibrils

α-syn monomers were diluted in 500 µL of PBS, pH 7.5 at a final concentration ~170 to 200 µM. The monomeric solution was filtered through a 100 kDa filter (Millipore, Switzerland) before being incubated under constant orbital agitation (1000 rpm) (Peqlab, Thriller, Germany) at 37°C for 5 days(1, 2). The extent of fibril formation and amyloid-like properties of α-syn aggregates were assessed by ThT fluorescence(1, 2). The fibrils were then sonicated on ice (Sonics Vibra cell) with a fine tip for 20 sec, 20% amplitude, pulse 1 second on/ 1 second off. Sonication of α-syn PPFs is a crucial step and should be carefully conducted in order to have sufficient breakage of the mature fibrils into smaller seeds with

a size length of ~50-100 nm (assessed after TEM imaging, Figure S1), with a minimum release of α-syn monomers (assessed by SDS-PAGE and Coomassie staining, see Figure S1)(1, 2). Sonicated α-syn fibrils were aliquoted, snap frozen in liquid nitrogen and stored at -80°C.

Long-term primary culture of hippocampal neurons

Primary hippocampal neurons were prepared from P0 pups of WT mice (C57BL/6JRccHsd, Harlan) or α-syn KO mice (C57BL/6J OlaHsd, Harlan) and cultured as previously described (2, 3). All procedures were approved by the Swiss Federal Veterinary Office (authorization number VD 3392). Briefly, the cerebral hippocampi were isolated stereoscopically in Hank's Balanced Salt Solution (HBSS) and digested by papain (20U/mL, Sigma-Aldrich, Switzerland) for 30 minutes at 37℃. After inhibition of the papain activity by a trypsin inhibitor (Sigma-Aldrich, Switzerland), the tissues were dissociated by mechanical trituration. The cells were finally resuspended in adhesion media (MEM, 10% Horse Serum, 30% glucose, L-glutamine and penicillin/streptomycin) (Life Technologies, Switzerland) and plated in 24- or 6-well plates previously treated with poly-L-lysine 0.1% w/v in water (Brunschwig, Switzerland) at a density of 300,000 cells/mL (for biochemistry analysis) or 250,000 cells/ml (for ICC/confocal microscopy analysis). After 3 hours, adhesion media was removed and replaced by Neurobasal medium (Life Technologies, Switzerland) containing B27 supplement (Life Technologies, Switzerland), L-glutamine and penicillin/streptomycin (100U/mL, Life Technologies, Switzerland) (table 1). Plating of the neurons in the black, clear-bottom, 96-well plates (Falcon, Switzerland) was performed directly in Neurobasal medium at a density of 200,000 cells/mL.

Culture Vessel	Volume of Neurobasal medium per well (Before PFF treatment)
6 well plate	4 ml
24 well plate	1 ml
96 well plate	0.2 ml

Table 1: Volume of the neuronal Growth media used to maintain the neurons in culture

To establish long-term culture of hippocampal primary neurons, we have observed that the change of fresh media once a week as often recommended in primary culture protocols(4-7) is deleterious for the neurons. In our hands, such extra manipulation caused additional stress to our primary culture that induced the neurons to grow as clusters and/or trigger unspecific cell death. Therefore, no further media changes was made until the end of the culture.

Primary culture treatment with mouse α-syn fibrils or PBS

As morphological (8-10), physiological (11-13), gene expression (14) and proteome (15) changes are observed during the different developmental stages of primary neurons in culture (Days *In vitro*, DIV), we have adapted the time-course of the PFFs treatment in primary neurons to be able to analyze the spatio-temporal effects of the seeding mechanism at the biochemical, proteomic, transcriptomic and ultrastructural level uncoupled to the intrinsic changes related to neuronal development and maturation.

Therefore, in our seeding model, the PFFs were added to the neuronal cell culture media at different DIV and PFFs-treated neurons were all harvested at the DIV 26 (See Figure S1F). This ensures that the developmental stage of primary neurons in culture was similar at the harvest time. For the control neurons, PBS was added at DIV 5. The day of the treatment, PFFs were thawed at RT and diluted to a final concentration of 70 nM using the Neurobasal media collected from wells containing the plated neurons (see table 2). The Neurobasal media left in the wells with neurons was then aspirated and

replaced by the diluted PFFs. Treated neurons were cultured for up to 21 days without any further media changes until the end of the treatment (see previous section on primary culture conditions for further information).

Culture Vessel	Volume of the neurobasal medium used to dilute the PFFs (per well)
6 well plate	2 ml
24 well plate	0.5 ml
96 well plate	0.1 ml

Table 2: Volume of the neuronal Growth media used to prepare the PFFs

Immunocytochemistry (ICC)

After α-syn PFFs treatment, primary hippocampal neurons were washed twice with PBS, fixed in 4% PFA for 20 min at RT, and then immunostained as previously described(2). The antibodies used are indicated in the corresponding legend section of each figure. The source and dilution of each antibody can be found in Figure S2. The cells plated on CS were then examined with a confocal laser-scanning microscope (LSM 700, Carl Zeiss Microscopy, Germany) with a 40× objective and analyzed using Zen software (RRID:SCR_013672). The cells plated in black, clear-bottom, 96-well plates were imaged using the IN Cell Analyzer 2200 (with a ×10 objective). For each independent experiment, two wells were acquired per tested condition, and in each well, nine fields of view were imaged. Each experiment was reproduced at least three times independently.

Quantitative high-content wide-field cell imaging analyses (HCA)

After α-syn PFFs treatment, primary hippocampal neurons plated in black, clear-bottom, 96-well plates (BD, Switzerland) were washed twice with PBS, fixed in 4% PFA for 20 min at RT and then immunostained as described above. Images were acquired using the Nikon 10×/ 0.45, Plan Apo, CFI/60 of the IN Cell Analyzer 2200 (GE Healthcare, Switzerland), a high-throughput imaging system equipped with a high-resolution 16-bits

sCMOS camera (2048×2048 pixels), using a binning of 2×2. For each independent experiment, duplicated wells were acquired per condition, and nine fields of view were imaged for each well. Each experiment was reproduced at least three times independently. Images were then analyzed using CellProfiler 3.0.0 software (RRID:SCR_007358) for identifying and quantifying the level of LB-like inclusions (stained with pS129 antibody) formed in neurons MAP2-positive cells, the number of neuronal cell bodies (co-stained with MAP2 staining and DAPI), or the number of neurites (stained with MAP2 staining).

Correlative Light and Electron Microscopy (CLEM)

Primary hippocampal neurons were grown on 35 mm dishes with alphanumeric searching grids etched to the bottom glass (MatTek Corporation, Ashland, MA, USA) and treated with WT PFFs. At the indicated time point, cells were fixed for 2 h with 1% glutaraldehyde and 2.0% PFA in 0.1 M phosphate buffer (PB) at pH 7.4. After washing with PBS, ICC was performed (for more details, see the corresponding section in the Materials and Methods). Neurons with LB-like inclusions (positively stained for pS129) were selected by fluorescence confocal microscopy (LSM700, Carl Zeiss Microscopy) for ultrastructural analysis. The precise position of the selected neuron was recorded using the alpha-numeric grid etched on the dish bottom. The cells were then fixed further with 2.5% glutaraldehyde and 2.0% paraformaldehyde in 0.1 M PB at pH 7.4 for another 2 h. After washing (5 times for 5 min) with 0.1 M cacodylate buffer at pH 7.4, cells were post-fixed with 1% osmium tetroxide in the same buffer for 1 h and washed with double-distilled water before contrasting with 1% uranyl acetate water for 1 h. The cells were then dehydrated in increasing concentrations of alcohol (twice at 50%, once at 70%, once at 90%, once at 95%, and twice at 100%) for 3 min each wash. Dehydrated cells were infiltrated with Durcupan resin diluted with absolute ethanol at 1:2 for 30 min, at 1:1 for 30 min, and 2:1

for 30 min, and twice with pure Durcupan (Electron Microscopy Sciences, Hatfield, PA, USA) for 30 min each. After 2 h of incubation in fresh Durcupan resin, the dishes were transferred into a 65°C oven for the resin to polymerize overnight. Once the resin had hardened, the glass CS on the bottom of the dish was removed by repeated immersion in hot (60°C) water, followed by liquid nitrogen. The cell of interest was then located using the alphanumeric coordinates previously recorded and a razor blade used to cut this region away from the rest of the resin. This piece was then glued to a resin block with acrylic glue, trimmed with a glass knife using an ultramicrotome (Leica Ultracut UCT, Leica Microsystems), and then ultrathin sections (50–60 nm) were cut serially from the face with a diamond knife (Diatome, Biel, Switzerland) and collected onto 2 mm single-slot copper grids coated with formvar plastic support film. Sections were contrasted with uranyl acetate and lead citrate and imaged with a transmission electron microscope (Tecnai Spirit EM, FEI, The Netherlands) operating at 80 kV acceleration voltage and equipped with a digital camera (FEI Eagle, FEI). Width of the microtubules compared to the newly formed fibrils was measured at D7. A minimum of 120 microtubules or newly formed fibrils were counted). Measurements confirmed that the width of newly formed α-syn fibrils of 11.94±3.97 nm (SD) is significantly smaller than the average width of the microtubules of 18.67±2.94 nm (SD).

Immunogold Staining

Primary hippocampal neurons were grown on 35 mm dishes with alphanumeric searching grids etched to the bottom glass (MatTek Corporation, Ashland, MA, USA) and treated with WT PFFs. At the indicated time point, cultured cells were fixed for 2 h with a buffered mix of paraformaldehyde (2%) and glutaraldehyde (0.2%) in PB (0.1M), then washed in PBS (0.01M). After washing with PBS, ICC was performed as described(2). Briefly, cells were incubated with pS129 antibody (81a, Figure S4B) for 2 h at RT diluted in the blocking

solution [(3% BSA and 0.1% Triton X-100 in PBS), (PBS-BSA-T)]. After five washes with PBS-BSA-T, neurons were incubated with the Alexa Fluor^{647} Fluoronanogold secondary antibody (Nanoprobes, USA) for 1 h at RT. Neurons were washed five times with PBS-BSA-T and mounted in polyvinyl alcohol mounting medium supplemented with anti-fading DABCO reagent. Neurons with LB-like inclusions (positively stained for pS129) were selected by fluorescence confocal microscopy (LSM700, Carl Zeiss Microscopy) for ultrastructural analysis. The precise position of the selected neuron was recorded using the alpha-numeric grid etched on the dish bottom. The cells were next washed in phosphate buffer (0.1M) and fixed again in 2.5% glutaraldehyde before being rinsed in distilled water. A few drops of a silver enhancement solution (Aurion, Netherlands) were then added to each CS to cover all of the cells and left in the dark for 1 h at RT. The solution was then removed, and the CS washed in distilled water followed by 0.5% osmium tetroxide for 30 min and 1% uranyl acetate for 40 min. Following this, the CS were dehydrated through increasing concentrations of ethanol and then transferred to 100% epoxy resin (Durcupan, Sigma Aldrich) for 4 h and then placed upside down on a glass CS in a 60°C oven overnight. Once the resin had cured, the CS was removed, and regions of interest were cut away with a razor blade and mounted onto a blank resin block for thin sectioning. Serial thin sections were cut at 50 nm thickness with a diamond knife (Diatome, Switzerland) in an ultramicrotome (UC7, Leica Microsystems) and collected onto a pioloform support firm on copper slot grids. These were further stained with lead citrate and uranyl acetate. Sections were imaged with a digital camera (Eagle, FEI Company) inside a transmission electron microscope (Tecnai Spirit, FEI Company) operating at 80 kV.

Cell lysis and WB analyses of primary hippocampal neurons

Preparation of soluble and insoluble fractions

After α-syn PFFs treatment, primary hippocampal neurons were lysed as described in Volpicelli-Daley *et al.* (4, 5). Briefly, treated neurons were lysed in 1% Triton X-100/ Tris-buffered saline (TBS) (50 mM Tris, 150 mM NaCl, pH 7.5) supplemented with protease inhibitor cocktail, 1 mM phenylmethane sulfonyl fluoride (PMSF), and phosphatase inhibitor cocktail 2 and 3 (Sigma-Aldrich, Switzerland). After sonication using a fine probe [(0.5-s pulse at an amplitude of 20%, ten times (Sonic Vibra Cell, Blanc Labo, Switzerland], cell lysates were incubated on ice for 30 min and centrifuged at 100,000 g for 30 min at 4°C. The supernatant (soluble fraction) was collected while the pellet was washed in 1% Triton X-100/TBS, sonicated as described above, and centrifuged for another 30 min at 100,000 g. The supernatant was discarded whereas the pellet (insoluble fraction) was resuspended in 2% sodium dodecyl sulfate (SDS)/TBS supplemented with protease inhibitor cocktail, 1 mM PMSF, and phosphatase inhibitor cocktail 2 and 3 (Sigma-Aldrich, Switzerland), and sonicated using a fine probe (0.5-s pulse at amplitude of 20%, 15 times).

Total cell lysates

After α-syn PFFs treatment, primary hippocampal neurons were lysed in 2% sodium dodecyl sulfate (SDS)/TBS supplemented with protease inhibitor cocktail, 1 mM PMSF, and phosphatase inhibitor cocktail 2 and 3 (Sigma-Aldrich, Switzerland) and boiled for 10 min at 95°C. The bicinchoninic acid (BCA) protein assay was performed to quantify the protein concentration in the total, soluble, and insoluble fractions before addition of Laemmli buffer 4× (4% SDS, 40% glycerol, 0.05% bromophenol blue, 0.252 M Tris-HCl pH 6.8, and 5% β-mercaptoethanol). Proteins from the total, soluble, and the insoluble fractions were then separated on a 16% tricine gel, transferred onto a nitrocellulose membrane (Fisher Scientific, Switzerland) with a semi-dry system (Bio-Rad, Switzerland), and immunostained as previously described (2).

Preparation of α-syn seeds from PFF-treated primary hippocampal neurons

70 nM of mouse α-syn PFFs were added to hippocampal primary neurons at *DIV* 5-6. After 10 days of treatment, seeded neurons were lysed in 1% Triton X-100/ Tris-buffered saline (TBS) (50 mM Tris, 150 mM NaCl, pH 7.5) supplemented with protease inhibitor cocktail, 1 mM phenylmethane sulfonyl fluoride (PMSF), and phosphatase inhibitor cocktail 2 and 3 (Sigma-Aldrich, Switzerland) and sequential biochemical fractionation of cell extracts was performed as described previously (4). After sonication using a fine probe [(0.5-s pulse at an amplitude of 20%, ten times (Sonic Vibra Cell, Blanc Labo, Switzerland], cell lysates were incubated on ice for 30 min and centrifuge at 100,000 g for 30 min at 4°C. The supernatant (soluble fraction) was collected while the pellet was washed in 1% Triton X-100/TBS, sonicated as described above, and centrifuged for another 30 min at 100,000 g. The supernatant was discarded whereas the pellet (insoluble fraction) was washed twice with PBS, pH 7.4. The pellet was then sonicated in PBS, pH 7.4 using a fine probe [(0.5-s pulse at an amplitude of 20%, ten times (Sonic Vibra Cell, Blanc Labo, Switzerland]. The bicinchoninic acid (BCA) protein assay was performed to quantify the protein concentration in the soluble and insoluble fractions. 2 µg of the insoluble fraction was then added to hippocampal primary neurons at *DIV* 5-6 to induce seeding.

Proteomic identification of the proteins enriched in the insoluble fraction of the PFF-treated neurons

Primary hippocampal neurons were treated with PBS or PFFs for 7, 14, or 21 days. Cells were lysed at the indicated time-points into the soluble and insoluble fractions as described above. Proteins from the insoluble fraction were then separated by SDS-PAGE on a 16% polyacrylamide gel, which was then stained with Coomassie Safestain (Life Technologies, Switzerland). Each gel lane was entirely sliced, and proteins were in-gel digested as previously described (16). Peptides were desalted on stageTips (17) and dried

under a vacuum concentrator. For LC-MS/MS analysis, resuspended peptides were separated by reversed phase chromatography on a Dionex Ultimate 3000 RSLC nano UPLC system connected in-line with an Orbitrap Lumos (Thermo Fisher Scientific, Waltham, USA). Label-free quantification (LFQ) was performed using MaxQuant 1.6.0.1 (18) against the UniProt mouse database (UniProt release 2017_05). Perseus was used to highlight differentially quantified proteins (19). Reverse proteins, contaminants, and proteins only identified by sites were filtered out. Biological replicates were grouped together. Protein groups containing a minimum of two LFQ values in at least one group were conserved. Empty values were imputed with random numbers from a normal distribution (Width: 0.5 and Downshift: 1.7). Significant hits were determined by a volcano plot-based strategy, combining t-test p-values with ratio information (20). Significance curves in the volcano plot corresponding to a SO value of 0.4 (D7 and D21) or 0.5 (D14) and 0.05 FDR were determined by a permutation-based method. Further graphical displays were generated using a homemade program written in R (https://www.R-project.org/). The mass spectrometry proteomics data (Dataset 1) have been deposited to the ProteomeXchange Consortium via the PRIDE (21) partner repository with the dataset identifier PXD016850.

Quantification of cell death in primary hippocampal neurons

Primary hippocampal neurons were plated in a 96-well plate and treated with α-syn PFFs (70 nM or up to 500 nM). After 7, 14, and 21 days of treatment, cell death was quantified using complementary cell death assays.

Quantification of active caspase 3

The CaspaTag fluorescein caspase 3 activity kit (ImmunoChemistry Technologies, MN, USA) allows the detection of active effector caspase (caspase 3) in living cells. These kits use the specific fluorochrome peptide inhibitor (FAM-DEVD-fmk) of the caspase 3

(FLICA). This probe passively enters the cells and binds irreversibly to the active caspases. Neurons were washed twice with PBS and incubated for 30 min at 37°C with FAM-DEVD-FMK in accordance with the supplier's instructions. Fluorescein emission was quantified using a Tecan infinite M200 Pro plate reader (Tecan, Maennedorf, Switzerland) with excitation and emission wavelengths of 487 nm and 519 nm respectively.

Quantification of LDH release

Using a CytoTox 96® Non-Radioactive Cytotoxicity Assay (Promega, Switzerland), the lactic acid dehydrogenase (LDH) released into culture supernatants was measured following the manufacturer's instructions. After a 30 min coupled enzymatic reaction, which results in the conversion of a tetrazolium salt (INT) into a red formazan product, the amount of color formed, that is proportional to the number of damaged cells, was measured using a Tecan infinite M200 Pro plate reader (Tecan, Maennedorf, Switzerland) at a wavelength of 490 nm.

TUNEL assay and NeuN counting

DNA fragmentation was detected using the TUNEL method as described by Gavrieli et al. PFFs- or PBS- treated neurons were fixed at the indicated times in 4% PFA for 15 min at RT. Cells were permeabilized in a solution composed of 0.1% Triton X-100 in 0.1% citrate buffer, pH 6.0, and then washed in PBS buffer before incubation with terminal deoxynucleotide transferase (In Situ Cell Death Detection kit; Roche, Switzerland) for 1 h at 37 °C in a solution containing TMR red dUTP. The nucleus was counterstained with DAPI at 1/5000 (Sigma-Aldrich, Switzerland) by 15 min of incubation in PBS. For the hippocampal primary neurons, the neurons were also specifically stained for NeuN, a nuclear neuronal marker (see Immunocytochemistry section) and pS129. The cells were washed five times in PBS before mounting in polyvinyl alcohol (PVA) mounting medium with the anti-fading DABCO reagent (Sigma-Aldrich, Switzerland). The cells plated on CS were then examined with a microscope (Axioplan, Carl Zeiss Microscopy) with a 20 ×

objective and analyzed using ImageJ (US National Institutes of Health, Bethesda, MD, USA). A minimum of 350 cells were counting for each condition and for each independent experiment.

Quantitative real-time RT-PCR and transcriptomic analysis

Primary hippocampal neurons were treated with WT PFFs or PBS buffer for 7, 14, and 21 days. Total RNA was isolated using the RNeasy Mini Kit (Qiagen, Switzerland) according to the manufacturer's protocol. The concentration of each sample was measured using a NanoDrop (NanoDrop Technologies, Wilmington, DE, USA), and the purity was confirmed using the ratios at (260/280) nm and (260/230) nm.

Quantitative real-time RT-PCR

RNA (2 µg) was used to synthesize cDNA using the High-Capacity RNA-to-cDNA Kit (Life Technologies) following the manufacturer's instructions. To quantify α-syn mRNAs levels, we used the SYBR Green PCR master mix (Pack Power SYBR Green PCR mix, Life Technologies). Q-PCR was performed using the following primers synthesized by Microsynth (Balgach, Switzerland):

Gene	**Forward sequence (5'-3')**	**Reverse sequence (5'-3')**
SNCA	AATGTTGGAGGAGCAGTGGT	GGCATGTCTTCCAGGATTCC
β-actin	TTGTGATGGACTCCGGAGAC	TGATGTCACGCACGATTTCC
GAPDH	AACGACCCCTTCATTGACCT	TGGAAGATGGTGATGGGCTT

Forty cycles of amplification were then performed in an ABI Prism 7900 (Applied Biosystem, Foster City, USA) using a 384-well plate, which allowed the simultaneous analysis of the genes of interest and the housekeeping genes (β-actin and GAPDH) that serve as references for the normalization step. For each independent experiment,

triplicated wells were acquired per condition, and each experiment was reproduced at least three times independently. To quantify the expression level of the genes of interest in the different conditions tested, the comparative $2^{-\Delta\Delta CT}$ method was used where ΔΔCT = ΔCT(target gene)−ΔCT(reference gene) and ΔCT = CT(target gene)−CT(reference gene). Results were expressed as the fold change relative to control neurons ($2^{-\Delta\Delta CT}$). The geNorm method (RRID: SCR_006763, https://genorm.cmgg.be/) was performed to assess the most stable reference gene that should be used for the normalization of the gene expression(22).

Temporal transcriptomic analysis

Libraries for mRNA-seq were prepared according to manufacturer's instructions with the TruSeq stranded mRNA kit (Illumina) starting from 300 ng of good-quality total RNAs (RNA quality scores >8.9 on the TapeStation 4200). Libraries were subsequently loaded at 1.44 pM on two High Output flow cells (Illumina) and sequenced in a NextSeq 500 instrument (Illumina) according to manufacturer instructions, yielding 75 nt paired-end reads.

RNA-seq reads were aligned to the mm10 mouse reference genome (GRCm38.p5) with STAR (version 2.5) (23). An average of 52 million of uniquely mapped reads per sample was then assigned to genes (gencode primary assembly v16) using HTSeq-count (version 0.9) (24). The analysis was focused on protein-coding and antisense RNA genes, representing a total of 23,057 studied genes. Lowly expressed genes (CPM < 5) and genes present in less than three samples were excluded prior to further processing. Normalization and differential expression analysis of the remaining 11,767 genes were done with the R package DEseq2 (version 1.2) (25), **using the internal DEseq and the results methods**. Genes with an absolute log2 fold-change greater than 1 and an FDR less than 0.01 were considered as significantly differentially expressed. Dataset 2 contains the final results and has been deposited in the Gene

Expression Omnibus (GEO) database, https://www.ncbi.nlm.nih.gov/geo (accession no. GSE142416). Datasets 3 and 4 contain respectively analyses of mitochondrial and synaptic genes significantly enriched shown in Figure 5 C and D.

Respirometry on detached primary neurons

Primary hippocampal neurons were plated 4 weeks before respiration experiments. At 21, 14, or 7 days before respiration, neurons were exposed to 70 nM PFFs. Immediately before respiration experiments, cells were carefully washed with PBS, and exposed to 0.05% trypsin for 35–40 min, until detachment of cells was clearly visible, after which DMEM F12 medium was used to neutralize the trypsin. Cells were gently spun down (300 g for 3 min), and the cells of 1.5 wells of 6 well plates were resuspended in DMEM F12 and used for high-resolution respirometry. The cell suspension was transferred to MiR05 (0.5 mM EGTA, 3 mM $MgCl_2$, 60 mM potassium lactobionate, 20 mM taurine, 10 mM KH_2PO_4, 20 mM HEPES, 110 mM sucrose and 0.1% (w/v) BSA, pH 7.1) at a concentration of 2.5% cell suspension in MiR05 directly in a 2 ml oxygraphy chamber. Respiration was measured in parallel to mitochondrial ROS production (O_2^- and H_2O_2) at 37°C in the Oroboros O2k (calibrated for each experiment) equipped with the O2K Fluo-LED2 Module (Oroboros Instruments, Austria). To the best of our knowledge this is the first report on high resolution respirometry in parallel to amplex red fluometry using the Oroboros setup in primary neurons.

Mitochondrial ROS measurements were performed as described previously (26) using LEDs for green excitation in the presence of 10 µM Amplex Red, 1 U/ml horseradish peroxidase, and 5 U/ml superoxide dismutase in 2 ml MiR05 per O2K chamber. Calibration was performed by titrations of 5 µL of 40 µM H_2O_2.

Routine respiration and associated mitochondrial ROS production were assessed from unpermeabilized cells, after which plasma membranes were permeabilized by

application of an optimized (optimal accessibility of substrates to mitochondria while maintaining mitochondrial outer membranes intact) concentration of digitonin (5 µg/mL).

A substrate-uncoupler-inhibitor-titration (SUIT) protocol was applied to measure oxygen flux at different respirational states on permeabilized cells, as described previously (27, 28). Briefly, NADH-pathway (N) respiration in the LEAK and oxidative phosphorylation (OXPHOS) state was analyzed in the presence of malate (2 mM), pyruvate (10 mM) and glutamate (20 mM) before and after the addition of ADP (5 mM), respectively (N_L, N_P). Addition of succinate (10 mM) allowed assessment of NADH- and Succinate-linked respiration in OXPHOS (NS_P) and the uncoupled state (NS_E) after incremental (Δ0.5 µM) addition of carbonyl cyanide m-chlorophenyl hydrazine (CCCP). Inhibition of Complex I by rotenone (0.5 µM) yielded succinate-linked respiration in the uncoupled state (S_E). Tissue-mass specific oxygen fluxes were corrected for residual oxygen consumption, *Rox*, measured after additional inhibition of the mitochondrial electron transfer system, ETS, Complex III with antimycin A. For further normalization, fluxes of all respiratory states were divided by ETS-capacity to obtain flux control ratios, *FCR*.

Terminology was applied according to http://www.mitoglobal.org/index.php/Gnaiger_2019_MitoFit_Preprint_Arch

Mitochondrial ROS values were corrected for background fluorescence, and respirational states before the addition of uncoupler were used for analysis.

Measurement of the mitochondrial membrane potential and the mitochondrial mass in PFF-treated neurons

Primary hippocampal neurons were plated in a 96-well plate and treated with α-syn PFFs (70 nM). After 7, 14, and 21 days of treatment, mitochondrial membrane potential and mitochondrial mass were quantified using the TMRE (tetramethylrhodamine, ethyl ester)

assay kit (Abcam, UK) and Mitotracker Green tracer (Life Technologies, Switzerland) assays respectively.

TMRE assay

TMRE is a permeant dye that accumulates in the active mitochondria. TMRE was added to cells at a final concentration of 200 nM and incubated for 20 min 37°C. After a wash with PBS, TMRE staining was quantified using a Tecan infinite M200 Pro plate reader (Tecan, Maennedorf, Switzerland) with excitation and emission wavelengths of 549 nm and 575 nm respectively.

Mitotracker Green assay

Mitotracker Green was added to cells at a final concentration of 20 nM and incubated for 30 min at 37°C. After a wash with PBS, Mitotracker Green staining was quantified using a Tecan infinite M200 Pro plate reader (Tecan, Maennedorf, Switzerland) with excitation and emission wavelengths of 487 nm and 519 nm respectively.

Measurement of the synaptic area

Images were acquired on an LSM 700 microscope (Carl Zeiss Microscopy, Germany), with a 40× objective (N.A. = 1.30). The pixel size was set to 78 nm and a z-step of 400 nm; the pinhole was set at 1 µm (equivalent 1A.U, channel 2).

To automatically analyze the z-stack images, the image analysis was performed in Fiji (29), using a custom script developed by Romain Guiet (in ImageJ macro language). Briefly, the script binarizes the different channels of the image using thresholds and measures the area and perimeter.

The script binaries user selected channels of the image using a threshold, either a fixed value or a value defined by an automatic threshold method (https://imagej.net/Auto_Threshold) (user defined the appropriate threshold by visual inspection, c1 = DAPI, c2 = Synapsin I, c3 = MAP2, c4 = pS129). From these resulting

images, the script applies median filtering to remove noisy pixels and outputs the final masks (user defined the radius of the median filter for each channel, c1 = DAPI, c2 = Synapsin I, c3 = MAP2, c4 = pS129). Finally, the script measures the area, the perimeter, and multiplies the perimeter value by the z-step (to get an estimate of the surface). The generated masks are merged and saved as an output for visual validation of the thresholding.

Relative Quantification of WBs and Statistical Analysis

The level of total α-syn (15 kDa, 12 kDa, or HMW) or pS129-α-syn were estimated by measuring the WB band intensity using Image J software (U.S. National Institutes of Health, Maryland, USA; RRID:SCR_001935) and normalized to the relative protein levels of actin. All the experiments were independently repeated three times. The statistical analyses were performed using Student's *t*-test or ANOVA test followed by a Tukey-Kramer *post-hoc* test using KaleidaGraph (RRID:SCR_014980). The data were regarded as statistically significant at $p<0.05$.

Supplemental information – Figures and Legends

Figure S1. Related to Figures 1-8

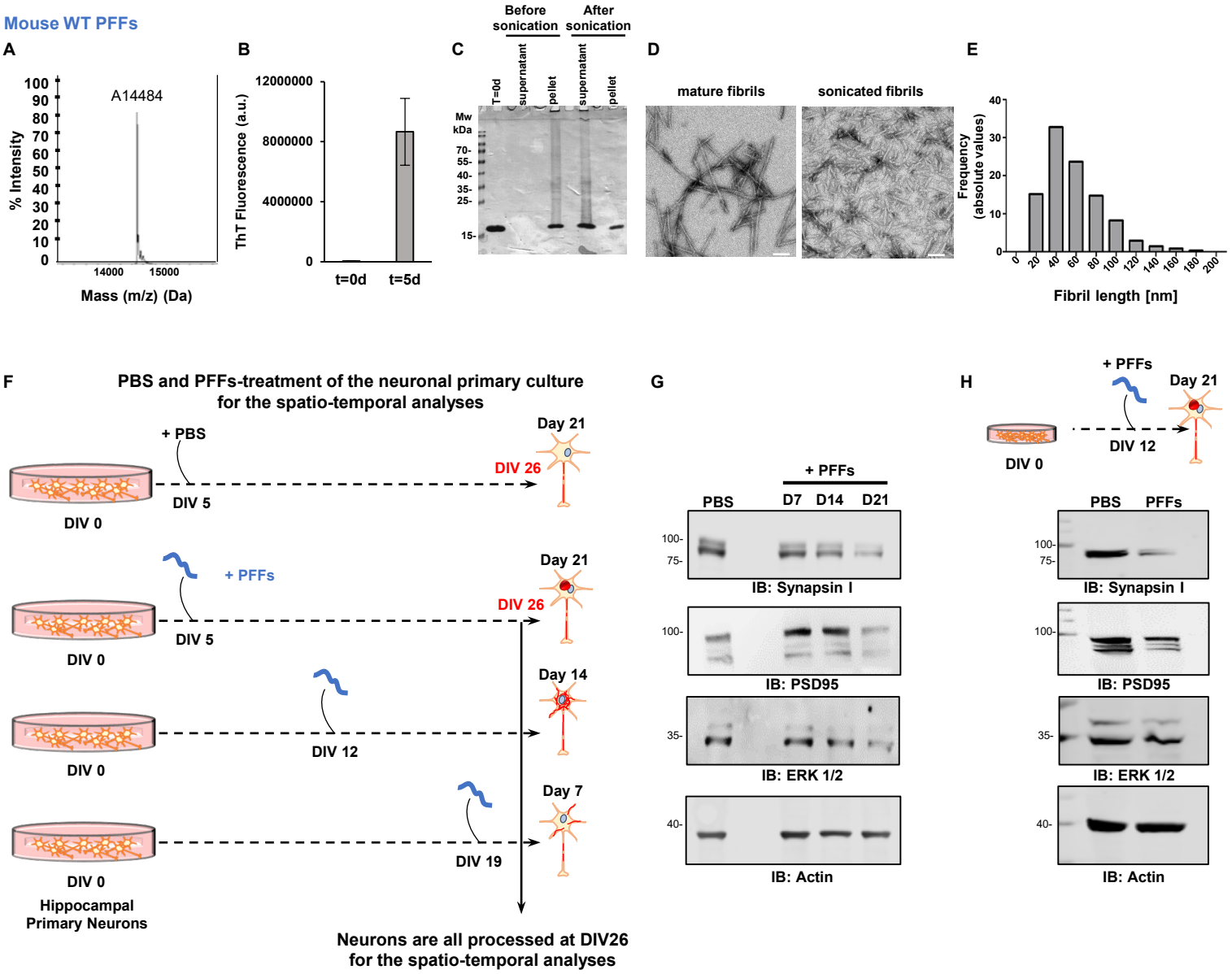

I

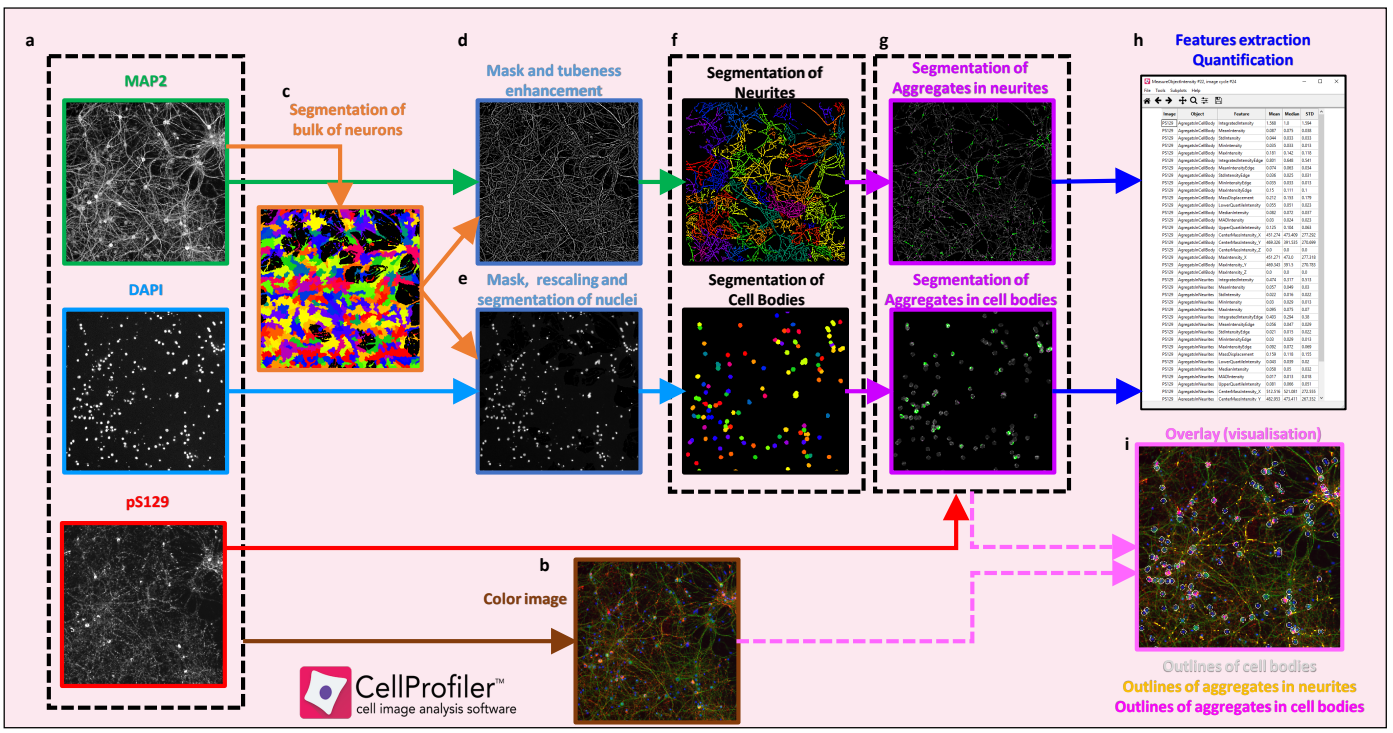

Fig. S1. Preparation and characterization of recombinant monomeric and PFFs α-syn species (related to Figures 1 to 8).

A. Purity and characterization of α-syn monomers.

Recombinant WT mouse α-syn was produced in *E. coli* and purified by anion exchange chromatography and size-exclusion chromatography, followed by a final chromatographic step using reverse-phase HPLC, as previously described (1). The purity of recombinant monomeric α-syn after purification was assessed by ESI-LC/MS, which showed the expected mass.

B-E. Purity and characterization of α-syn fibrils.

α-syn fibrils were formed by incubation of monomeric α-syn for 5 days at 37°C under constant agitation at 1000 rpm. (**B**). After sonication, fibril formation was assessed by ThT fluorometry. All data represent the average ± SD (n=3). (**C**). Purity of α-syn fibrils was verified by SDS-PAGE and Coomassie blue staining. After sonication, fibril preparations were centrifuged, and the presence of the fibrils was verified in the pellet fraction, while the absence of monomer release after the sonication step was assessed in the supernatant fraction or after filtration through a 100 kDa filter (filtration). (**D-E**). α-syn fibrils were characterized by transmission electron microscopy (TEM) imaging. (**D**) Representative images of negatively stained α-syn fibrils before and after sonication. All α-syn fibrils showed the characteristic rigid non-branched fibrillar morphology. Scale bars = 100 nm. (**E**) Average length of the fibrils after sonication.

F-H. Treatment of hippocampal primary neurons by α-syn PFFs seeds.

F. Schematic of experiments for the *time course* of the primary culture *treatment* with α-syn PFFs seeds. Morphological (8-10), physiological (11-13), gene expression (14) and proteome (15) changes are observed during the different developmental stages of primary neurons in culture (Days *In vitro*, DIV). Therefore, we adapted the time-course of the PFFs treatment in primary neurons to be able to analyze the spatio-temporal effects of the

seeding mechanism at the biochemical, proteomic, transcriptomic and ultrastructural level uncoupled to the intrinsic changes related to neuronal development and maturation. PFFs were added to the neuronal cell culture media at different DIV and PFFs-treated neurons were all harvested at the DIV 26. This ensures that the developmental stage of primary neurons in culture was similar at the harvest time.

G-H. To validate our method, we compare the level of synaptic markers at D21 when PFFs were added prior to synapse assembly in culture (DIV 5-6, as depicted in **F**) or after synapse formation has peaked (DIV 12). In both treatments, the synaptic markers decreased likewise compared to PBS-treated neurons.

I. Image analysis workflow. Images were analyzed using CellProfiler software. **a.** Raw images were acquired in green channel (MAP2 staining), blue channel (DAPI) and red channel (pS129 staining) for each well and each field of view. **b.** An RGB color image was produced and rescaled from individual grayscale images, MAP2 in green, DAPI in blue and pS129 in red, for visualization purpose. **c.** Bulk of neurons area was first identified based on MAP2 staining using otsu thresholding. **d.** MAP2 image was masked to exclude all non-neuronal areas, based on bulk neurons segmentation, and tubeness method was used to enhance neurites. **e.** DAPI image was rescaled and masked to exclude all non-neuronal areas, therefore excluding all glial cells from the analysis, and neuronal nuclei were segmented using minimum cross entropy thresholding. **f.** Neurites are then segmented on image **d** using minimum cross entropy thresholding and using a watershed algorithm with neuronal nuclei as seeds. Cell Bodies are identified as the perinuclear region by expanding by 3 pixels the previously identified neuronal nuclei. **g.** Image from pS129 staining is rescaled and used to segment individual α-syn aggregates in neurites and cell bodies using the segmentation from **f**. **h.** Features are then extracted and quantified from all identified objects: nuclei, neurons, neurites, cell bodies, aggregates in neurites, aggregates in cell bodies. Measurements were made on pS129 channel and

composed of counts, size, shape and intensity criteria. **i.** For control / visualization purpose, an overlay image was finally created and recorded, composed of the color image from **b** and the outlines of some segmented objects: cell bodies and α-syn aggregates in cell bodies and neurites.

Figure S2. Related to Figures 1 to 8

A

Primary Antibody	Catalog #	Company	Clone	RRID	Host	Concentration	WB dilution	ICC dilution	Epitope
anti-α-syn **total**	LASHUEL	-	LASH-EGT1-20	-	Rabbit	Not provided	1:1000	1:1000	**1-20**
anti-α-syn **total**	LASHUEL	-	LASH-BL-A15110B	-	Mouse	1.2 mg/ml	1:1000	1:500	**34-45**
anti-α-syn **total**	LASHUEL	-	LASH-BL-A15115A	-	Mouse	0.8 mg/ml	1:1000	1:500	**80-96**
anti-α-syn **total**	610787	BD	SYN-1	RRID:AB_398108	Mouse	0.25 mg/ml	1:1000	1:1000	**91-99**
anti-α-syn **total**	AB5336P	Millipore	-	RRID:AB_2192954	Sheep	1 mg/ml	1:500	1:500	**108-120**
anti-α-syn **total**	ab131508	Abcam	-	RRID:AB_11155736	Rabbit	1 mg/ml	1:500	1:500	**134-138**

B

Primary Antibody	Catalog #	Company	Clone	RRID	Host	Concentration	WB dilution	ICC dilution	Epitope
anti-**pS129**-α-syn	Ab168381	Abcam	MJF-R13	RRID:AB_2728613	Rabbit	4.229 mg/ml	1:3000	1:1000	Not provided
anti-**pS129**-α-syn	825701	BioLegend	P-syn/81A	RRID:AB_2564891	Mouse	1.0 mg/ml	1:1000	1:1000	AYEMPpSEEGYQ
anti-**pS129**-α-syn	GTX82738	GeneTex	-	AB_11176838	Rabbit	-	1:500	1:1000	Synthetic phospho-peptide corresponding to amino acid residues surrounding Ser129 conjugated to KLH

C

Primary Antibody	Catalog #	Company	Clone	RRID	Host	Concentration	WB dilution	ICC dilution	Epitope
anti-**actin**	ab6276	Abcam	AC-15	RRID:AB_2223210	Mouse	2.2 mg/ml	1:5000	Not tested	DDDIAALVIDNGSGK
anti-**MAP2**	ab92434	Abcam	-	RRID:AB_2138147	Chicken	Not provided	Not tested	1:2000	Recombinant full length protein
anti-**p62**	H00008878	Abnova	2C11	RRID:AB_437085	Mouse	1 mg/ml	1:1000	1:500	Raised against a full length recombinant SQSTM1
anti-**LC3**	ab48394	Abcam	-	-	Rabbit	1 mg/ml	1:500	1:500	A synthetic peptide made to an Nterminal portion of the human LC3 protein sequence (between residues 1-100)
anti-**ubiquitin**	Sc-8017	Santa-Cruz	P4D1	RRID:AB_628423	Mouse	0.2 mg/ml	1:500	1:500	1-76
anti-**OXPHOS**	ab110413	Abcam	-	-	Mouse	1.5 mg/ml	1:1000	-	Cocktail of high quality antibodies for analyzing relative levels of OXPHOS complexes
anti-**Tom 20**	sc-17764	Santa-Cruz	F-10	RRID:AB_628381	Mouse	0.2 mg/ml	1:500	1:200	Raised against amino acids 1-145
anti-**Tim 23**	sc-514463	Santa-Cruz	H-8	-	Mouse	0.2 mg/ml	1:500	1:200	Raised against amino acids 31-209
anti-**VDAC1**	ab14734	Abcam	20B12AF2	-	Mouse	1 mg/ml	1:500	1:200	Recombinant full length protein corresponding to Human VDAC1/ Porin.
anti-**OPA1**	612606	BD biosciences	18/OPA1	RRID:AB_399888	Mouse	0.25 mg/ml	1:1000	-	Raised against amino acids 708-830
anti-**Citrate Synthase**	ab96600	Abcam	-	-	Rabbit	1.03 mg/ml	1:1000	-	Recombinant fragment within Human Citrate synthetase aa 44-316
anti-**Mitofusin 2**	ab50843	Abcam	-	-	Rabbit	1.1 mg/ml	1:1000	-	Synthetic peptide corresponding to Human Mitofusin 2 aa 557-576
anti-**Synapsin I**	ab64581	Abcam	-	-	Rabbit	1 mg/ml	1:1000	1:500	Synthetic peptide corresponding to Rat Synapsin I aa 600-700
anti-**PSD95**	MAB N68	Millipore	K28/43	-	Mouse	1 mg/ml	1:1000	1:500	Recombinant protein corresponding to human PSD95
anti-**Synaptophysin**	ab8049	Abcam	SY38	-	Mouse	1 mg/ml	1:1000	1:500	Not provided
anti-**ERK**	4696	Cell signalling	L34F12	-	Mouse	-	1:1000	-	Synthetic peptide corresponding to the sequence of p42 MAP Kinase
anti-**p-ERK**	9101	Cell signalling	-	-	Rabbit	-	1:1000	-	Synthetic phosphopeptide corresponding to residues surrounding Thr202/Tyr204 of human p44 MAP kinase
anti-**LAMP1**	ab62562	Abcam	-	RRID:AB_2134489	Rabbit		-	1:500	A 15 amino acid peptide from near the centre of human LAMP1
anti-**BIP/Grp78**	ab21685	Abcam	-	RRID:AB_2119834	Rabbit	1 mg/ml	1:1000	1:500	
anti-**NeuN**	ab177487	Abcam	EPR12763	RRID:AB_2532109	Rabbit	1 mg/ml	-	1:500	Synthetic peptide within Human NeuN aa 1-100
anti-**VAMP2**	ab181869	Abcam	EPR12790	RRID:AB_2721005	Rabbit	1 mg/ml	-	1:500	Synthetic peptide within Human VAMP2 aa 1-100
anti-**SNAP25**	ab5666	Abcam	-	RRID:AB_305033	Rabbit	1 mg/ml	-	1:500	Synthetic peptide corresponding to Mouse SNAP25 aa 195-206
anti-**NSE**	MMS-518P	BioLegend	-	RRID:AB_291449	Mouse	1 mg/ml	1:1000	-	synthetic peptide corresponding to amino acids 416-433
anti-**β-Tubulin III**	ab18207	Abcam	-	RRID:AB_444319	Rabbit	1 mg/ml	1:1000	-	-
anti-**Tau**	MABN827	Millipore	T49	-	Mouse	1 mg/ml	-	1:500	-

D

Secondary Antibody	Catalog #	Company	RRID	Concentration	WB dilution	ICC dilution
Goat anti-**mouse Alexa Fluor 680**	A21058	Invitrogen	RRID:AB_2535724	2 mg/ml	1:5000	-
Goat anti-**rabbit Alexa Fluor 680**	A21109	Invitrogen	RRID:AB_2535758	2 mg/ml	1:5000	-
Goat anti-**mouse Alexa Fluor 800**	926-32210	Li-Cor	RRID:AB_621842	1 mg/ml	1:5000	-
Goat anti-**rabbit Alexa Fluor 800**	926-32211	Li-Cor	RRID:AB_621843	1 mg/ml	1:5000	-
Goat anti-**mouse Alexa Fluor 647 + nanogold particles**	7502	Nanoprobes	-		-	1:800
Donkey anti-**mouse Alexa Fluor 568**	A10037	Invitrogen	RRID:AB_2534013	2 mg/ml	-	1:800
Donkey anti-**rabbit Alexa Fluor 568**	A10042	Invitrogen	RRID:AB_2534017	2 mg/ml	-	1:800
Donkey anti-**rabbit Alexa Fluor 647**	A31573	Invitrogen	RRID:AB_2536183	2 mg/ml	-	1:800
Donkey anti-**mouse Alexa Fluor 647**	A31571	Invitrogen	RRID:AB_162542	2 mg/ml	-	1:800
Donkey anti-**Sheep Alexa Fluor 647**	A21448	Invitrogen	RRID:AB_1500712	2 mg/ml	-	1:800
Donkey anti-**chicken Alexa Fluor 405**	703-475-155	Jackson Immunoresearch	RRID:AB_2340373	1 mg/ml	-	1:400
Donkey anti-**chicken Alexa Fluor 488**	703-545-155	Jackson Immunoresearch	RRID:AB_2340375	1 mg/ml	-	1:400
Goat anti-**chicken Alexa Fluor 568**	A11041	Invitrogen	RRID:AB_2534098	2 mg/ml	-	1:500
Donkey anti-**chicken Alexa Fluor 647**	703-605-155	Jackson Immunoresearch	RRID:AB_2340379	1 mg/ml	-	1:500

E

Dyes	Catalog #	Company	RRID	Concentration	WB dilution	ICC dilution
Amytracker**680**	Amytracker™680	Ebba Biotech	-		-	1:500
Mitotracker **Green FM**	M7514	Invitrogen	-	1 mg/ml	-	20 nM
Neutral lipid **Lipidox Red**	H34476	Invitrogen	-		-	1:500
Ceramide **BODIPY TR**	B34400	Invitrogen	-		-	1:500
Phospholipid **Lipidox Red**	H34158	Invitrogen	-		-	1:500
Cholesteryl **BODIPY 524/563**	C12680	Invitrogen	-		-	1:500
C12-Sphingomyelin **BODIPY FL**	D7711	Invitrogen	-		-	1:500
Methyl Ester **BODIPY FL**	C34556	Invitrogen	-		-	1:500

Fig. S2. List of the antibodies used in this study (related to Figures 1 to 8).

A. Antibodies used for the detection of total α-syn.

B. Antibodies used for the detection of α-syn phosphorylated on S129 residue.

C. Other antibodies used in the study.

D. Secondary antibodies or dyes used for immunoblotting or confocal imaging.

Figure S3. Related to Figure 1

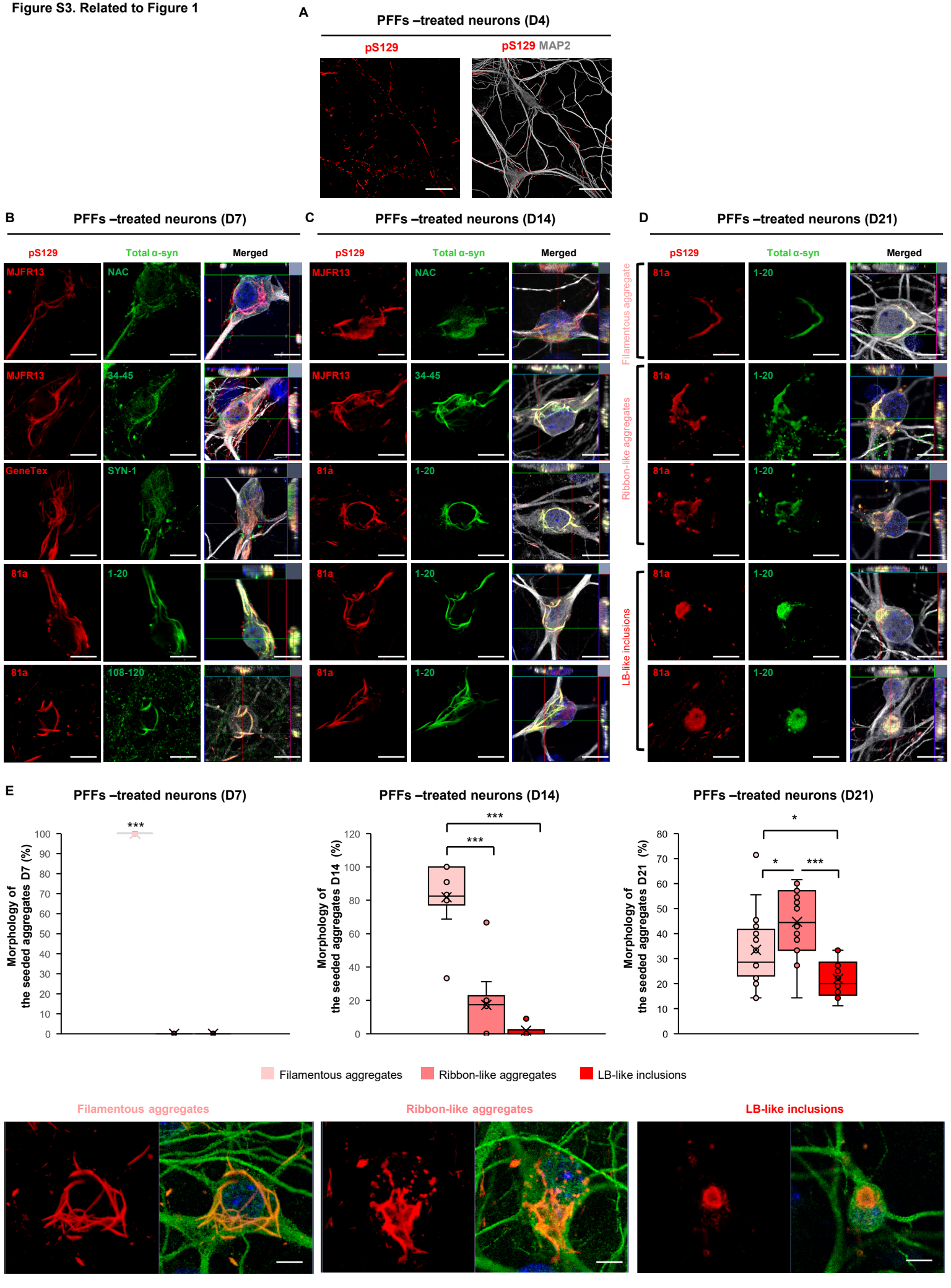

Figure S3. Related to Figure 1

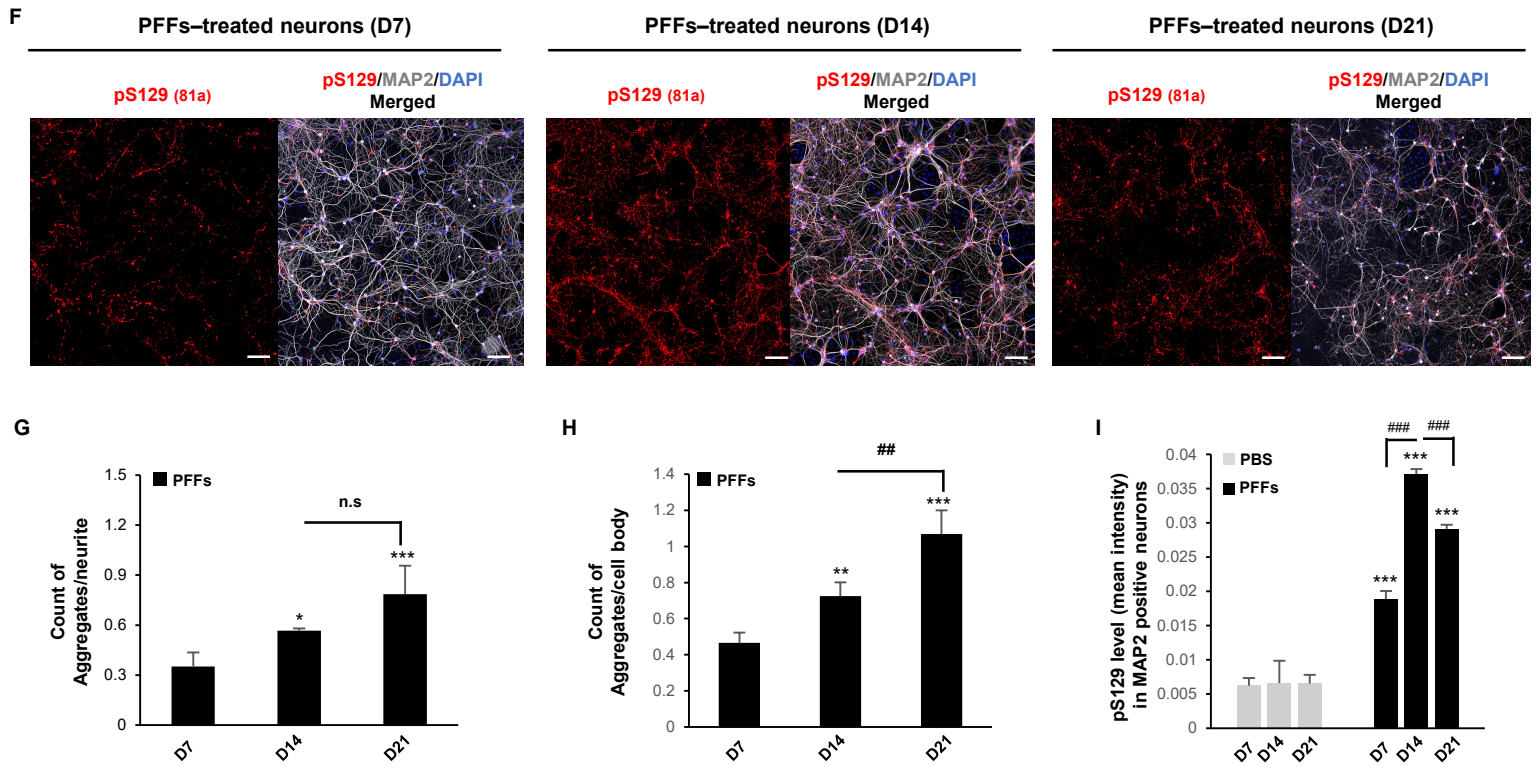

Figure S3. Related to Figure 2

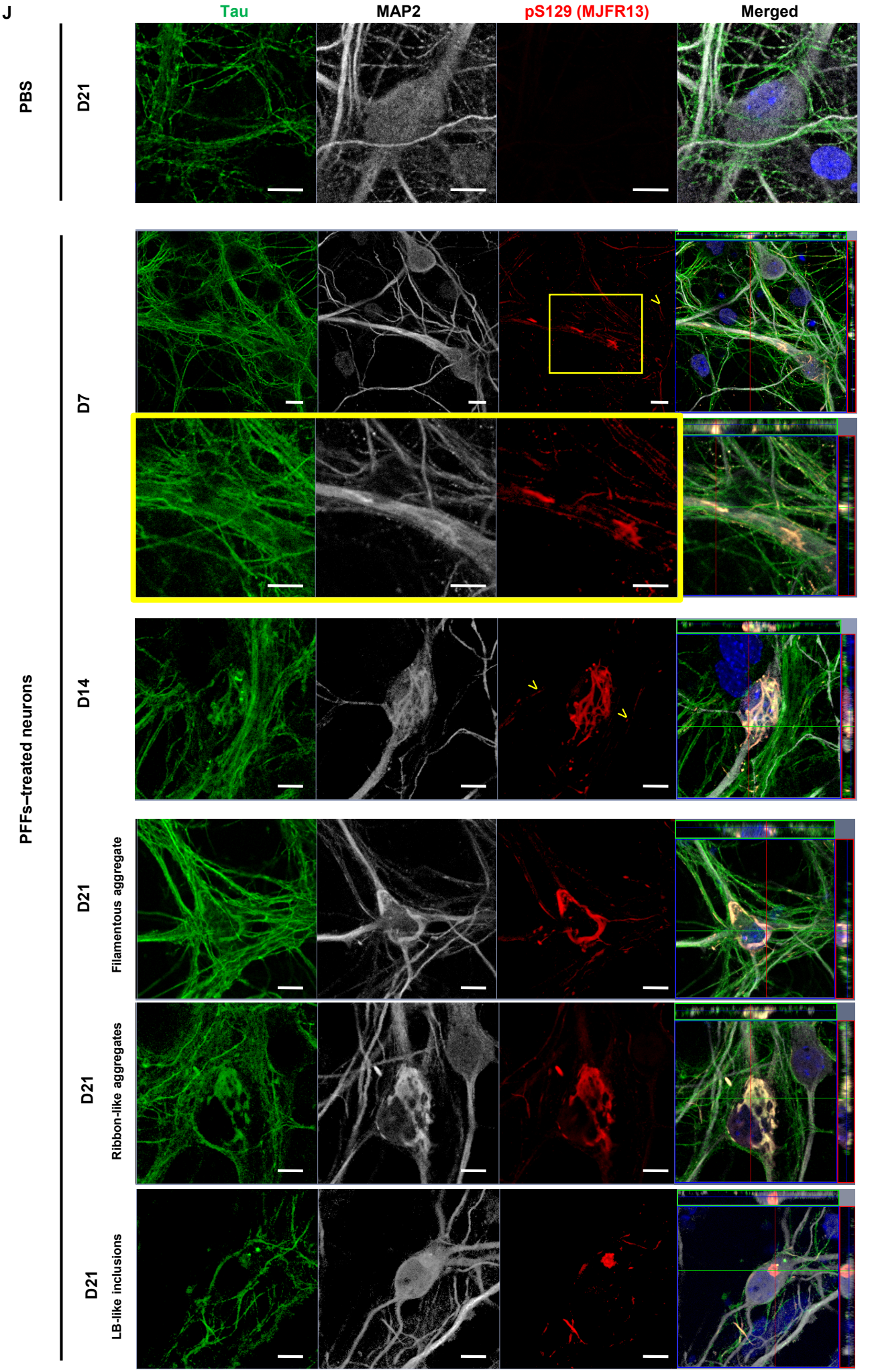

Figure S3. Related to Figure 1

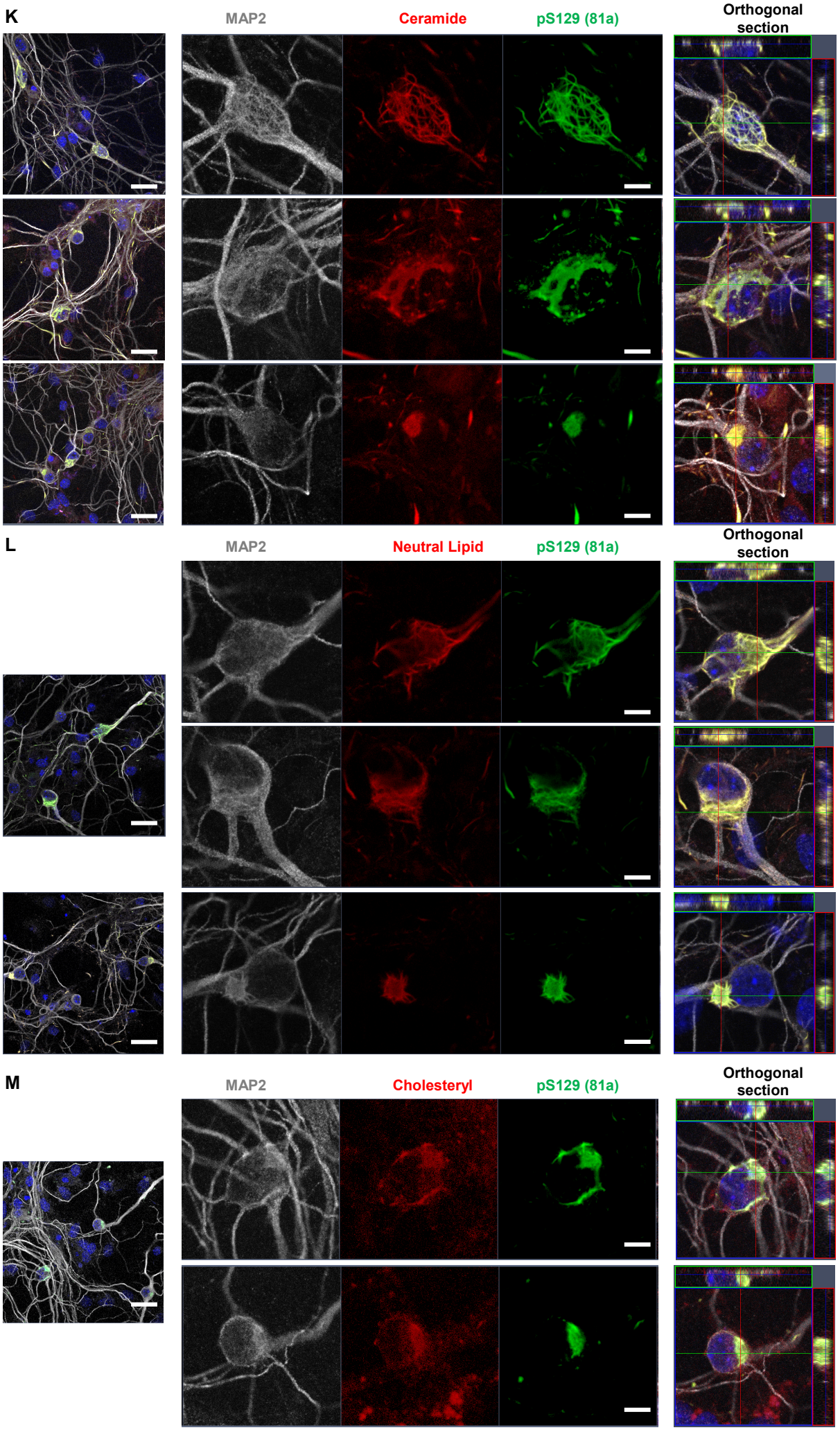

Figure S3. Related to Figure 1

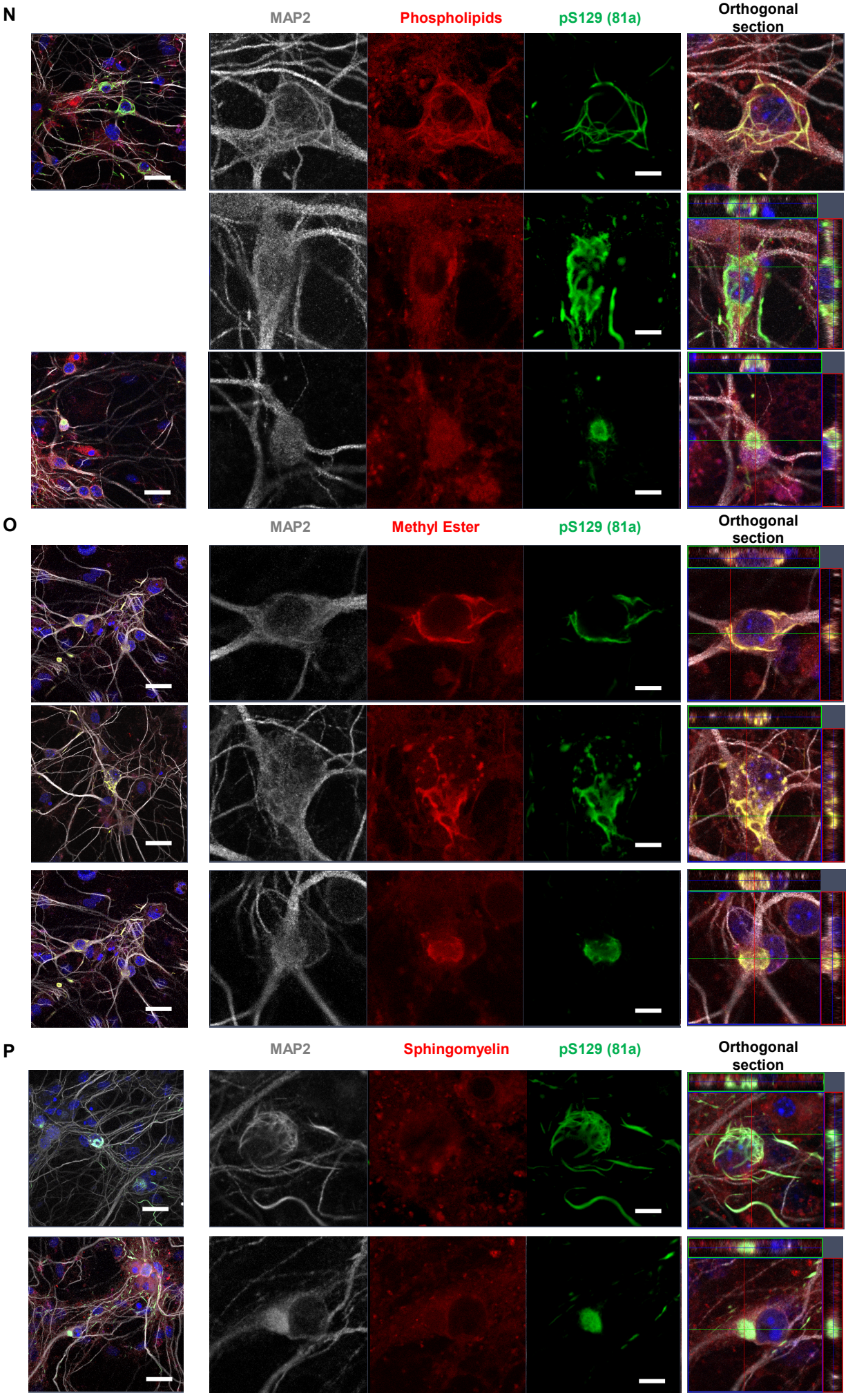

Fig. S3. Morphological and spatial distribution changes of α-syn seeded aggregates formed in PFFs-treated neurons over time (related to Figure 1).

A. 70 nM of mouse sonicated PFFs were added to neurons at DIV 5 (days *in vitro*). α-syn aggregates appear first in the neuronal extension after 4 days of PFFs-treatment. Aggregates were detected by ICC using pS129 (MJFR13). Neurons were counterstained with microtubule-associated protein (MAP2) antibody, and the nucleus was counterstained with DAPI staining. Scale bars = 10 μm.

B-D. Temporal analysis of α-syn aggregates formed at D7 (**B**), at D14 (**C**) and at D21(**D**) in WT neurons after addition of α-syn PFFs. Aggregates were detected by ICC using pS129 (MJFR13, 81a or GenTex antibodies) in combination with total α-syn (epitopes: 1-20 or 34-45 or NAC/ or 108-120) antibodies. Neurons were counterstained with microtubule-associated protein (MAP2) antibody, and the nucleus was counterstained with DAPI staining. Scale bars = 10 μm.

E. Quantification of the different types of morphologies observed by ICC (**B-D**) for α-syn seeded aggregates in PFFs-treated neurons at D7, D14 and D21. Representative images of the filamentous-, ribbon- and LB-like inclusions are depicted in the bottom panel, scale bar = 10 μm. Our classification of the seeded-aggregates is based on their morphology imaged by confocal microscopy as follows: 1) filamentous inclusion when several bundles of fibrils are observed in the neurites and/or in the neuronal cell bodies; 2) ribbon-like inclusion corresponds to intermediate aggregates in which filamentous α-syn is not detectable anymore but has not yet evolved in a round inclusion; 3) LB-like inclusion when α-syn newly formed fibrils are all packed in a round inclusion

A minimum of 300 α-syn seeded aggregates were measured in three independent experiments. $p<0.01$=*, $p<0.0001$=*** (ANOVA followed by Tukey HSD post-hoc test, filamentous vs ribbon-like vs round LB-like inclusions).

F-I. Spatial distribution of the α-syn seeded aggregates formed in PFFs-treated neurons over time was assessed by high content imaging analysis (HCA) that allows the total count of α-syn seeded aggregates (**F**) in neurites (**G**) or in cell bodies (**H**). **I**. Total level of pS129 in MAP2 positive neurons (dendrites + cell bodies).

For each independent experiment, duplicated wells were acquired per condition, and nine fields of view were imaged for each well. Images were then analysed using CellProfiler software to identify and quantify the number of α-syn seeded aggregates in neuronal cell bodies (DAPI and MAP2-positive cells) or in dendrites (MAP2-positive).

The graphs (**G-I**) represent the mean +/- SD of three independent experiments. $p<0.01$=*, $p<0.01$=**, $p<0.0001$=*** (ANOVA followed by Tukey HSD post-hoc test, PBS vs PFFs-treated neurons). $p<0.001$= ##, $p<0.001$= ### (ANOVA followed by Tukey HSD post-hoc test, PFFs-treated neurons D14 vs D21).

J. Confocal images put in evidence that although present in the axons at D7 and D14 (Tau positive/MAP2-negative neurites; α-syn-seeded aggregates are indicated by the yellow arrows), the majority of the seeded aggregates were detected in the dendrites (MAP2-positive neurites) at all the time-points. In addition, our analysis demonstrated that Tau protein was recruited inside α-syn-seeded aggregates at D7, D14 and D21. Nucleus was counterstained with DAPI.

K-P. Colocalization of lipids with pS129-positive inclusions at D21. Ceramide (**K**), neutral lipid (**L**), cholesteryl (**M**), phospholipids (**N**), methyl ester (**O**) and sphingomyelin (**P**) were stained using specific fluorescent probes (Figure S2E). pS129-positive aggregates were stained with MJFR13 antibody. Neurons were counterstained with microtubule-associated protein (MAP2) antibody, and the nucleus was counterstained with DAPI staining. Scale bars = 10 μm

Figure S4. Related to Figure 1

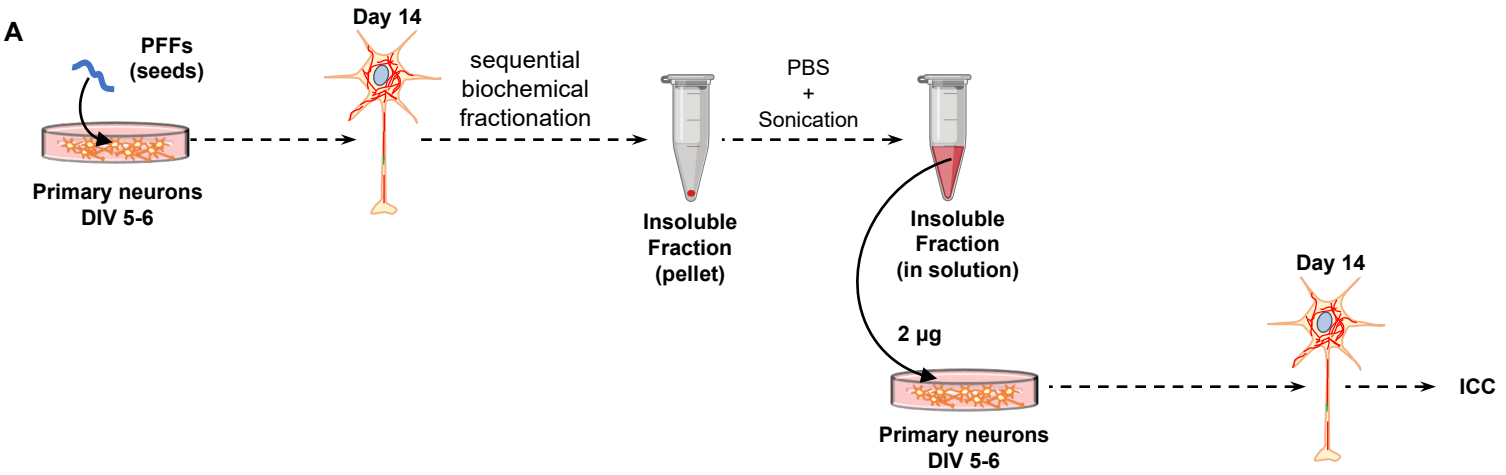

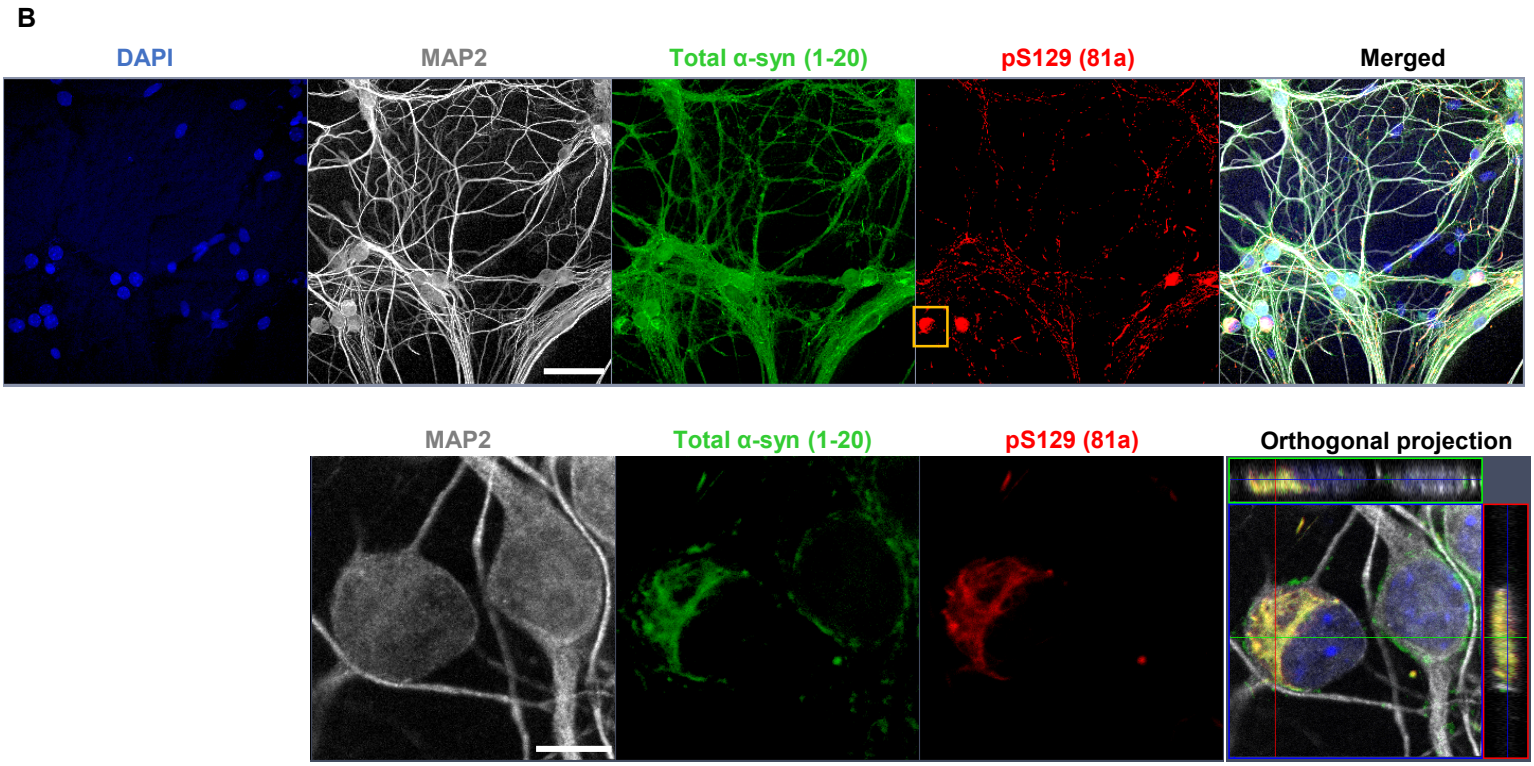

Fig. S4. α-syn seeds prepared from PFF-seeded primary neurons have high seeding activity (related to Figure 1).

A. 70 nM of mouse α-syn PFFs were added to hippocampal primary neurons at *DIV* 5-6. After 14 days of treatment, seeded neurons were lysed and sequential biochemical fractionation of cell extracts was performed. The pellet corresponding to the insoluble fraction was resuspended in PBS and dispersed by sonication. 2 µg of this fraction was then added to naïve hippocampal primary neurons at *DIV* 5-6 for 14 days.

B. Newly formed fibrils were detected by ICC using pS129 (81a antibody) in combination with total α-syn (epitope: 1-20) antibody. Neurons were counterstained with microtubule-associated protein (MAP2) antibody, and the nucleus was counterstained with DAPI staining. Neurons highlighted in yellow in the top panel was observed at higher magnification (bottom panel). Top panel, scale bar = 40 µm. Bottom panel, scale bar = 10 µm.

Figure S5. Related to Figure 2

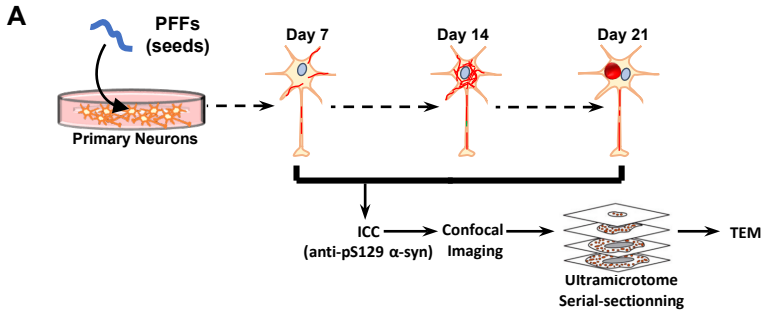

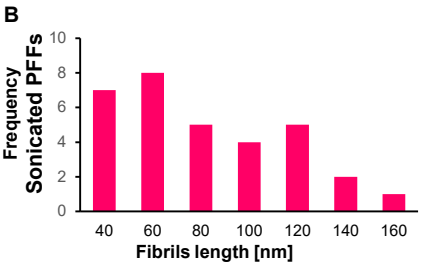

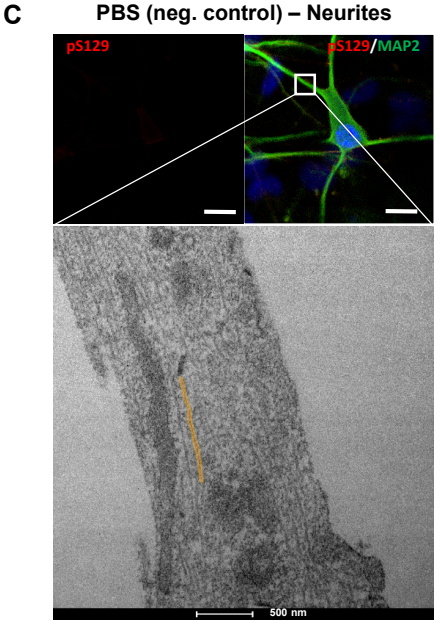

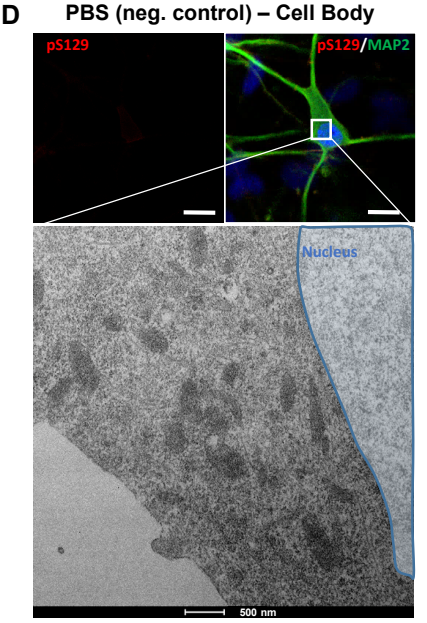

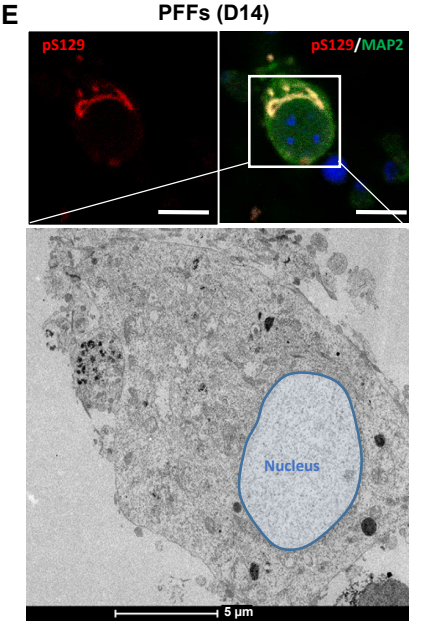

Figure S5. Related to Figure 2

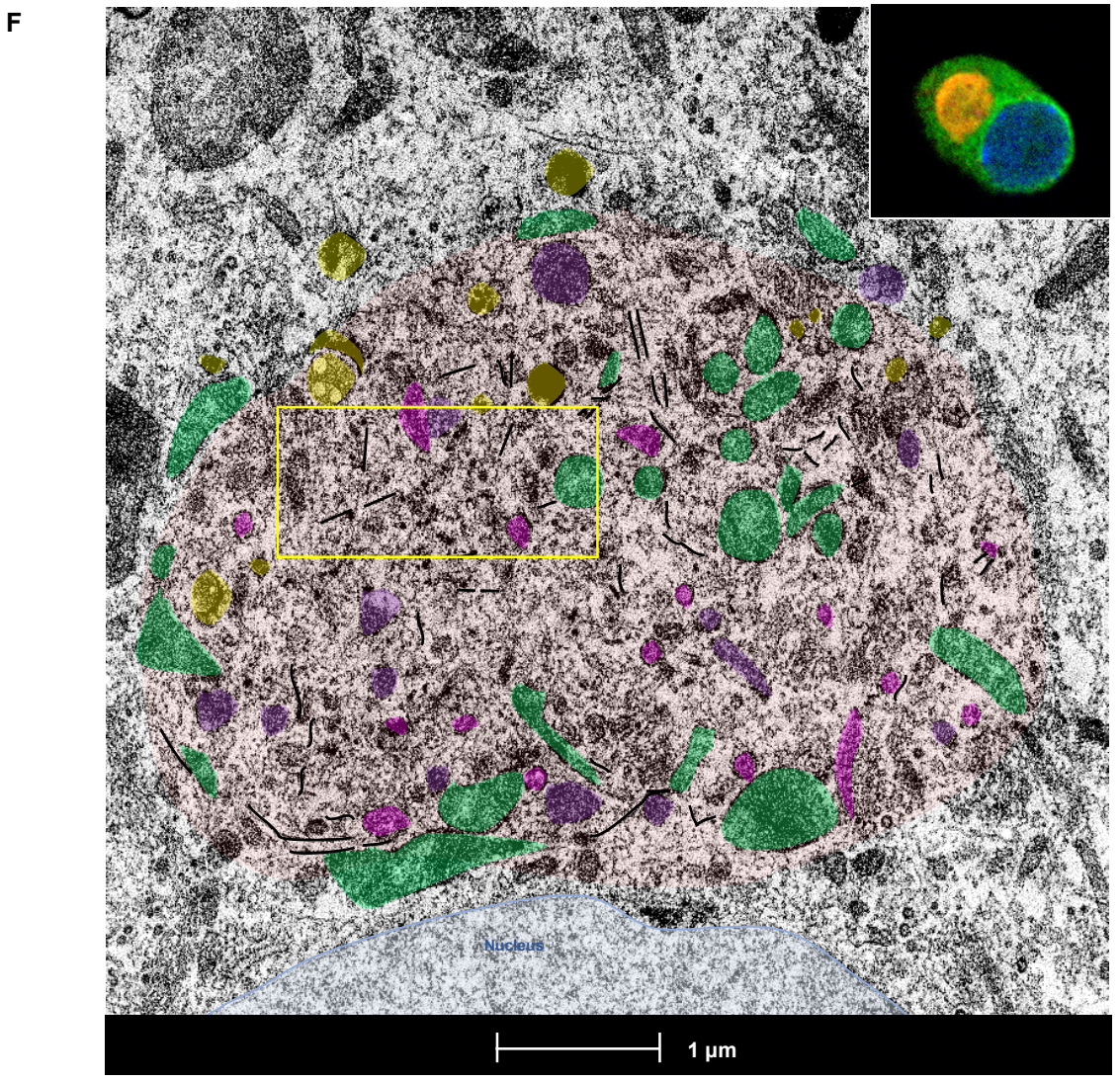

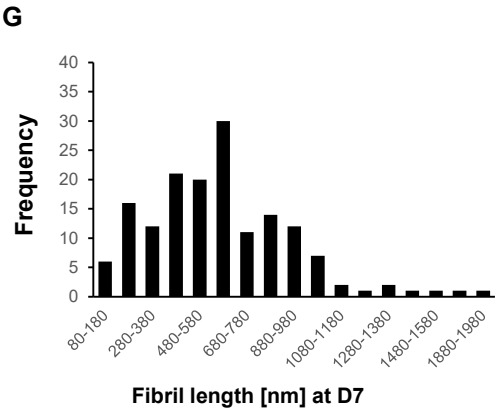

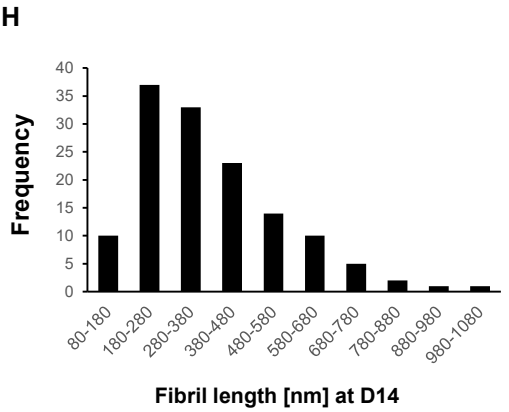

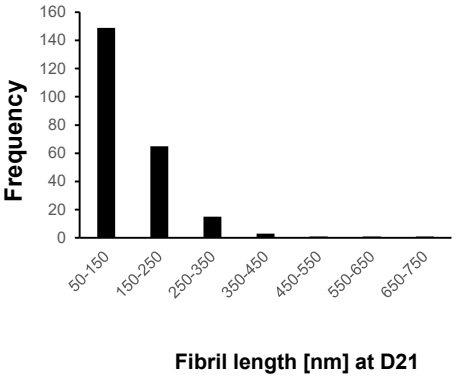

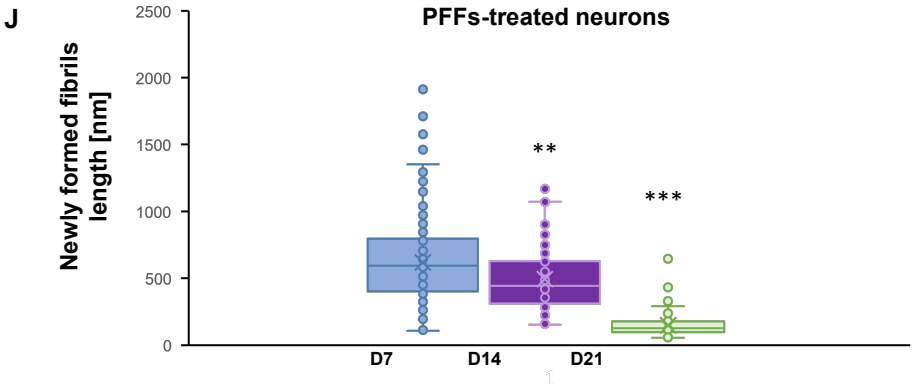

Fig. S5. Temporal profiling of the LB-like inclusions formation by correlative light electron microscopy (related to Figure 2).

A. PFFs were added for 7, 14, and 21 days to the extracellular media of hippocampal neurons plated on dishes with alpha-numerical searching grids imprinted on the bottom, allowing an easy localization of the cells. Neurons were fixed at the indicated time and imaged by confocal microscopy (**C-E**, top images, scale bars = 10 µm). The selected neurons were embedded and cut by an ultramicrotome. Serial sections were examined by TEM. **B.** Graph representing the mean +/- SD of the width of the microtubules compared to the newly formed fibrils at D7 (a minimum of 120 microtubules or newly formed fibrils were counted). Measurements confirmed that the width of newly formed α-syn fibrils of 11.94±3.97 nm (SD) is significantly smaller than the average width of the microtubules of 18.67±2.94 nm (SD). $p<0.001$=*** (student t-test for unpaired data with equal variance), indicating that this parameter can be used to discriminate the newly formed fibrils from the cytoskeletal proteins. **C-E**. Representative confocal images (top images) and EM micrographs (bottom images) of the control neurons treated with PBS buffer for 7 days (**C-D**) or neurons treated with PFFs for 14 days (**E**). Microtubule is highlighted in orange (**C**), and nucleus is highlighted in blue. **E.** CLEM imaging confirmed that PFFs did not accumulate on the outer side of the plasma membrane when used at a nanomolar concentration, as previously shown when higher concentrations were applied to the neurons (2). **G.** Colored EM images of α-syn inclusions formed at D21 shown in Figure 2F. Autophagolysosomal-like vesicles are colored in yellow, mitochondrial compartments in green and endomembranous compartments are colored in pink (endosomes-like vesicles) and purple (lysosomes-like vesicles). Nuclei are highlighted in blue. **H-K.** The length of newly formed fibrils was measured over time. A minimum of 160 fibrils were counted for each condition. **C-D.** Scale bar = 500 nm. **E**. Scale bar = 5 µm. **F**. Scale bar = 10 µm. **G.** Scale bar = 1 µm

Figure S6. Related to Figure 3

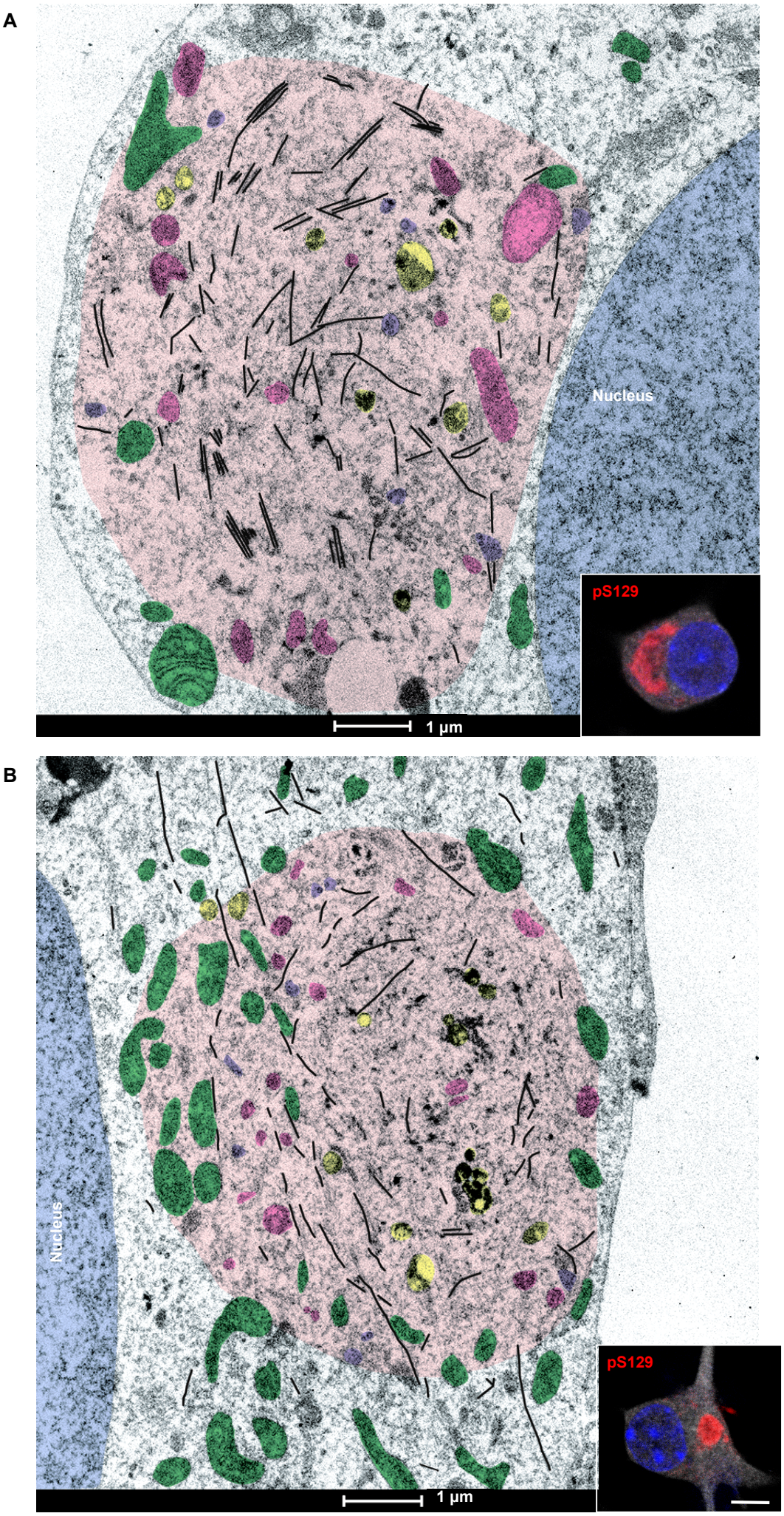

Figure S6. Related to Figure 3

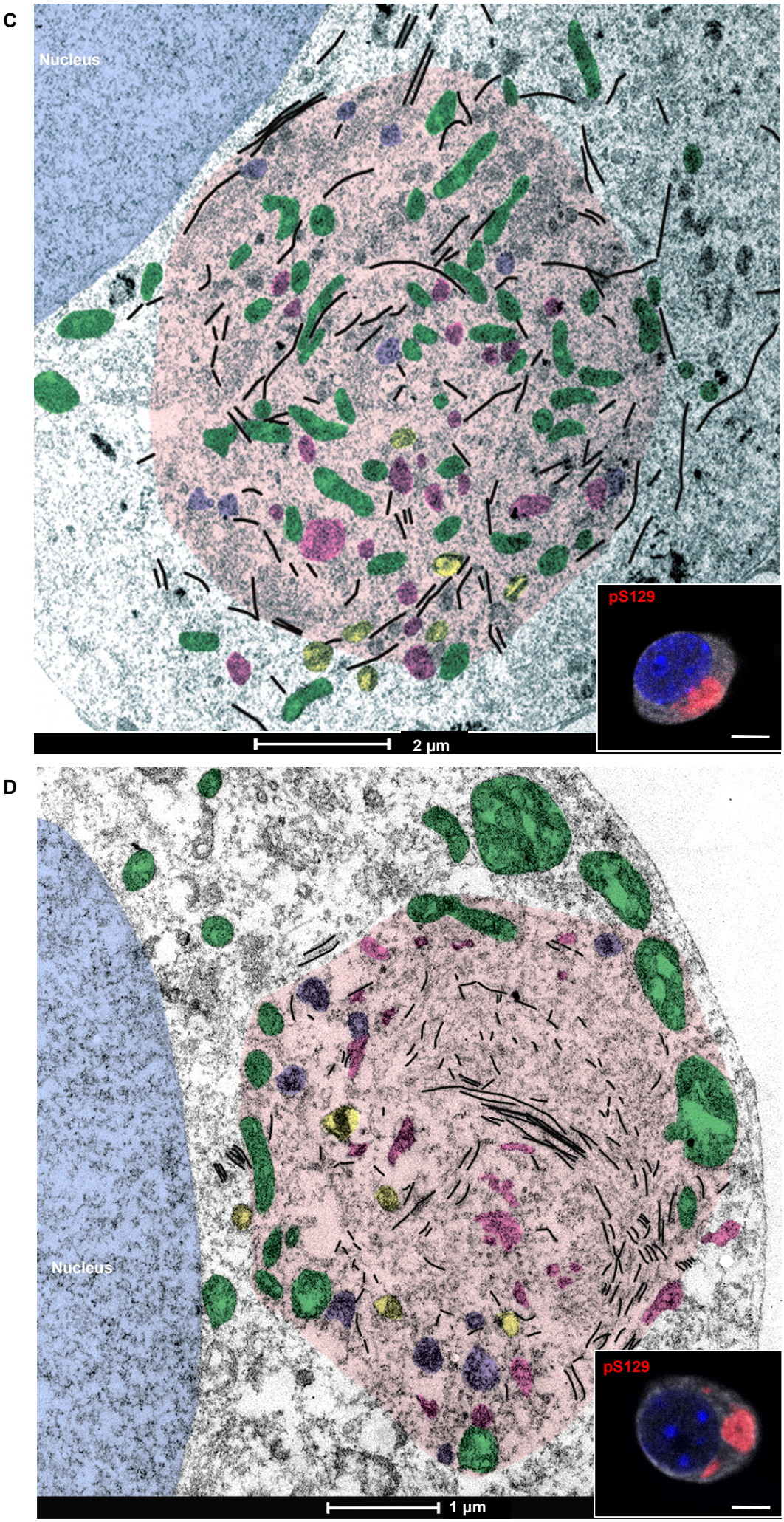

Figure S6. Related to Figure 3

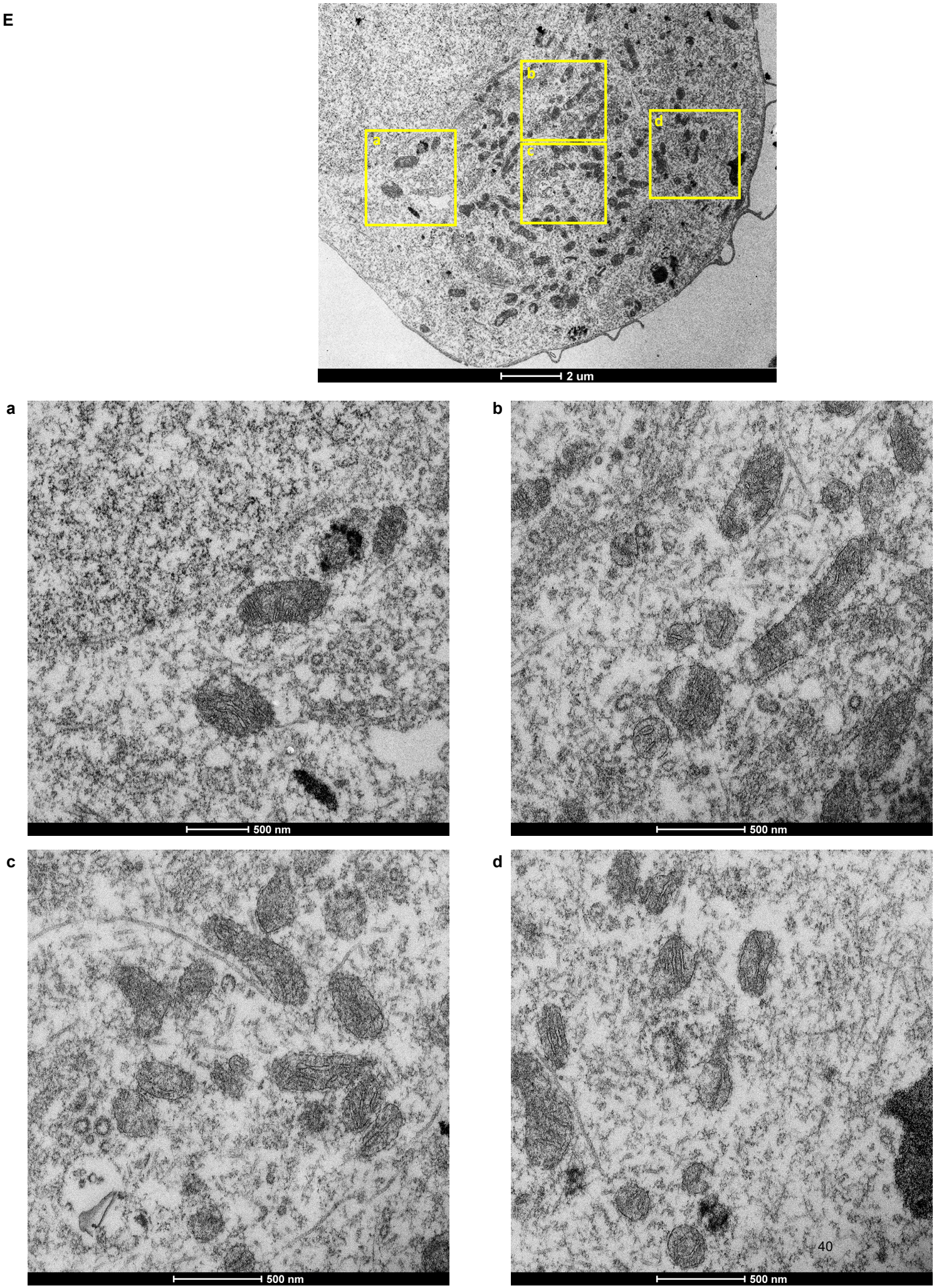

Figure S6. Related to Figure 3

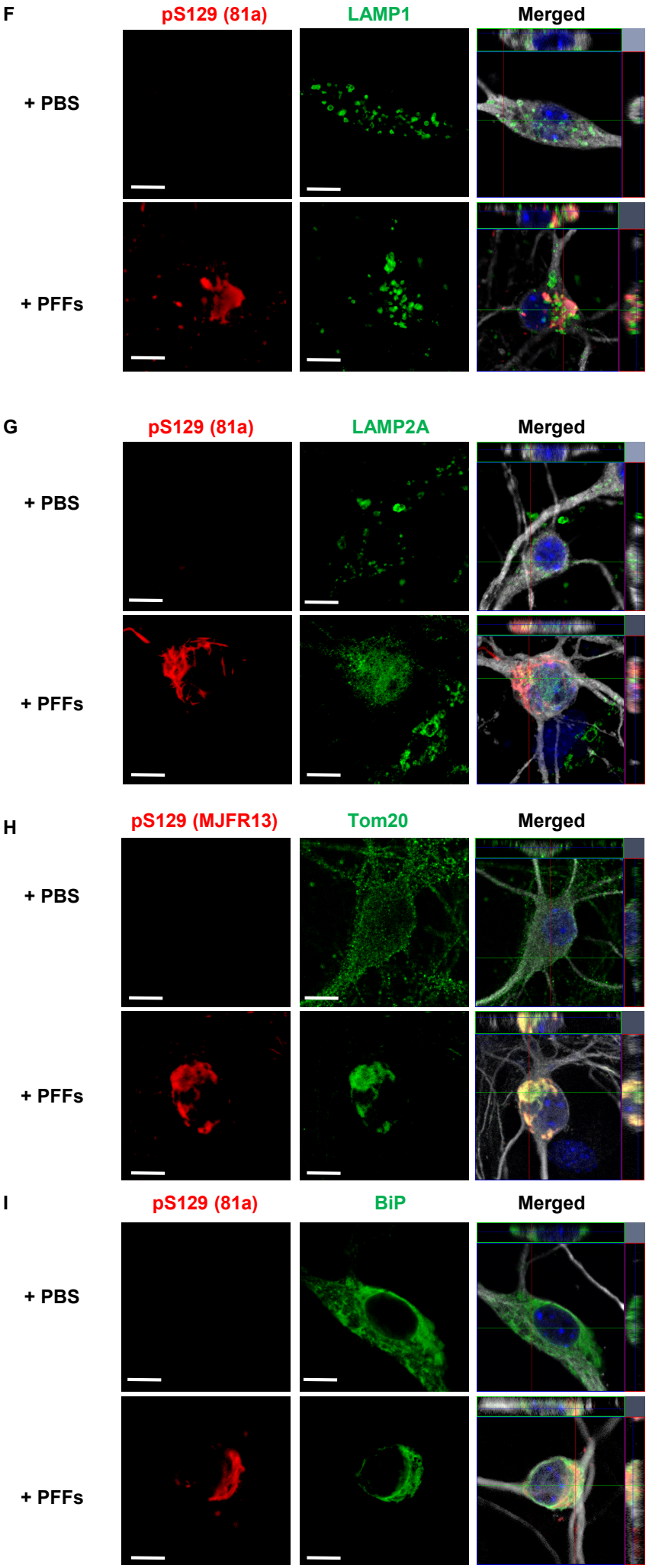

Fig. S6. LB-like inclusions imaged by correlative light electron microscopy at D21 (related to Figure 3).

A-D. Colored EM images of α-syn inclusions formed at D21 shown in Figure 3A-D. α-syn newly formed fibrils are highlighted in black. Autophagolysosomal-like vesicles are indicated by a yellow asterisk (**D**) or colored in yellow (**F**), mitochondrial compartments by a green asterisk (**D**) or colored in green (**F**). Accumulation of endomembranous compartment at a late stage (D21) are colored in pink (endosomes-like vesicles) and purple (lysosomes-like vesicles). Nuclei are highlighted in blue.

A-B, D. Scale bars = 1 µm. **C**. Scale bar = 2 µm.

E. Different fields of view (indicated by a yellow rectangle) of the organelles sequestered into the LB-like inclusion at D21 were imaged by EM at higher magnification (**a-d,** Scale bar = 500 µm).

F-I. LB-like inclusions were detected by ICC using pS129 in combination with LAMP1 (**F**), LAMP2A (**G**), Tom20 (**H**), or BiP (**I**) antibodies. PBS- (top panel) or PFFs- (bottom panel) treated neurons were counterstained with MAP2 antibody and nucleus with DAPI.

Figure S7. Related to Figures 1-3

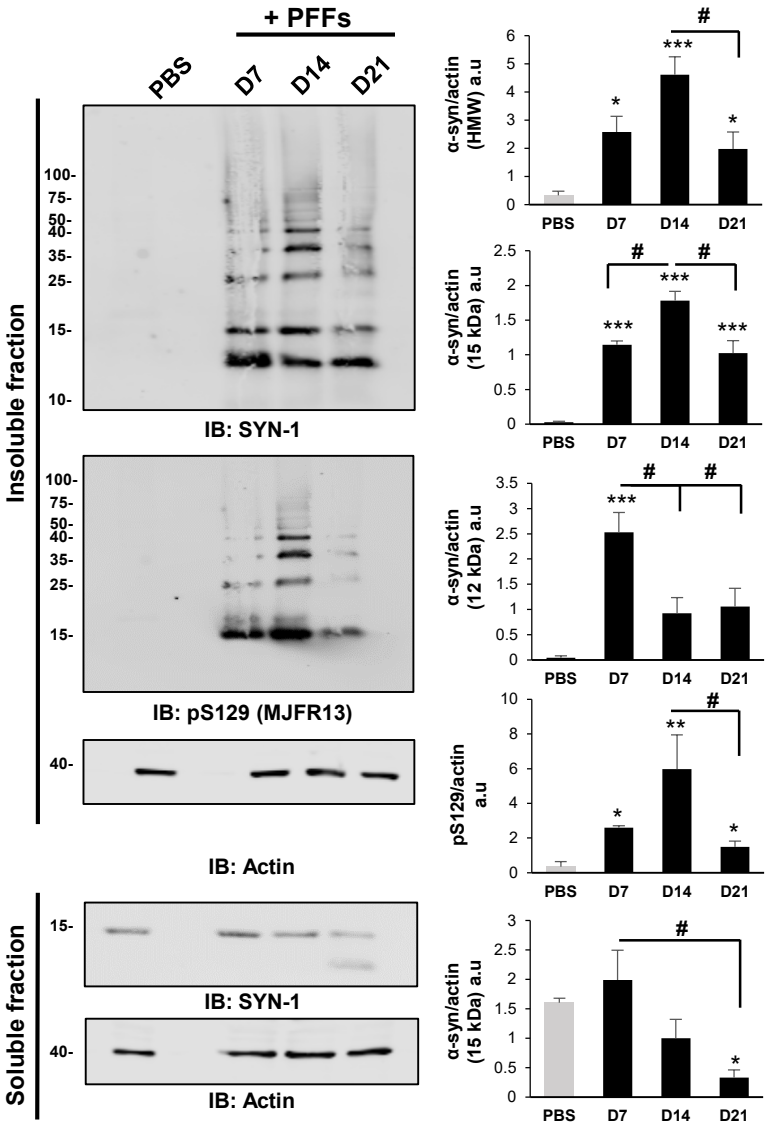

Fig. S7. WB analysis of α-syn seeded-aggregates formed 7, 14 or 21 days after adding mouse PFFs to WT neurons (related to Figures 1-3).

Control neurons were treated with PBS. After sequential extractions, the insoluble fractions of neuronal cell lysates were analyzed by immunoblotting. Total α-syn, pS129 and actin were respectively detected by SYN-1, pS129 (MJFR13), and actin antibodies. The higher molecular weights (HMWs) corresponding to the newly formed fibrils are detected from 25 kDa to the top of the gel. A minimum of three independent experiments was performed. $p<0.001$=**, $p<0.0001$=*** (ANOVA followed by Tukey HSD post-hoc test, PBS vs D7 or D14 or D21).

Figure S8. Related to Figure 4

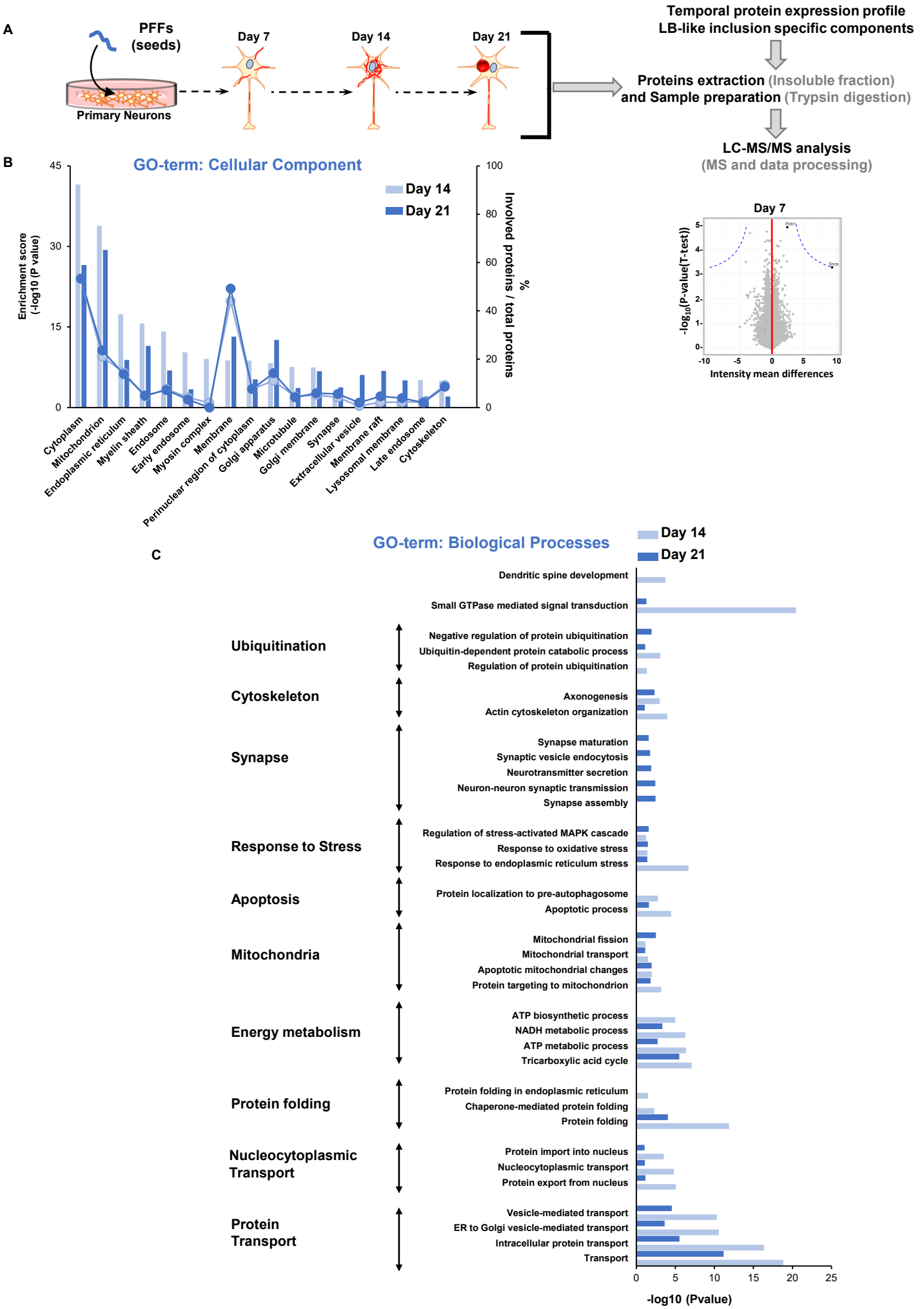

Figure S8. Related to Figure 4

D

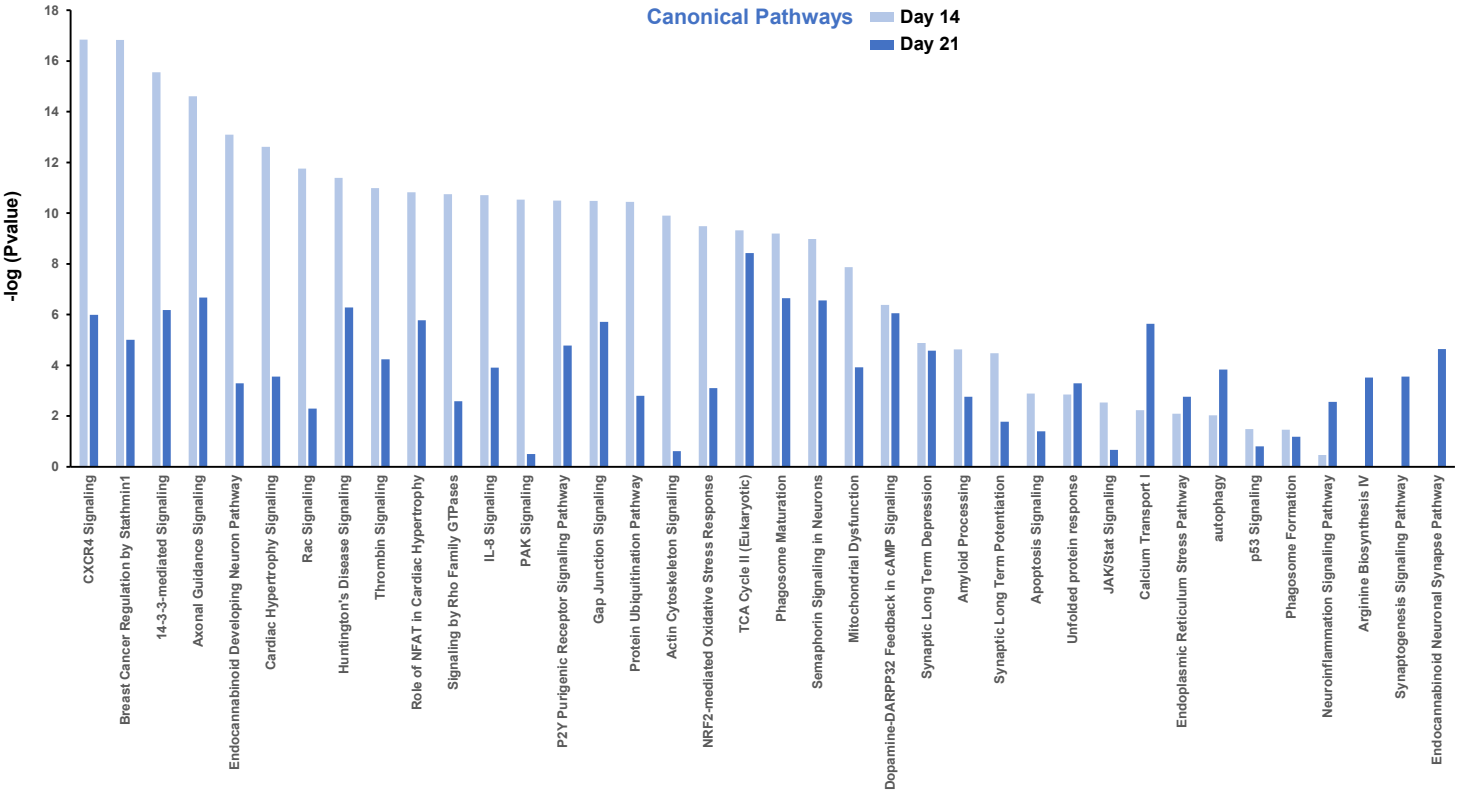

E

Proteins name (Hendersen et al., 2017)	Insoluble Fraction (D14)	Insoluble Fraction (D21)
Collagen alpha-1(XII) chain	+	+
MAP/microtubule affinity-regulating kinase 1	-	-
p21-activated kinase	-	-
α-synuclein	+	+
TBC1 domain family, member 10	+	+
β-synuclein	-	-
Sequestosome-1	+	+
Ubiquitin C	+	
Phospholipase C, β1	+	+
HECT and RLD domain containing E3 ubiquitin protein ligase family member 1	-	-
Hectd1 HECT domain containing 1	+	+
Transformation-related protein 53 binding protein 1	+	+

Figure S8. Related to Figure 4

F

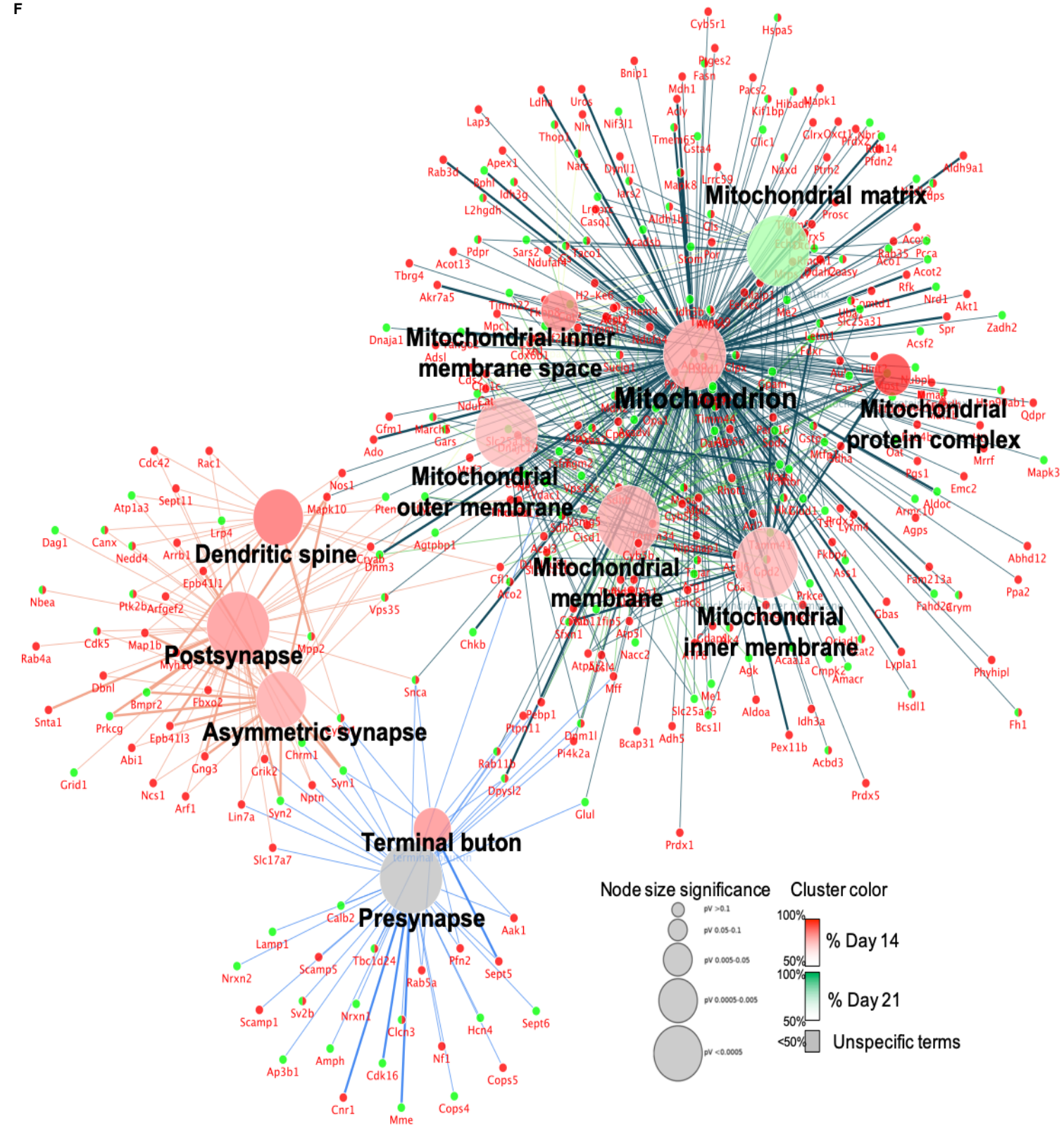

Figure S8. Related to Figure 4 and the discussion

G

Proteins name	Insoluble Fraction (D14)	Insoluble Fraction (D21)	References
acyl-CoA synthetase long-chain family member 4 isoform 1	+	+	Xia, Q., et al. (2008)
aggresome related proteins	+	+	Wakabayashi, K., et al. (2013)
a2-macroglobulin	+	+	Wakabayashi, K., et al. (2013)
amphiphysin isoform 1	-	+	Xia, Q., et al. (2008)
a-synuclein	+	+	Wakabayashi, K., et al. (2013), Xia, Q., et al. (2008); Leverenz, J. B., et al. (2007)
Amyloid precursor protein	+	+	Wakabayashi, K., et al. (2013)
atlastin	+	+	Xia, Q., et al. (2008)
band 4.1-like protein	+	-	Leverenz, J. B., et al. (2007)
C terminus of Hsp70-interacting protein	+	-	Wakabayashi, K., et al. (2013)
Calcium/calmodulin-dependent protein kinase II	-	+	Wakabayashi, K., et al. (2013)
calnexin	+	+	Xia, Q., et al. (2008)
calreticulin precursor	-	+	Xia, Q., et al. (2008)
cathepsin D preproprotein	-	+	Xia, Q., et al. (2008)
coatomer protein complex	+	+	Xia, Q., et al. (2008)
coatomer protein complex, subunit beta	+	+	Xia, Q., et al. (2008)
coatomer protein complex, subunit zeta 1	+	+	Xia, Q., et al. (2008)
cofilin 1	+	-	Xia, Q., et al. (2008)
coronin, actin binding protein, 1A	+	-	Xia, Q., et al. (2008)
crystallin mu	+	+	Xia, Q., et al. (2008)
Cyclin-dependent kinase 5	+	+	Wakabayashi, K., et al. (2013)
cysteine-rich protein 2	+	+	Xia, Q., et al. (2008)
cytosolic nonspecific dipeptidase (EC 3.4.13.18)	-	+	Xia, Q., et al. (2008)
Cytochrome c	+	+	Wakabayashi, K., et al. (2013)
dihydropyrimidinase-like 2	+	+	Xia, Q., et al. (2008) and Leverenz, J. B., et al. (2007)
Di-Ras2	+	+	Xia, Q., et al. (2008)
doublecortin and CaM kinase-like 1	+	+	Xia, Q., et al. (2008)
dynamin 3	-	+	Leverenz, J. B., et al. (2007)
dynein, cytoplasmic, heavy polypeptide 1	+	+	Xia, Q., et al. (2008) and Leverenz, J. B., et al. (2007)
dynein, cytoplasmic, intermediate polypeptide 1	+	+	Xia, Q., et al. (2008)
dynein, cytoplasmic, light intermediate polypeptide 2	+	+	Xia, Q., et al. (2008)
electron-transferring-flavoprotein dehydrogenase	+	+	Xia, Q., et al. (2008)
elongation factor 1 α2	+	-	Leverenz, J. B., et al. (2007)
eukaryotic translation elongation factor 2	+	-	Xia, Q., et al. (2008)
exportin 1	+	-	Xia, Q., et al. (2008)
fascin 1	+	+	Xia, Q., et al. (2008) and Leverenz, J. B., et al. (2007)
fatty acid synthase	+	+	Xia, Q., et al. (2008)
G-protein-coupled receptor kinase 5	-	+	Wakabayashi, K., et al. (2013)
GATE-16/GABARAPL1	+	-	Wakabayashi, K., et al. (2013)
glutamate dehydrogenase 1	+	+	Xia, Q., et al. (2008)
glutamate-cysteine ligase regulatory protein	-	+	Xia, Q., et al. (2008)
glutathione S-transferase	+	+	Xia, Q., et al. (2008)
GSK3 b (glycogen synthase kinase 3b)	+	+	Wakabayashi, K., et al. (2013)
Heat-shock proteins 27	-	-	Wakabayashi, K., et al. (2013)
Heat-shock proteins 40	-	-	Wakabayashi, K., et al. (2013)
Heat-shock proteins 60	+	+	Wakabayashi, K., et al. (2013)
Heat-shock proteins 70	+	-	Wakabayashi, K., et al. (2013)
Heat-shock proteins 90	+	+	Wakabayashi, K., et al. (2013) and Xia, Q., et al. (2008)
Heat-shock proteins 110	-	-	Wakabayashi, K., et al. (2013)
Heme oxygenase	-	+	Wakabayashi, K., et al. (2013)
HDAC 6	+	+	Wakabayashi, K., et al. (2013)
importin 7	+	-	Xia, Q., et al. (2008)
kinesin family member 3A	+	+	Xia, Q., et al. (2008)
LIM and SH3 protein 1	+	-	Xia, Q., et al. (2008)
Microtubule-associated protein 1	+	-	Wakabayashi, K., et al. (2013) and Xia, Q., et al. (2008)
Microtubule-associated protein 1B	+	-	Wakabayashi, K., et al. (2013) and Xia, Q., et al. (2008)
Microtubule-associated protein 1A	+	-	Wakabayashi, K., et al. (2013) and Xia, Q., et al. (2008)
mitofusin 2	+	-	Xia, Q., et al. (2008)
mitogen-activated protein kinase 1	+	+	Xia, Q., et al. (2008)
NEDD8	+	-	Wakabayashi, K., et al. (2013)
neuronal membrane glycoprotein	-	+	Leverenz, J. B., et al. (2007)
nuclear receptor binding protein	-	+	Xia, Q., et al. (2008)
OTU domain, ubiquitin aldehyde binding 1	+	-	Xia, Q., et al. (2008)
P450 (cytochrome) oxidoreductase	+	-	Xia, Q., et al. (2008)
peroxiredoxin 5, mitochondrial precursor	+	-	Leverenz, J. B., et al. (2007)
phosphatidylinositol-4-phosphate 5-kinase type II beta isoform a	+	-	Xia, Q., et al. (2008)
phosphoglycerate mutase 1 (brain)	+	-	Xia, Q., et al. (2008)
Phospholipase C b1	+	+	Wakabayashi, K., et al. (2013)
platelet-activating factor acetylhydrolase, isoform Ib, alpha subunit (45kD)	+	+	Xia, Q., et al. (2008)
p62/sequestosome 1	+	+	Wakabayashi, K., et al. (2013)
profilin 1	+	-	Xia, Q., et al. (2008)
progesterone receptor membrane component 1	+	-	Xia, Q., et al. (2008)
Proteasome	+	+	Wakabayashi, K., et al. (2013)
Proteasome activators (PA700, PA28)	+	+	Wakabayashi, K., et al. (2013)
protein disulfide isomerase-related protein	+	+	Xia, Q., et al. (2008)
protein kinase C, beta 1	+	+	Xia, Q., et al. (2008)
protein kinase C, gamma	+	+	Xia, Q., et al. (2008)
protein phosphatase 1, catalytic subunit, gamma isoform	+	-	Xia, Q., et al. (2008)
regulator of nonsense transcripts 1	-	+	Xia, Q., et al. (2008)
reticulon 3 isoform a	+	+	Xia, Q., et al. (2008)
rho-associated protein kinase 2	+	-	Leverenz, J. B., et al. (2007)
ROC1 (E3 ubiquitin-protein ligase RBX1)	+	-	Wakabayashi, K., et al. (2013)
SEC23-related protein A	+	-	Xia, Q., et al. (2008)
similar to aminopeptidase puromycin sensitive	-	+	Xia, Q., et al. (2008)
SLC25A3	+	+	Leverenz, J. B., et al. (2007)
Sodium/potassium-transporting ATPase α1 chain	-	+	Leverenz, J. B., et al. (2007)
Sodium/potassium-transporting ATPase β1 chain	-	+	Leverenz, J. B., et al. (2007)
solute carrier family 30 (zinc transporter), member 9	+	+	Xia, Q., et al. (2008)
STIP1 homology and U-Box containing protein 1	+	-	Xia, Q., et al. (2008)
succinate dehydrogenase complex, subunit B, iron sulfur (Ip)	+	-	Xia, Q., et al. (2008)
Superoxide dismutase 2 (Mn superoxide dismutase)	-	+	Xia, Q., et al. (2008)
synaptic vesicle glycoprotein 2	+	+	Xia, Q., et al. (2008)
synaptotagmin	-	+	Xia, Q., et al. (2008)
triosephosphate isomerase 1	+	-	Xia, Q., et al. (2008)
Tubulin α1 chain	+	+	Wakabayashi, K., et al. (2013) and Leverenz, J. B., et al. (2007)
TUBB β Tubulin 1	+	+	Leverenz, J. B., et al. (2007)
Tubulin β	+	+	Wakabayashi, K., et al. (2013) and Leverenz, J. B., et al. (2007) and xia
Tubulin β2 chain	-	+	Leverenz, J. B., et al. (2007)
Tubulin β4 chain	+	+	Leverenz, J. B., et al. (2007)
Tubulin β5	+	-	Leverenz, J. B., et al. (2007)
Tubulin β5 chain	+	-	Leverenz, J. B., et al. (2007)
βTubulin	+	+	Wakabayashi, K., et al. (2013) and Leverenz, J. B., et al. (2007)
γ Tubulin	+	+	Wakabayashi, K., et al. (2013) and Leverenz, J. B., et al. (2007)
Tubulin polymerization promoting protein/p25	-	-	Wakabayashi, K., et al. (2013)
Ubiquitin	+	+	Wakabayashi, K., et al. (2013) and Xia, Q., et al. (2008)
Ubiquitin conjugating enzyme UbcH7 (E2)	+	-	Wakabayashi, K., et al. (2013)
Ubiquitin C-terminal hydrolase	+	+	Wakabayashi, K., et al. (2013)
vacuolar protein sorting 33B	+	+	Xia, Q., et al. (2008)
vacuolar protein sorting 35	+	+	Xia, Q., et al. (2008)
vesicle trafficking protein sec22b	+	-	Xia, Q., et al. (2008)
voltage dependent anion channel 1	-	+	Leverenz, J. B., et al. (2007)

Figure S8. Related to Figure 4 and the discussion

H

Protein degradation machineries	Proteins name	Insoluble Fraction (D14)	Insoluble Fraction (D21)
Ubiquitin Proteasome Pathway	Anaphase-promoting complex subunit 5	+	-
	Cell division cycle protein 23 homolog	+	-
	Cullin-2	+	-
	Cullin-3	-	+
	Cullin-5	-	+
	Cullin-associated NEDD8-dissociated protein 1	+	+
	E2/E3 hybrid ubiquitin-protein ligase UBE2O	-	+
	E3 ubiquitin-protein ligase HECTD1	+	+
	E3 ubiquitin-protein ligase MARCH5	+	-
	E3 ubiquitin-protein ligase NEDD4	+	+
	E3 ubiquitin-protein ligase RBX1	+	+
	E3 ubiquitin-protein ligase RNF14	+	-
	E3 ubiquitin-protein ligase RNF126	-	+
	E3 ubiquitin-protein ligase TRIM32	+	-
	NEDD8-activating enzyme E1 catalytic subunit	+	-
	NEDD8-activating enzyme E1 regulatory subunit	-	+
	NEDD8-conjugating enzyme Ubc12	+	-
	Proteasome-associated protein ECM29 homolog	+	+
	Proteasome complex activator	+	+
	SUMO-activating enzyme subunit 1	+	+
	SUMO-activating enzyme subunit 2	+	+
	SUMO-conjugating enzyme UBC9	+	-
	Transcription elongation factor B polypeptide 1	+	+
	Transcription elongation factor B polypeptide 2	+	+
	Ubiquitin C-terminal hydrolase isozyme L1 UCHL1	+	-
	Ubiquitin C-terminal hydrolase 5 USP5	+	-
	Ubiquitin C-terminal hydrolase FAF-X USP9x	+	+
	Ubiquitin C-terminal hydrolase 14 USP14	+	-
	Ubiquitin Cl-terminal hydrolase 15 USP15	+	-
	Ubiquitin C-terminal hydrolase 47 USP47	+	-
	Ubiquitin conjugating enzyme UbcH7	+	-
	Ubiquitin-conjugating enzyme E2 D2	+	+
	Ubiquitin-conjugating enzyme E2 D3	+	-
	Ubiquitin-conjugating enzyme E2 E2	-	+
	Ubiquitin-conjugating enzyme E2 L3	+	-
	Ubiquitin-conjugating enzyme E2 O	+	-
	Ubiquitin-conjugating enzyme E2Q-like protein 1	-	+
	Ubiquitin-like modifier-activating enzyme 1	+	+
	Ubiquitin-like modifier-activating enzyme 1	-	+
	Ubiquitin-like modifier-activating enzyme 6	+	-
	Ubiquitin-protein ligase E3B	+	-
Autophagy	Autophagy-related protein 9	+	-
	Cathepsin D	-	+
	Cathepsin F	-	+
	Lysosome-associated membrane glycoprotein 1	-	+
	Microtubule-associated proteins 1A/1B light chain 3A – LC3 A	+	-
	Next to BRCA1 gene 1 protein	-	+
	Sequestosome-1	+	+
	Serine/threonine-protein kinase mTOR	-	+
	Ubiquitin-like modifier-activating enzyme ATG7	+	-
	Vacuolar protein sorting-associated protein 16 homolog	-	+
	Vacuolar protein sorting-associated protein 33A	+	-
	Vacuolar protein sorting-associated protein 33B	+	+
Aggresome related proteins	Histone deacetylase 6	+	+
	Dynein, cytoplasmic, heavy chain	+	+
	Dynein, cytoplasmic, intermediate chain	+	+
	Microtubule-associated protein 1B	+	-
	Microtubule-associated proteins 1A/1B light chain 3A	+	-
	Regulator of microtubule dynamics protein 1	-	+

Protein degradation machineries	Proteins name	Insoluble Fraction (D14)	Insoluble Fraction (D21)
Unfolded Protein Response	78 kDa glucose-regulated protein	+	+
	Calnexin	+	+
	Calreticulin	-	+
	Endoplasmin	+	+
	Heat shock 70 kDa protein 4	+	-
	Mitogen-activated protein kinase 8	+	+
	Protein disulfide-isomerase	-	+
	Protein disulfide-isomerase A6	+	-
	Protein sel-1 homolog 1	+	-
	Transitional endoplasmic reticulum ATPase	+	+
Chaperones	78 kDa glucose-regulated protein Hsp5a	+	+
	DnaJ homolog subfamily C member 5 Dnajc5	+	-
	DnaJ (Hsp40) homolog	-	+
	Endoplasmin Hsp90b1	+	+
	Heat shock 70 kDa protein 12A Hspa12a	+	+
	Heat shock 70 kDa protein 13 Hspa13	+	+
	Heat shock 70 kDa protein 4 Hspa4	+	-
	Heat shock protein 60 kDa, mitochondrial Hspd1	+	+
	Heat shock protein HSP 90-alpha Hsp90aa1	+	-
	Heat shock protein HSP 90-beta Hsp90ab1	+	+
	Histone chaperone ASF1A	-	+
	Mitochondrial chaperone BCS1	-	+
	Proteasome assembly chaperone 1	+	-
	Tubulin-specific chaperone E	+	+
Sumoylation Pathway	C-terminal-binding protein 1	-	+
	Dual specificity mitogen-activated protein kinase kinase 4	+	+
	Mitochondrial Rho GTPase 1	+	-
	Mitogen-activated protein kinase 10	+	-
	Mitogen-activated protein kinase 8	+	+
	Rab GDP dissociation inhibitor alpha	-	+
	Rab GDP dissociation inhibitor beta	+	+
	Rab GDP dissociation inhibitor beta	+	-
	Rho-related GTP-binding protein RhoB	+	-
	SUMO-activating enzyme subunit 1	+	+
	SUMO-activating enzyme subunit 2	+	+
	SUMO-conjugating enzyme UBC9	+	-
Endolysosomal Pathway	Argininosuccinate synthase	-	+
	Calpain-2 catalytic subunit	+	+
	Cathepsin D	-	+
	Cathepsin F	-	+
	CD63 antigen	-	+
	Chitinase domain-containing protein 1	-	+
	Lysosomal acid phosphatase	-	+
	Lysosome membrane protein 2	-	+
	Lysosome-associated membrane glycoprotein 1	-	+
	Membrane protein MLC1	-	+
	Next to BRCA1 gene 1 protein	-	+
	Ragulator complex protein LAMTOR2	+	-
	Ragulator complex protein LAMTOR3	+	-
	Ras-related GTP-binding protein A	-	+
	Ras-related protein Rab-7a	+	-
	Sequestosome-1	+	+
	Serine/threonine-protein kinase mTOR	-	+
	Vacuolar fusion protein CCZ1 homolog	-	+
	Vacuolar protein sorting-associated protein 16 homolog	-	+
	Vacuolar protein sorting-associated protein 33B	+	+
	Vacuolar protein sorting-associated protein 35	+	+

Fig. S8. Temporal proteomic analyses of the protein contents found in the insoluble fraction of the PFFs-treated neurons reveals a high increase in proteins related to the endomembrane system (related to Figure 4 and dataset S1).

A. Insoluble proteins from neurons treated with PBS and PFFs for 7, 14 or 21 days were extracted and analyzed using LC-MS/MS (**Dataset S1**). Identified proteins were plotted using volcano plot. Mean difference (log_2) between the insoluble fractions of PFFs-treated neurons and PBS neurons treated for 7 days, were plotted against $-log_{10}$ P value (t-test). Dotted lines represent the FDR <0.05 (False Discovery Rate) and threshold of significance SO=1 assigned for the subsequent analysis. At D7, only α-syn and Plcb1 proteins were significantly enriched in the insoluble fraction of the PFFs-treated neurons.

B-C. Classification of the proteins significantly enriched in the insoluble fractions of the PFF-treated neurons at D14 and D21 by cellular component (**B**) and biological processes (**C**) using Gene Ontology (GO) and DAVID enrichment analyses.

D. Canonical pathways enriched in the insoluble fractions of the PFFs-treated neurons at D14 and D21 using Ingenuity Pathway Analysis (IPA).

E. Comparison of our proteomic results with previous published proteomic analyses using the same neuronal seeding model**.** 8 out of the 12 proteins shown by Henderson et al(30) to be significantly enriched in the insoluble fraction of PFFs-treated neurons were also present in our proteomic data. However, in this study, only twelve proteins were found to be significantly enriched in the insoluble fraction of PFF-treated neurons, and eight out of the twelve were also present in our proteomic data.

F. Cytoscape visualization. The nodes represent gene ontology terms; node color represents the group and node size represents the significance of each gene ontology term.

G. The proteome of the neuronal LB-like inclusions overlaps significantly with that of LBs from human PD brain tissues. The table depicts the comparison of the proteins enriched in the insoluble fraction of PFFs-treated neurons (at D14 and D21) to the proteins contents of human *bona fide* LBs established by IHC (32) or by proteomic (33, 34) analyses.

H. Temporal proteomic analyses of the protein contents found in LB-like inclusions formed in PFFs-treated neurons. The table depicts the proteins involved in the protein degradation machinery that were enriched in the insoluble fraction of PFFs-treated neurons at D14 and D21.

Figure S9. Related to Figure 5

A

Differentially-expressed genes (FDR cutoff of adjusted p value <0.01)			
Gene count	**Total genes**	**Up-regulated**	**Down-Regulated**
PBS vs D7	75	27	48
PBS vs D14	435	106	223
PBS vs D21	1017	455	562
D14 vs D21	194	83	111

B

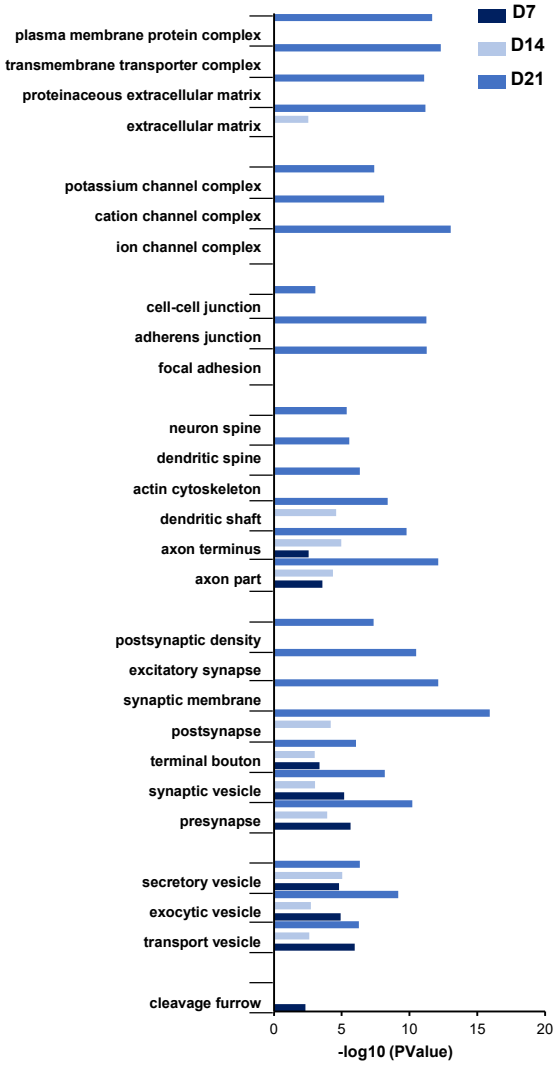

C

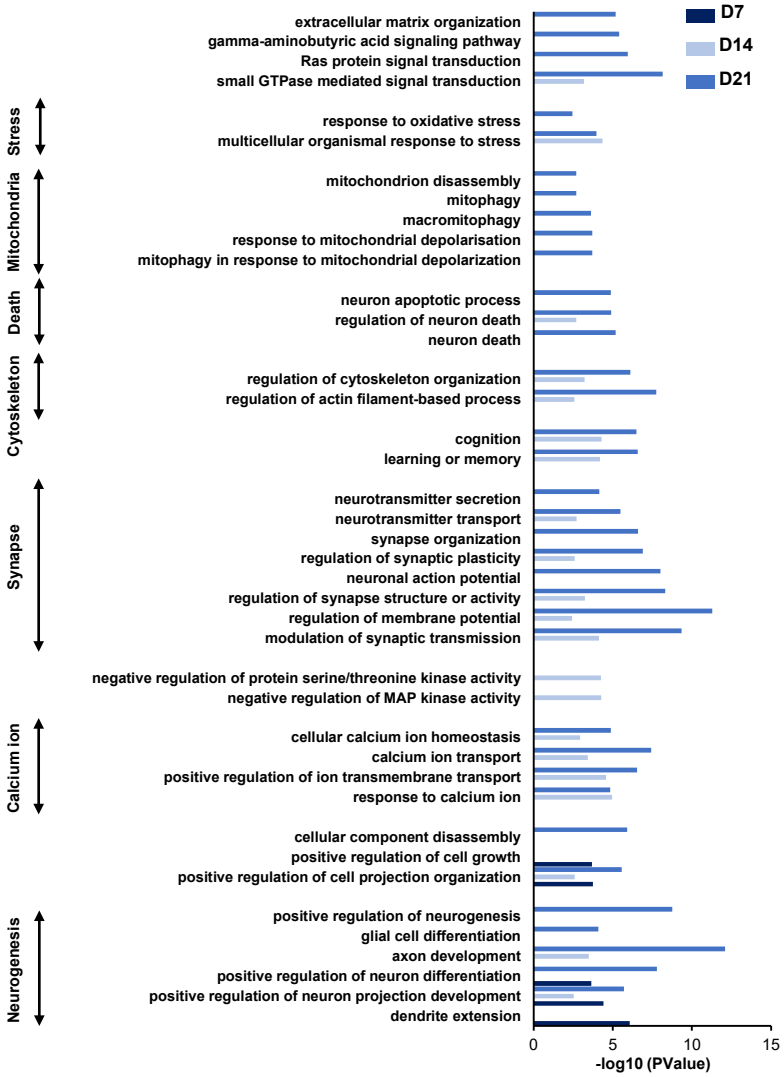

Figure S9. Related to Figure 5

D

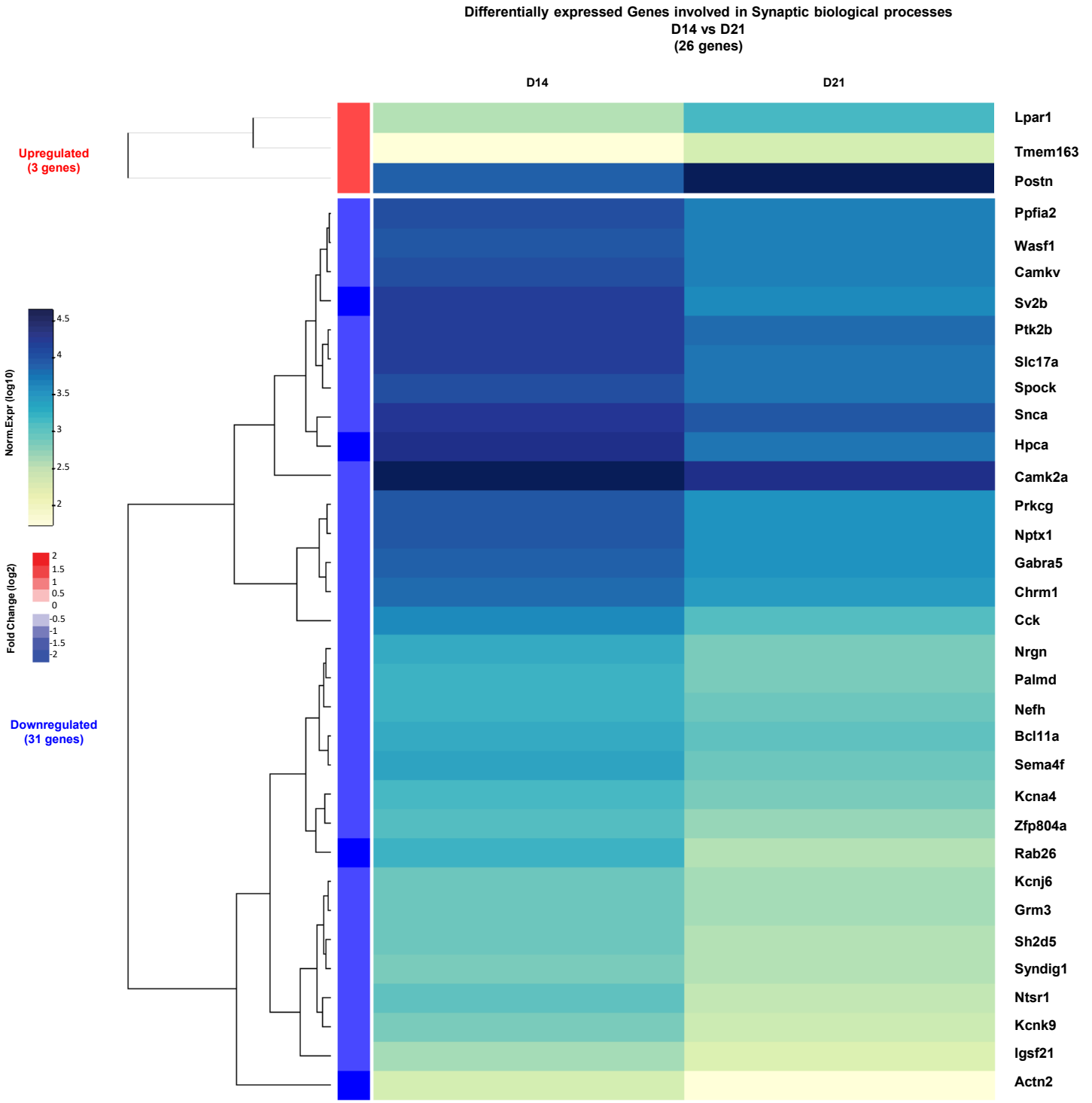

Fig. S9. Gene expression level changes during the formation of the newly formed fibrils and their maturation into LB-like inclusions (related to Figure 5 and Dataset S2).

A. Temporal transcriptomic analysis of the gene expression level in PBS-treated neurons vs PFFs-treated neurons treated for 7, 14 or 21 days. Genes with an absolute log2 fold-change greater than 1 and an FDR less than 0.01 were considered as significantly differentially expressed. The table depicts the number of genes up or down-regulated in PFFs-treated neurons over time.

B-C. Significant GO terms enrichment associated with cellular components (**B**) and biological processes (**C**) from differentially regulated genes were plotted against $-\log_{10}$ P value (t-test, PBS-treated neurons vs. PFF-treated neurons, **Dataset S2**).

D. The heatmap depicts the synaptic genes that are up- or down-regulated in PFFs-treated neurons between D14 and D21.

Figure S10. Related to Figure 6 and Discussion

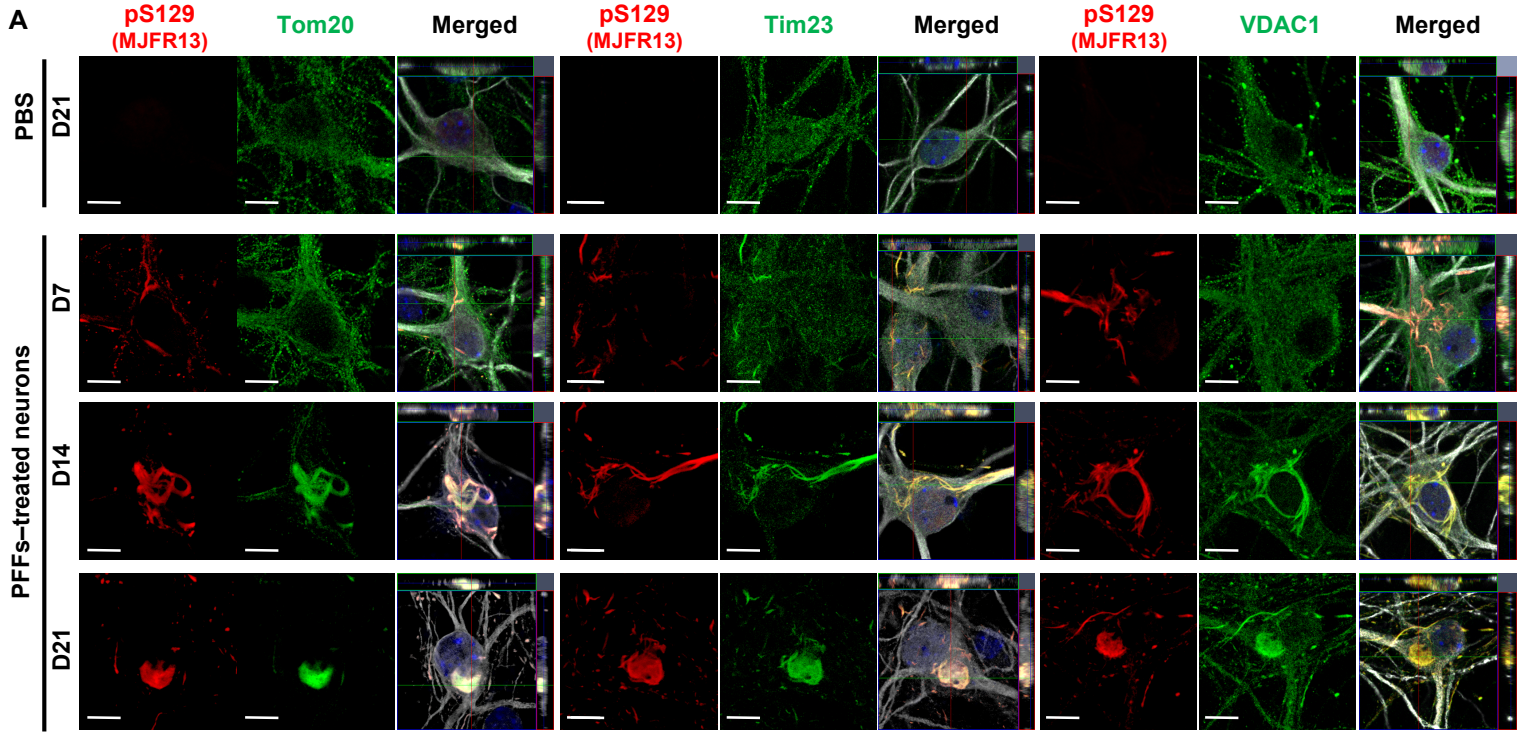

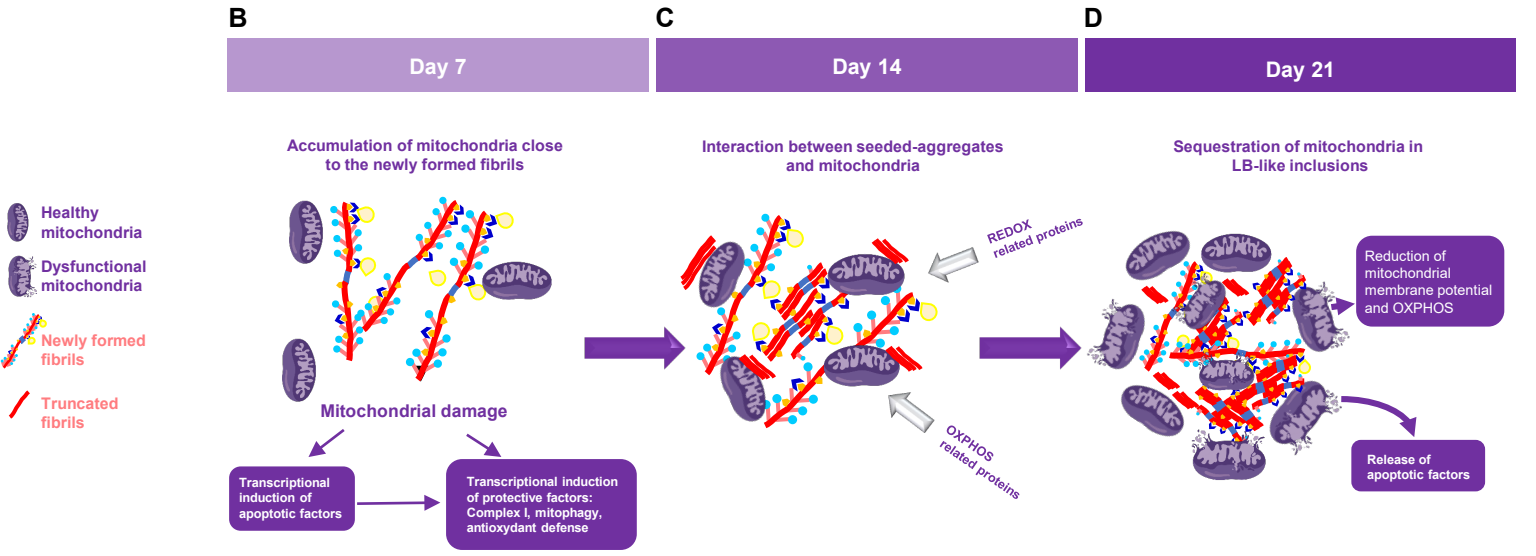

Stage		D7: Cellular responses related to mitochondrial damage during the process of fibrils formation	D14: Interaction of mitochondrial and antioxidant defense components with α-syn seeded aggregates	D21: Mitochondrial sequestration into LB-like inclusions induces mitochondrial dysfunctions and cell death
Evidence for aggregate-mitochondria interaction	ICC	Moderate colocalization of pS129 positive aggregates with TOM20, TIM23 and VDAC1	Strong colocalization of pS129 positive aggregates with TOM20, TIM23 and VDAC1	Strong colocalization of pS129 positive aggregates with TOM20, TIM23 and VDAC1
	EM	Mitochondria accumulate in proximity to cytoplasmic, fibrillar aggregates (not in the neuritic ones)	Mitochondria interact with fibrillar aggregates	Mitochondria get incorporated into maturing LB-like inclusions
	proteomics	No mitochondrial proteins detected in insoluble fraction of PFF-treated neurons	Many mitochondrial components, such as OXPHOS proteins and MFN2 are enriched in the insoluble fraction of PFF-treated neurons	Reduction of mitochondrial components found in the insoluble fraction of PFF-treated neurons as compared to D14
Observations		a. Transcriptional upregulation (until D21) of antioxidant defense systems, mitochondrial quality control, OXPHOS b. Reduced mitochondrial ROS production. c. Maintenance of OXPHOS performance and mitochondrial membrane potential	a. Sequestration of OXPHOS and antioxidant defense components b. Mitochondrial ROS back to baseline level c. Despite compact aggregate-organelle associations OXPHOS performance and mitochondrial membrane potential remain high	a. Mitochondrial membrane potential reduced b. Heavily impaired OXHOS capacities c. Reduced levels of CI-NDUFB8, OPA1 and MFN2
Interpretation		a. Aggregates start to coordinate mitochondria in neuronal soma b. Interaction is unstable c. Neuronal damage signalling induces protective pathways counteracting mitochondrial dysfunction	a. Oxidation and other associated PTMs stabilize aggregates, immobilizing interacting mitochondria b. Enhanced fibril growth on membraneous substrate provided by mitochondrial envelop	a. Dynamics of mitochondria-enclosing aggregates mechanically disrupt membranes → reduced mitochondrial membrane potential and release of apoptotic factors b. Accumulating defective mitochondria surpass neuronal clearance capacities

Fig. S10. Model of how the interaction of mitochondria and LB-like inclusions might induce neurodegeneration (related to Figure 6 and discussion).

A. ICC co-staining of α-syn pS129 (MJFR13) with VDAC1, TOM20, and TIM23 in PFF-treated neurons. Scale bars = 5 µm.

B. α-syn aggregates interact with mitochondrial membranes, mitochondrial transmembrane proteins and soluble α-syn localized in or close to mitochondria, accelerating α-syn aggregation and the formation of LB-like inclusions. Aggregation kinetics and perturbation of mitochondrial membrane integrity (potentially caused by mitochondrial reactive oxygen species) induce damage signalling that on D7 is translated in transcriptional upregulation of both pro-apoptotic factors (e.g. BAX, Aifm3) and potentially protective factors, including subunits of mitochondrial complex I, as well as mitophagy-related PINK1 and oxidative response genes (e.g. Gpx1). These processes are accompanied by reduced mitochondrial reactive oxygen species (ROS) generation and maintenance of efficient oxidative phosphorylation.

C. Continuous recruitment of α-syn to mitochondria and stimulated aggregation in presence of mitochondrial membranes cause maturation of LB-like inclusions with detectable sequestration of mitochondrial proteins, such as mitofusin2 (MFN2) or proteins related to oxidative phosphorylation (OXPHOS), and proteins related to REDOX-mechanisms. Cellular resilience is still sufficient to secure oxidative phosphorylation performance.

D. Aggregating α-syn mechanically disrupts mitochondrial membranes resulting in dense assemblies of fibrillary α-syn, mitochondrial components and other sequestered constituents of LB-like inclusions. Increasing recruitment of mitochondria to inclusions renders the organelles dysfunctional and results in massive respirational deficits, associated with reduced levels of numerous mitochondrial proteins and the induction of the apoptotic machinery.

Figure S11. Related to Figures 6-8

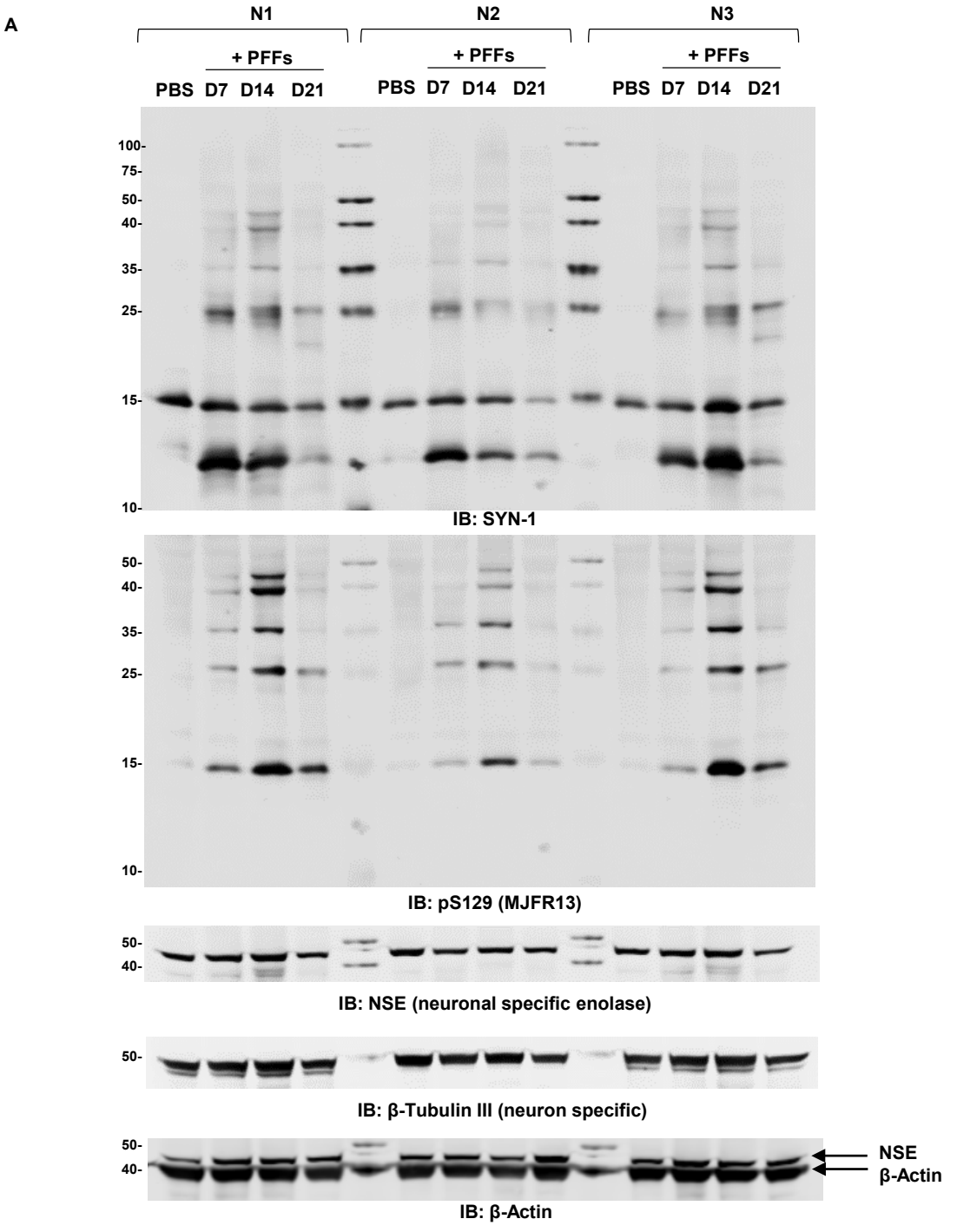

Figure S11. Related to Figures 6-8

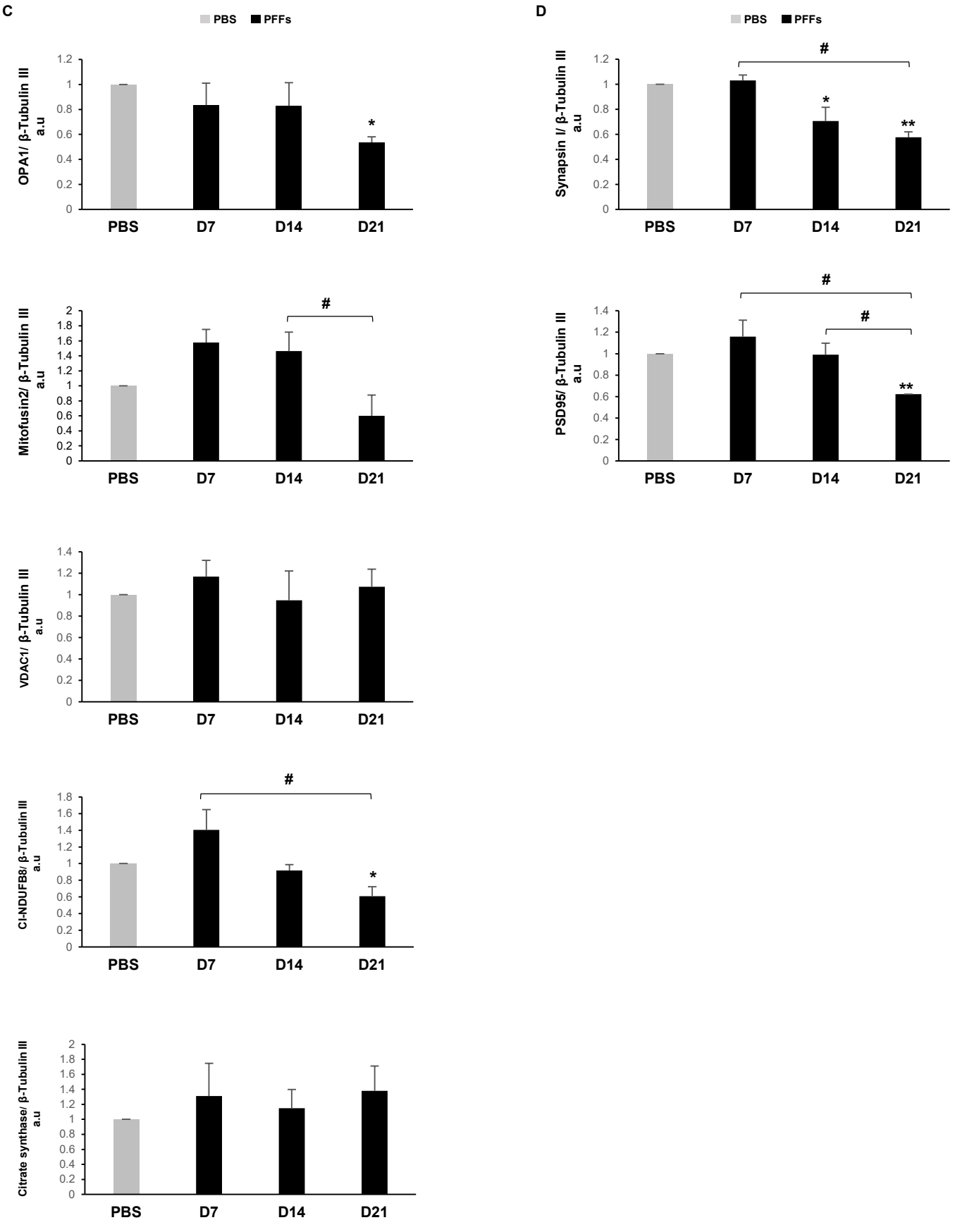

Fig. S11. Synaptic and mitochondria dysfunctions were associated with the formation and maturation of the LB-like inclusions (related to Figures 6 and 7).

A-B. Western blot analyses of the total fractions immunoblotted with antibodies against total α-syn (SYN-1) and pS129 (MJFR13). In addition to actin found in both neurons and glial cells, we also used two neuronal markers [neuronal specific enolase (NSE) and β-Tubulin III] to specifically measured proteins levels changes (Figures 6F and 7A) in the neuronal population (**A**). Densitometry (**B**) showed that over time the overall level of Actin was not significantly changed while NSE and β-Tubulin III significantly decreased between D14 and D21.

C-D. Western blot analyses of the total fractions immunoblotted with antibodies against mitochondria markers (Figure 6F) (OXPHOS, complexes I-V), mitofusin 2, OPA1, citrate synthase and VDAC1 proteins **(C)** or against synaptic markers (Figure 7A) Synapsin I, PSD95, total and phosphorylated ERK1/2 (**D**). The densitometry was performed using the specific neuronal marker β-Tubulin III for normalisation. The graphs (**C-D**), represent the mean +/- SD of a minimum of three independent experiments. $p<0.05$ = *, $p<0.005$=** (ANOVA followed by Tukey HSD post-hoc test, PBS vs. PFF-treated neurons). $p<0.05$ = *, (D14 vs. D21 PFF-treated neurons).

Figure S12. Related to Figure 7

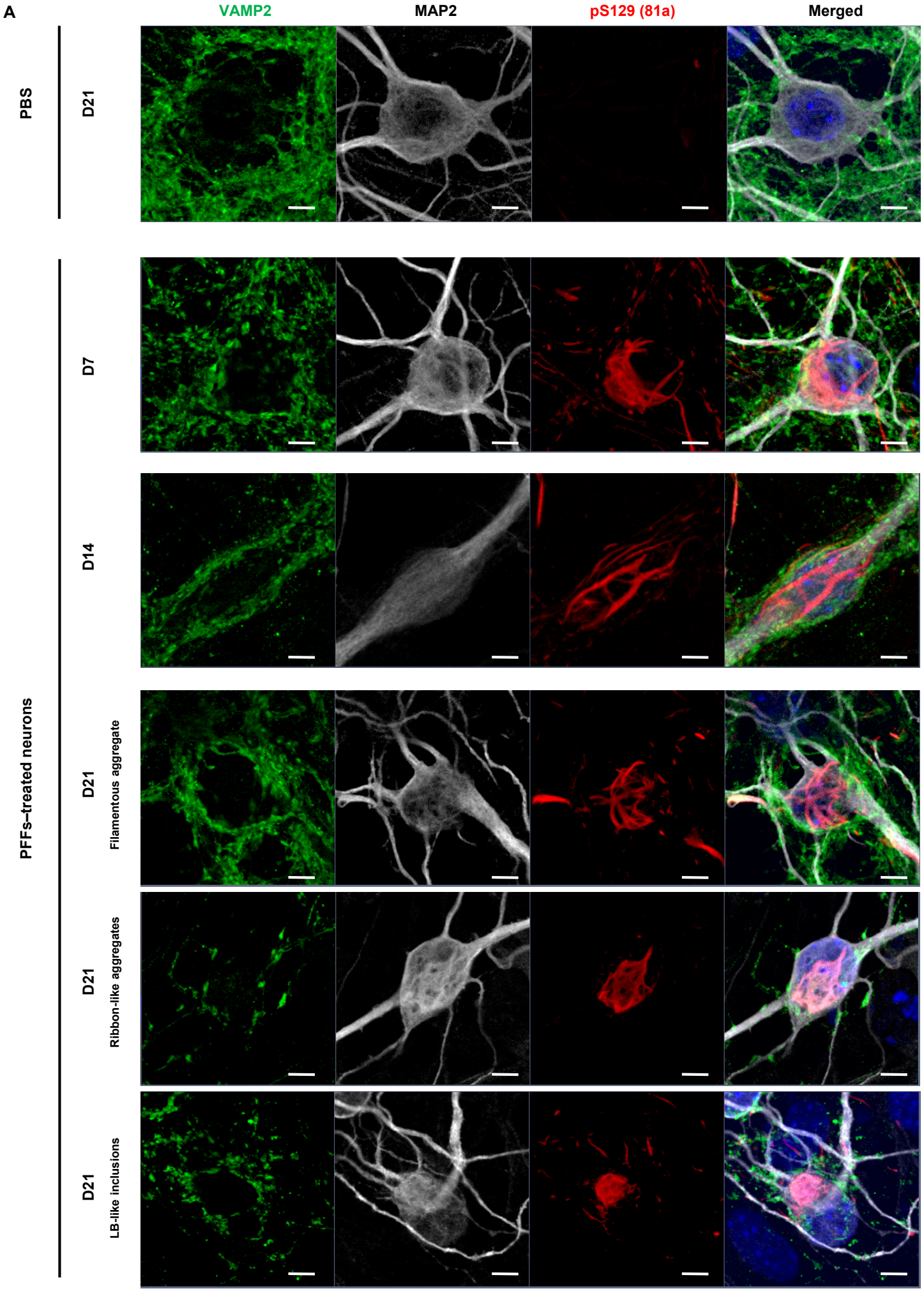

Figure S12. Related to Figure 7

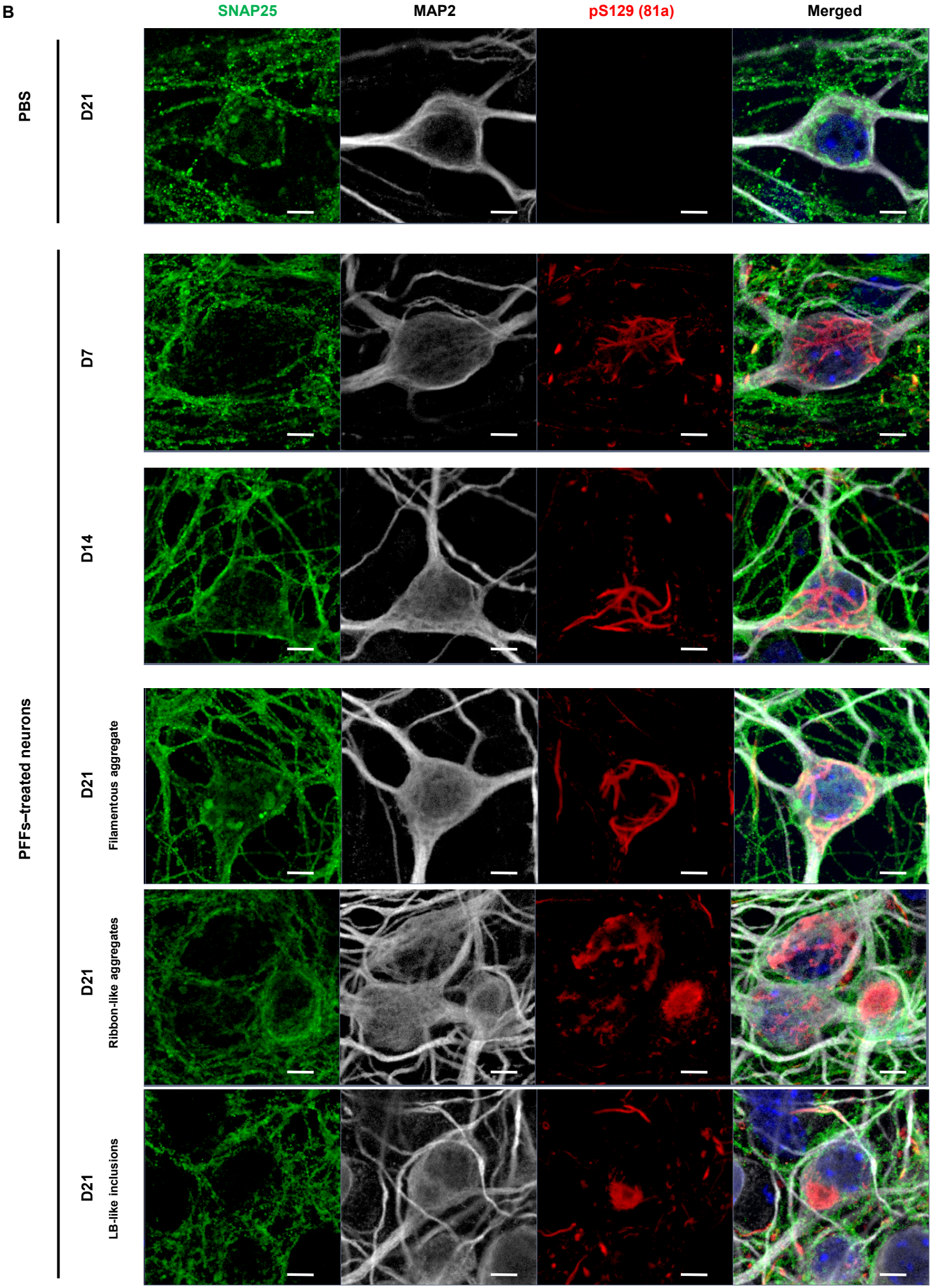

Figure S12. Related to Figure 7

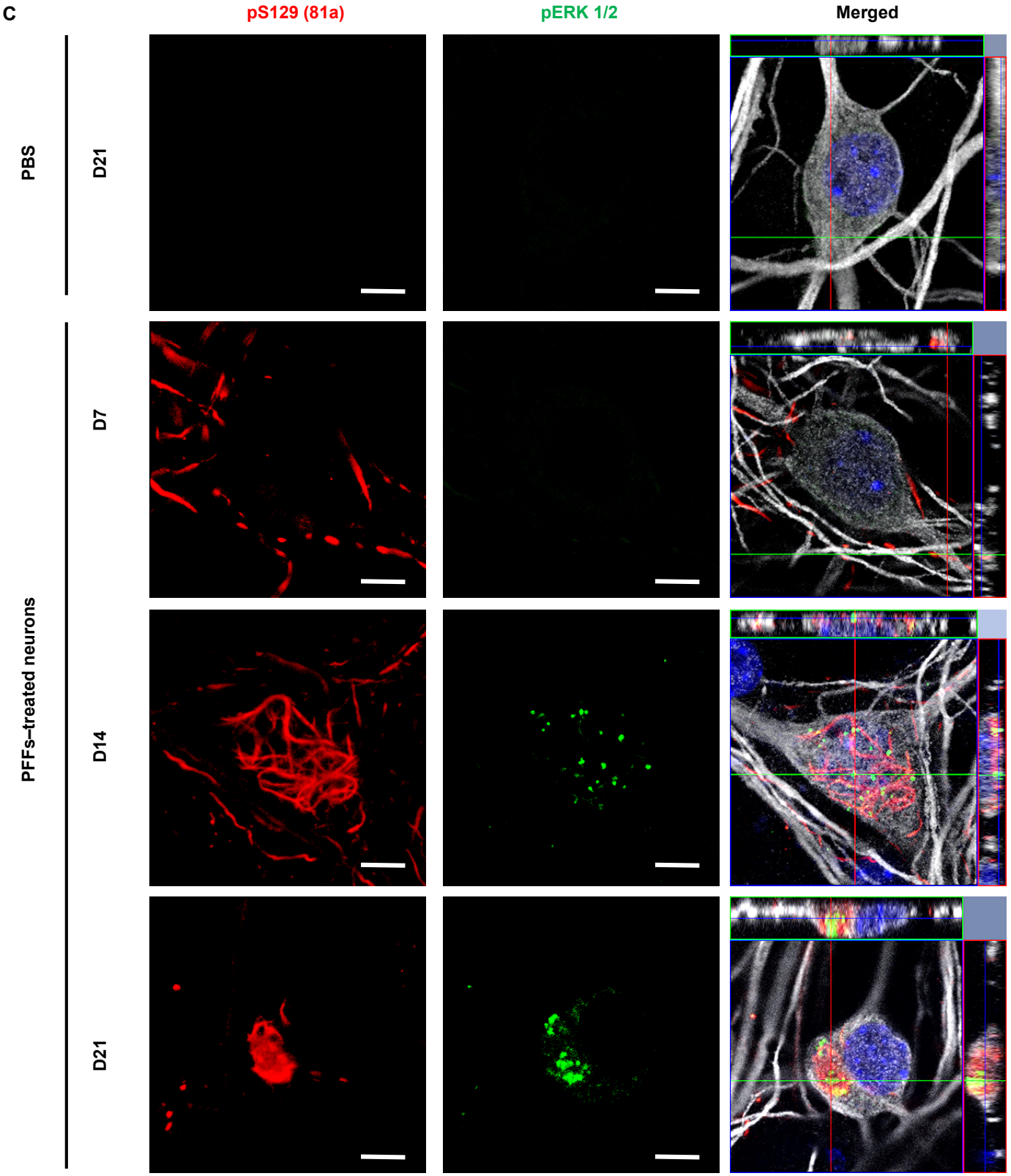

Fig. S12. Synaptic area decreases in PFF-treated neurons (related to Figure 7).

α-syn seeded aggregates were detected by ICC using pS129 (MJFR13) in combination with VAMP2 (**A**), SNAP25 (**B**), p-ERK 1/2 (**C**) antibodies. Neurons were counterstained with MAP2 antibody, and the nucleus with DAPI. Scale bar = 5 µm.

Figure S13

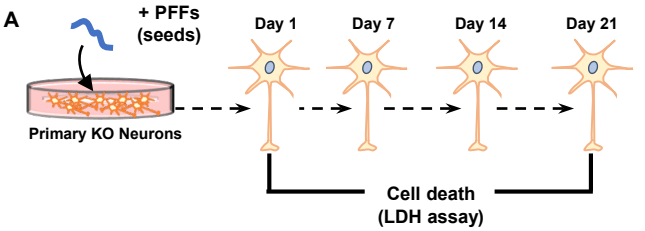
A
+ PFFs
(seeds)
Day 1
Day 7
Day 14
Day 21
Primary KO Neurons
Cell death
(LDH assay)

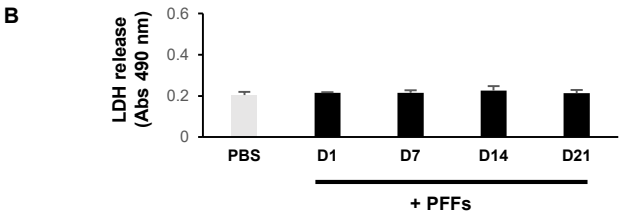
B
LDH release
(Abs 490 nm)
0.6
0.4
0.2
0
PBS
D1
D7
D14
D21
+ PFFs

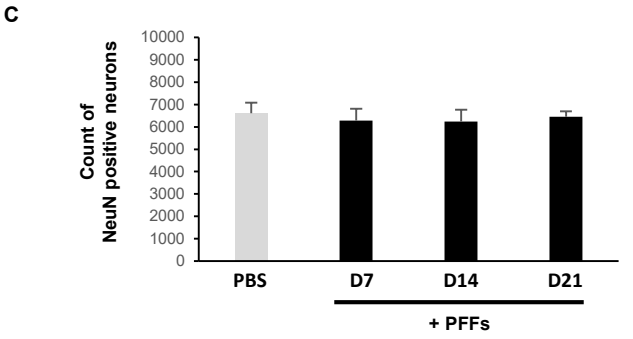
C
Count of
NeuN positive neurons
10000
9000
8000
7000
6000
5000
4000
3000
2000
1000
0
PBS
D7
D14
D21
+ PFFs

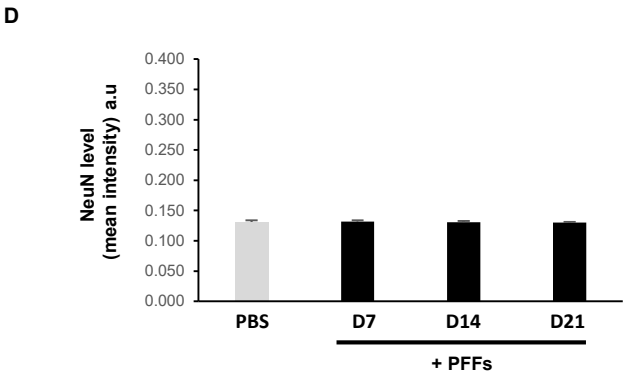
D
NeuN level
(mean intensity) a.u
0.400
0.350
0.300
0.250
0.200
0.150
0.100
0.050
0.000
PBS
D7
D14
D21
+ PFFs

Fig. S13. Addition of α-syn PFFs to primary neurons does not induce cell death in KO neurons.

A-B. Cell death level was assessed in KO neurons treated with PFFs (70 nm) for up to D21 (**A**) using lactate dehydrogenase (LDH) release assay (31) (**B**), and NeuN staining by high content image analysis (**C-D**). For each independent experiment, the total count of NeuN positive neurons (**C**) and the intensity of NeuN staining (**D**) were measured in a minimum of 7'000 neurons. For each independent experiment, triplicate wells were measured per condition. A minimum of three independent experiments was performed.

Figure S14

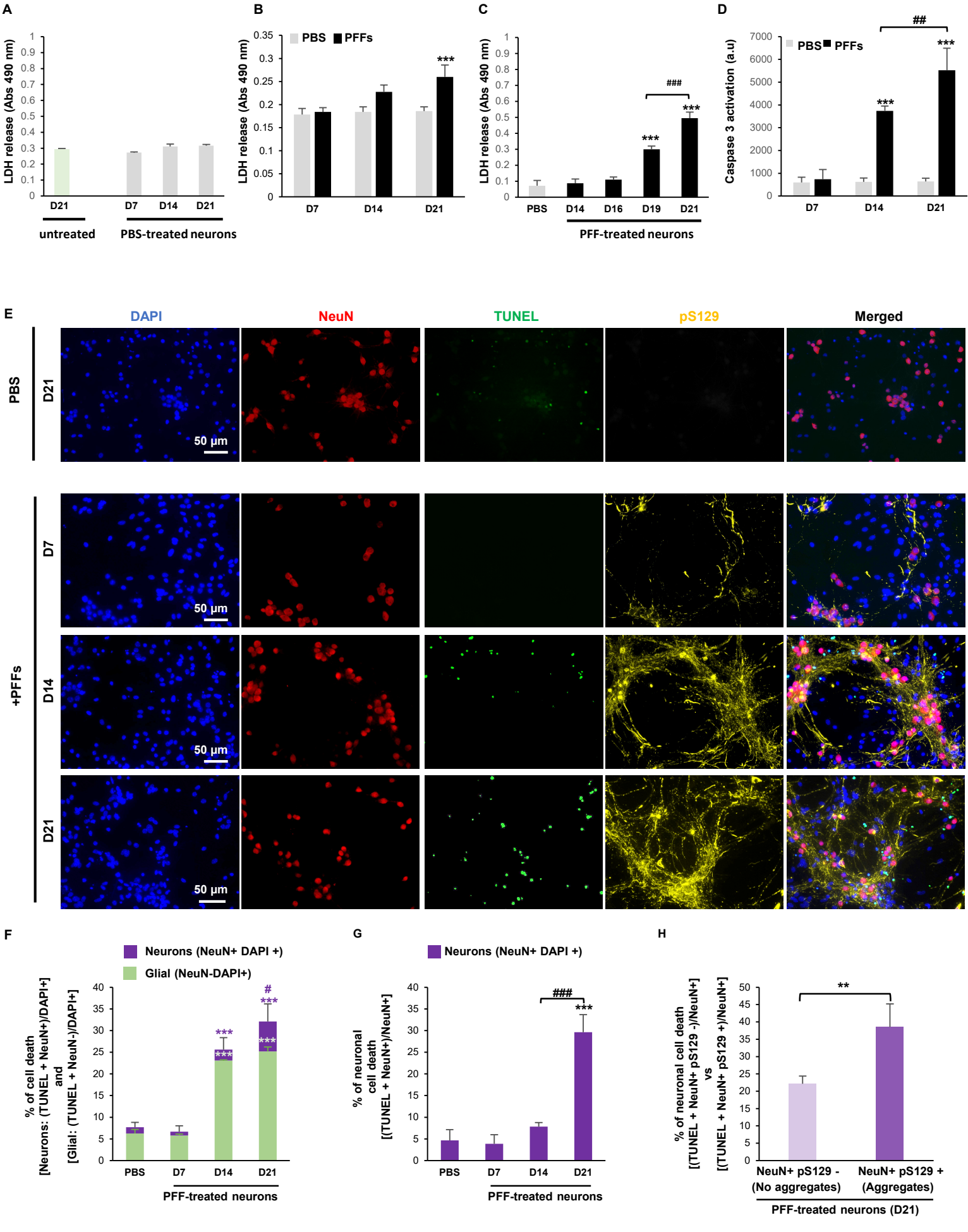
A
LDH release (Abs 490 nm)
D21
D7
D14
D21
untreated
PBS-treated neurons
B
PBS
PFFs
LDH release (Abs 490 nm)
***
D7
D14
D21
C
LDH release (Abs 490 nm)
###
***
***
PBS
D14
D16
D19
D21
PFF-treated neurons
D
Caspase 3 activation (a.u)
PBS
PFFs
##
***
***
D7
D14
D21
E
DAPI
NeuN
TUNEL
pS129
Merged
PBS
D21
+PFFs
D7
D14
D21
50 µm
F
Neurons (NeuN+ DAPI +)
Glial (NeuN-DAPI+)
% of cell death
[Neurons: (TUNEL + NeuN+)/DAPI+]
and
[Glial: (TUNEL + NeuN-)/DAPI+]
#
***
***
***
PBS
D7
D14
D21
PFF-treated neurons
G
Neurons (NeuN+ DAPI +)
% of neuronal cell death
[(TUNEL + NeuN+)/NeuN+]
###
***
PBS
D7
D14
D21
PFF-treated neurons
H
% of neuronal cell death
[(TUNEL + NeuN+ pS129 -)/NeuN+]
vs
[(TUNEL + NeuN+ pS129 +)/NeuN+]
**
NeuN+ pS129 -
(No aggregates)
NeuN+ pS129 +
(Aggregates)
PFF-treated neurons (D21)

Figure S14

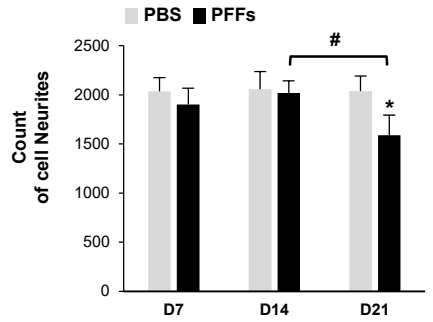
I
PBS
PFFs
Count of cell Neurites
2500
2000
1500
1000
500
0
#
*
D7
D14
D21

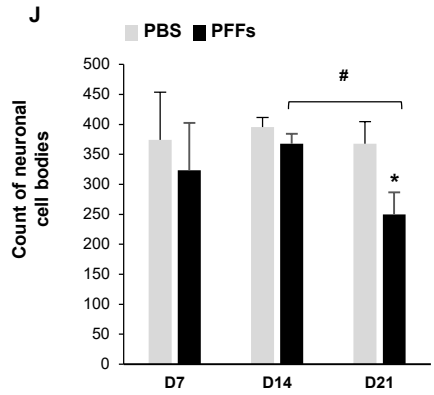
J
PBS
PFFs
Count of neuronal cell bodies
500
450
400
350
300
250
200
150
100
50
0
#
*
D7
D14
D21

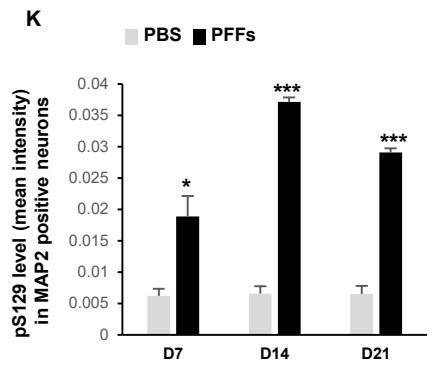
K
PBS
PFFs
pS129 level (mean intensity) in MAP2 positive neurons
0.04
0.035
0.03
0.025
0.02
0.015
0.01
0.005
0
*
***
***
D7
D14
D21

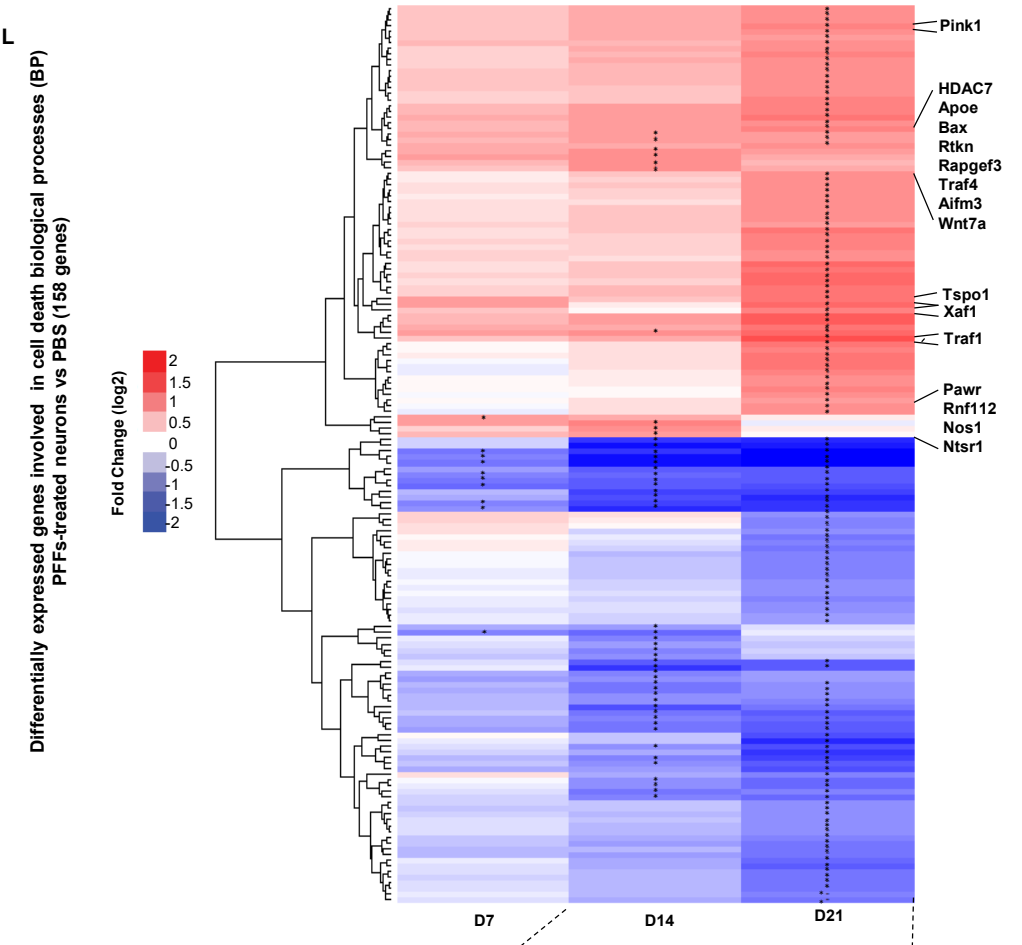
L
Differentially expressed genes involved in cell death biological processes (BP)
PFFs-treated neurons vs PBS (158 genes)
Fold Change (log2)
2
1.5
1
0.5
0
-0.5
-1
-1.5
-2
Pink1
HDAC7
Apoe
Bax
Rtkn
Rapgef3
Traf4
Aifm3
Wnt7a
Tspo1
Xaf1
Traf1
Pawr
Rnf112
Nos1
Ntsr1
D7
D14
D21

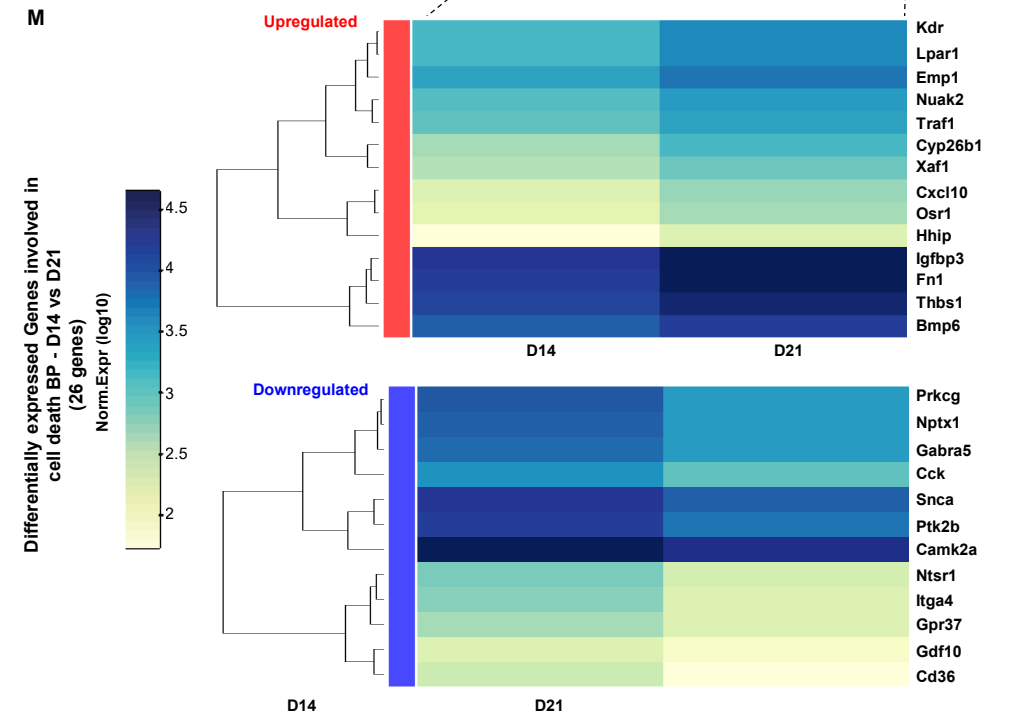
M
Differentially expressed Genes involved in cell death BP - D14 vs D21 (26 genes)
Norm.Expr (log10)
4.5
4
3.5
3
2.5
2
Upregulated
Kdr
Lpar1
Emp1
Nuak2
Traf1
Cyp26b1
Xaf1
Cxcl10
Osr1
Hhip
Igfbp3
Fn1
Thbs1
Bmp6
D14
D21
Downregulated
Prkcg
Nptx1
Gabra5
Cck
Snca
Ptk2b
Camk2a
Ntsr1
Itga4
Gpr37
Gdf10
Cd36
D14
D21

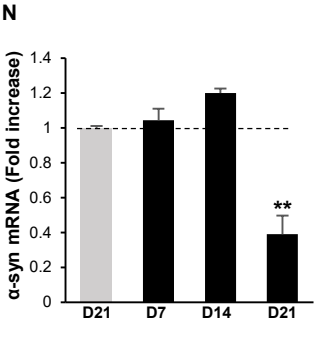
N
α-syn mRNA (Fold increase)
1.4
1.2
1
0.8
0.6
0.4
0.2
0
**
D21
D7
D14
D21

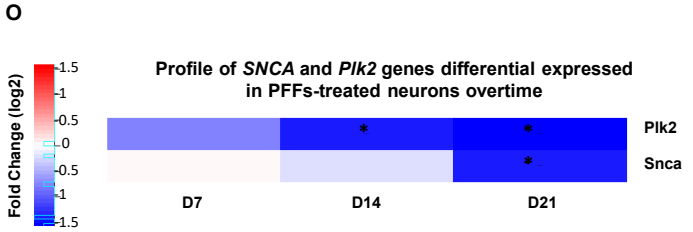
O
Profile of SNCA and Plk2 genes differential expressed in PFFs-treated neurons overtime
Fold Change (log2)
1.5
1
0.5
0
-0.5
-1
-1.5
*
*
*
Plk2
Snca
D7
D14
D21

Fig. S14. At late stages, the processes of formation and maturation of the LB-like inclusions are associated with neuronal toxicity.

A. Cell death level was assessed in WT neurons untreated or treated with PBS for up to D21 using lactate dehydrogenase (LDH) release assay (31). No significant toxicity was observed. **B-H.** Addition of α-syn PFFs to primary neuronal culture induces apoptotic cell death in a time-dependent manner between D14 and D21 as shown by the significant release of LDH (**B-C**) and the activation of the Caspase 3 (**D**). **E-H**. TUNEL (Terminal dUTP Nick End-Labeling) assay confirmed the activation of cell death through apoptotic pathways in PFFs-treated neurons at D14 and D21 as shown by confocal imaging (**E,** scale bars = 50 µm). Under these conditions, the neuronal population, positively stained for a specific neuronal marker (NeuN+), was significantly affected at D21 (TUNEL+/NeuN+) (**F-G**). Among the neuronal population, those in which seeded-aggregates were formed were the most affected by cell death (TUNEL+ NeuN+ pS129+) (**H**). **I-K**. The neuritic loss (**I**), the reduction in the number of neuronal cell bodies (**J**) and the level of pS129 (**K**) were also assessed by HCA. The graphs (**A-D, F-K**) represent the mean ± SD of three independent experiments. ANOVA followed by Tukey HSD post-hoc test was performed. $p<0.01$=*, $p<0.001$=**, $p<0.0001$=*** (PBS vs. PFF-treated neurons). $p<0.01$= #, $p<0.001$= ##, $p<0.0001$= ### (PFF-treated neurons D14 vs. D21).

L-O. Temporal transcriptomic analysis of the gene expression level. **L**. Log2 fold changes of the cell death genes at D7, D14, and D21 (**Dataset S2**). **M**. Expression level of cell death genes D14 vs. D21. **N.** Quantitative qRT-PCR. The graphs represent the mean ± SD of three independent experiments. $p<0.005$=** (ANOVA followed by Tukey HSD post-hoc test, PBS vs. PFF-treated neurons). **O**. Fold changes of *SNCA* and *PLK2* genes (PBS vs. PFF-treated neurons).

Figure S15. Related to Discussion

Day 7

Subcellular localization	Neurites	+++
	Cell bodies	+
LB markers	p62 (autophagy) and ub (proteasome)	√
α-syn PTMs	pS129	√
	C-ter truncation	x
Ultrastructure	Fibrils length	Long filaments (length: 600 nm to 2µm)
	Lateral association and packing	x
	Organelles interaction	x
Transcriptomic	Differentially-expressed genes	75 genes
LB Proteome	Enrichment of the insoluble fraction	Only 2 proteins
Biological Processes	Mitochondria dysfunctions	x
	Synaptic impairment	x
	Cell death	x

Day 14

Subcellular localization	Neurites	++
	Cell bodies	++
LB markers	p62 (autophagy) and ub (proteasome)	√
α-syn PTMs	pS129	√
	C-ter truncation	√
Ultrastructure	Fibrils length	Shorter filaments (~450 nm)
	Lateral association and packing	√
	Organelles interaction	√
Transcriptomic	Differentially-expressed genes	435 genes
LB Proteome	Enrichment of the insoluble fraction	633 proteins
Biological Processes	Mitochondria dysfunctions	x
	Synaptic impairment	√ (early event – reduction pre-synaptic area)
	Cell death	√ (early event – caspase 3 activation)

Day 21

Subcellular localization	Neurites	++
	Cell bodies	+++
LB markers	p62 (autophagy), ub (proteasome) and lipids	√
α-syn PTMs	pS129	√
	C-ter truncation	√
Ultrastructure	Fibrils length	Short filaments (~300 nm)
	Lateral association and packing	√
	Organelles interaction and sequestration	√
Transcriptomic	Differentially-expressed genes	1017 genes
LB Proteome	Enrichment of the insoluble fraction	568 proteins
Biological Processes	Mitochondria dysfunctions ↑ -Respiration ↓ -Mitochondria membrane potential ↓ -Mitochondrial protein levels ↓	√
	Synaptic impairment ↑ -Neurites ↓ -Pre-synaptic area ↓ -Synaptic plasticity ↓ -Pre and Post synaptic protein levels ↓	√
	Cell death (late events – loss of plasma membrane integrity)	√

Fig. S15. The dynamics of Lewy body formation, rather than simply alpha-synuclein fibrillization, is the primary cause of mitochondrial alterations, synaptic dysfunction and neurodegeneration (related to Figures 1-8 and discussion).

The table recapitulates the main events that occur during the formation of α-syn seeded aggregates and their maturation into LB-like inclusions over time.

Supplemental information – List of Datasets

Dataset S1. ***Proteomic identification of the proteins enriched in the insoluble fraction of the PFF-treated neurons (see corresponding excel dataset)***

Dataset S2. Transcriptomic identification of the genes significantly differentially expressed in PFF-treated neurons over time ***(see corresponding excel dataset)***

Dataset S3. Transcriptomic identification of the mitochondrial genes significantly differentially expressed in PFF-treated neurons over time ***(see corresponding excel dataset)***

Dataset S4. Transcriptomic identification of the synaptic genes significantly differentially expressed in PFF-treated neurons over time ***(see corresponding excel dataset)***

Supplemental information – References

1. Fauvet B*, et al.* (2012) alpha-Synuclein in central nervous system and from erythrocytes, mammalian cells, and Escherichia coli exists predominantly as disordered monomer. *The Journal of biological chemistry* 287(19):15345-15364.
2. Mahul-Mellier AL*, et al.* (2015) Fibril growth and seeding capacity play key roles in alpha-synuclein-mediated apoptotic cell death. *Cell death and differentiation* 22(12):2107-2122.
3. Steiner P*, et al.* (2002) Modulation of receptor cycling by neuron-enriched endosomal protein of 21 kD. *The Journal of cell biology* 157(7):1197-1209.
4. Volpicelli-Daley LA, Luk KC, & Lee VM (2014) Addition of exogenous alpha-synuclein preformed fibrils to primary neuronal cultures to seed recruitment of endogenous alpha-synuclein to Lewy body and Lewy neurite-like aggregates. *Nature protocols* 9(9):2135-2146.
5. Volpicelli-Daley LA*, et al.* (2011) Exogenous alpha-synuclein fibrils induce Lewy body pathology leading to synaptic dysfunction and neuron death. *Neuron* 72(1):57-71.
6. Catlin R*, et al.* (2016) Using Cultured Mammalian Neurons to Study Cellular Processes and Neurodegeneration: A Suite of Undergraduate Lab Exercises. *Journal of undergraduate neuroscience education : JUNE : a publication of FUN, Faculty for Undergraduate Neuroscience* 14(2):A132-137.
7. Hilgenberg LG & Smith MA (2007) Preparation of dissociated mouse cortical neuron cultures. *Journal of visualized experiments : JoVE* (10):562.
8. Dotti CG, Sullivan CA, & Banker GA (1988) The establishment of polarity by hippocampal neurons in culture. *The Journal of neuroscience : the official journal of the Society for Neuroscience* 8(4):1454-1468.
9. Fletcher TL & Banker GA (1989) The establishment of polarity by hippocampal neurons: the relationship between the stage of a cell's development in situ and its subsequent development in culture. *Developmental biology* 136(2):446-454.
10. Baj G, Patrizio A, Montalbano A, Sciancalepore M, & Tongiorgi E (2014) Developmental and maintenance defects in Rett syndrome neurons identified by a new mouse staging system in vitro. *Frontiers in cellular neuroscience* 8(18).
11. Cameron P, Mundigl O, & De Camilli P (1993) Traffic of synaptic vesicle proteins in polarized and nonpolarized cells. *Journal of cell science. Supplement* 17:93-100.
12. Gartner A, Fornasiero EF, Valtorta F, & Dotti CG (2014) Distinct temporal hierarchies in membrane and cytoskeleton dynamics precede the morphological polarization of developing neurons. *Journal of cell science* 127(Pt 20):4409-4419.
13. Yogev S & Shen K (2017) Establishing Neuronal Polarity with Environmental and Intrinsic Mechanisms. *Neuron* 96(3):638-650.

14. Dabrowski M*, et al.* (2003) Gene profiling of hippocampal neuronal culture. *Journal of neurochemistry* 85(5):1279-1288.
15. Frese CK*, et al.* (2017) Quantitative Map of Proteome Dynamics during Neuronal Differentiation. *Cell reports* 18(6):1527-1542.
16. Dorin-Semblat D*, et al.* (2015) Malaria Parasite-Infected Erythrocytes Secrete PfCK1, the Plasmodium Homologue of the Pleiotropic Protein Kinase Casein Kinase 1. *PloS one* 10(12):e0139591.
17. Rappsilber J, Mann M, & Ishihama Y (2007) Protocol for micro-purification, enrichment, pre-fractionation and storage of peptides for proteomics using StageTips. *Nature protocols* 2(8):1896-1906.
18. Cox J*, et al.* (2014) Accurate proteome-wide label-free quantification by delayed normalization and maximal peptide ratio extraction, termed MaxLFQ. *Molecular & cellular proteomics : MCP* 13(9):2513-2526.
19. Tyanova S*, et al.* (2016) The Perseus computational platform for comprehensive analysis of (prote)omics data. *Nature methods* 13(9):731-740.
20. Hubner NC*, et al.* (2010) Quantitative proteomics combined with BAC TransgeneOmics reveals in vivo protein interactions. *The Journal of cell biology* 189(4):739-754.
21. Perez-Riverol Y*, et al.* (2019) The PRIDE database and related tools and resources in 2019: improving support for quantification data. *Nucleic acids research* 47(D1):D442-D450.
22. Vandesompele J*, et al.* (2002) Accurate normalization of real-time quantitative RT-PCR data by geometric averaging of multiple internal control genes. *Genome biology* 3(7):RESEARCH0034.
23. Dobin A*, et al.* (2013) STAR: ultrafast universal RNA-seq aligner. *Bioinformatics (Oxford, England)* 29(1):15-21.
24. Anders S, Pyl PT, & Huber W (2015) HTSeq--a Python framework to work with high-throughput sequencing data. *Bioinformatics (Oxford, England)* 31(2):166-169.
25. Love MI, Huber W, & Anders S (2014) Moderated estimation of fold change and dispersion for RNA-seq data with DESeq2. *Genome biology* 15(12):550.
26. Makrecka-Kuka M, Krumschnabel G, & Gnaiger E (2015) High-resolution respirometry for simultaneous measurement of oxygen and hydrogen peroxide fluxes in permeabilized cells, tissue homogenate and isolated mitochondria. *Biomolecules* 5(3):1319-1338.
27. Burtscher J, Zangrandi L, Schwarzer C, & Gnaiger E (2015) Differences in mitochondrial function in homogenated samples from healthy and epileptic specific brain tissues revealed by high-resolution respirometry. *Mitochondrion* 25:104-112.
28. Pesta D & Gnaiger E (2012) High-resolution respirometry: OXPHOS protocols for human cells and permeabilized fibers from small biopsies of human muscle. *Methods in molecular biology (Clifton, N.J.)* 810:25-58.
29. Schindelin J*, et al.* (2012) Fiji: an open-source platform for biological-image analysis. *Nature methods* 9(7):676-682.

30. Henderson MX*, et al.* (2017) Unbiased Proteomics of Early Lewy Body Formation Model Implicates Active Microtubule Affinity-Regulating Kinases (MARKs) in Synucleinopathies. *The Journal of neuroscience : the official journal of the Society for Neuroscience* 37(24):5870-5884.
31. Parhamifar L, Andersen H, & Moghimi SM (2019) Lactate Dehydrogenase Assay for Assessment of Polycation Cytotoxicity. *Methods in molecular biology (Clifton, N.J.)* 1943:291-299.
32. Wakabayashi K*, et al.* (2013) The Lewy body in Parkinson's disease and related neurodegenerative disorders. *Molecular neurobiology* 47(2):495-508.
33. Leverenz JB*, et al.* (2007) Proteomic identification of novel proteins in cortical lewy bodies. *Brain pathology (Zurich, Switzerland)* 17(2):139-145.
34. Xia Q*, et al.* (2008) Proteomic identification of novel proteins associated with Lewy bodies. *Frontiers in bioscience : a journal and virtual library* 13:3850-3856.

Author contributions

H.A.L conceived and supervised the study. H.A.L and A.L.M.M designed all the experiments and wrote the paper. A.L.M.M performed and analyzed the experiments shown in Figures 1-5, 6A, 6D-F, 7-9, and Figures S1B-S15. J.B designed, performed, and analyzed the experiments shown in Figures 6A-B and S10B-D. N.M analyzed the experiments shown in Figures 4 and S8. L.W performed and analyzed the experiments shown in Figures 6F and 7A. M.L. analyzed the transcriptomic data (Datasets S2-S4) and participated to the Figures 4, 5, S9 and S14L-O. F.K developed the pipeline for High Content Image Analysis (HCA) using CellProfiler software shown in Figures S3G-I and Figure S14 I-K. M.C prepared the samples for CLEM analysis and acquired EM images in Figures 2, 3, and S5. G.K supervised the experiments shown in Figures 1L, 2-3, and S5 and contributed to the interpretation of the data. All authors reviewed and contributed to the writing.

Competing interests statement

Authors declare no competing financial interests in association with this manuscript.